Functional analyses of the proteins involved in DNA mismatch repair

DNA ミスマッチ修復に関与するタンパク質群の機能解析

Doctoral Thesis

Atsuhiro Shimada

Department of Biological Sciences, Graduate School of Science
Osaka University
2013

CONTENTS

ABBREVIATIONS

aaMutL	*Aquifex aeolicus* MutL
aaMutS	*Aquifex aeolicus* MutS
ABC	ATP-binding cassette
CCC form	covalently closed circular form
CFU	colony forming units
CTD	C-terminal domain
CRP	cyclic AMP receptor protein
DLS	dynamic light scattering
DSB	double-strand break
MMR	DNA mismatch repair
dsDNA	double-stranded DNA
ecMutL	*Escherichia coli* MutL
ecMutS	*Escherichia coli* MutS
EDTA	ethylenediaminetetraacetic acid
FT-ICR MS	Fourier transform ion cyclotron resonance mass spectrometer
GHL	gyrase, Hsp90, MutL
IPTG	isopropyl-β-D-thiogalactopyranoside
L form	linear form
NTD	N-terminal domain
OC form	open circular form
ssDNA	single-stranded DNA
ssExo	single-stranded DNA-specific exonuclease
Tth ExoI	*Thermus thermophilus* TTHB178
ttMutL	*Thermus thermophilus* MutL
ttMutS	*Thermus thermophilus* MutS
UV	ultraviolet
WT	wild type

GENERAL INTRODUCTION

During DNA replication, DNA polymerases generate misincorporation, deletion, and insertion errors (Kolodner and Marsischky, 1999; Kunkel and Erie, 2005; Modrich and Lahue, 1996). To prevent these errors from being fixed as mutations, DNA mismatch repair (MMR), a highly conserved DNA repair system, recognizes and repairs mispairs such as G-T and small insertion/deletion loops that give rise to frameshift mutations (Morita *et al*., 2010; Schofield and Hsieh, 2003; Marti and Fleck, 2002) (Fig. G-1 and Table G-1). MMR genes are involved not only in repairing DNA synthesis errors, but also in numerous cellular functions including repairing double-strand DNA breaks, antirecombination, cell cycle checkpoints and apoptotic responses to DNA damaging agents (Hsieh and Yamane, 2008; Li *et al*., 2008; Jirincy *et al*., 2006). These responsibilities make MMR proteins extremely important in the basic maintenance of the genetic material and the regulation of the cellular cycle. Mutations or epigenetic silencing of MMR genes can cause Lynch syndrome (also known as hereditary nonpolyposis colorectal cancer) in humans (Fishel *et al*., 1993; Leach *et al*., 1993; Peltomäki, 2005). This highlights the essential role of MMR in maintaining genomic fidelity and stability.

The overview of MMR pathways and conserved MMR components therein are described in Fig. G-1 and Table G-1, respectively. In eukaryotic MMR, MutSα and MutLα function during the initial steps of the MMR process (Table G-1, Eukaryote). First, MutSα binds to the DNA and searches for a replication error (Fishel *et al*., 1994; Gorman *et al*., 2007; Gorman *et al*., 2012) (Fig. G-1, Steps 1 and 2). Second, mismatch-bound MutSα forms the complex with MutLα and the DNA, and MutLα cleaves the strand containing the error (Kadyrov *et al*., 2006; Kadyrov *et al*., 2007) (Fig. G-1, Step 3). Finally, EXO1 exonuclease removes the error-contianing strand, DNA polymerases resynthesize the correct strand, and a DNA ligase seals the nick to complete the repair reaction (Fig. G-1, Steps 4 and 5) (Genschel *et al*., 2002; Szankasi and Smith, 1992;

Tishkoff *et al*., 1997; Tran *et al*., 2001). In the majority of bacteria, with the exception of a few species (e.g., *E. coli*), fundamental properties of MutS and MutL homodimers are similar to those of eukaryotic MutSα and MutLα (Fukui *et al*., 2011). In MMR of the majority bacteria, mismatch-bound MutS forms the complex with MutL on the DNA, and then MutL introduces a nick into the error-containing strand (Fig. G-1, Most bacteria Step 1-3). Subsequently, the DNA helicase unwinds the double-stranded DNA starting at the nick (Mechanic *et al*., 2000; Robertson *et al*., 2006), and single-stranded DNA-specific exonucleases degrade the unwound DNA (Burdett *et al*., 2001; Shimada *et al*., 2010) (Fig. G-1, Most bacteria Step 4). The single-stranded DNA region generated by removal of the error-containing DNA is immediately protected by a bacterial single-stranded DNA-binding protein. Finally, DNA polymerases resynthesize the correct strand and a DNA ligase seals the nick (Fig. G-1, Most bacteria Step 5).

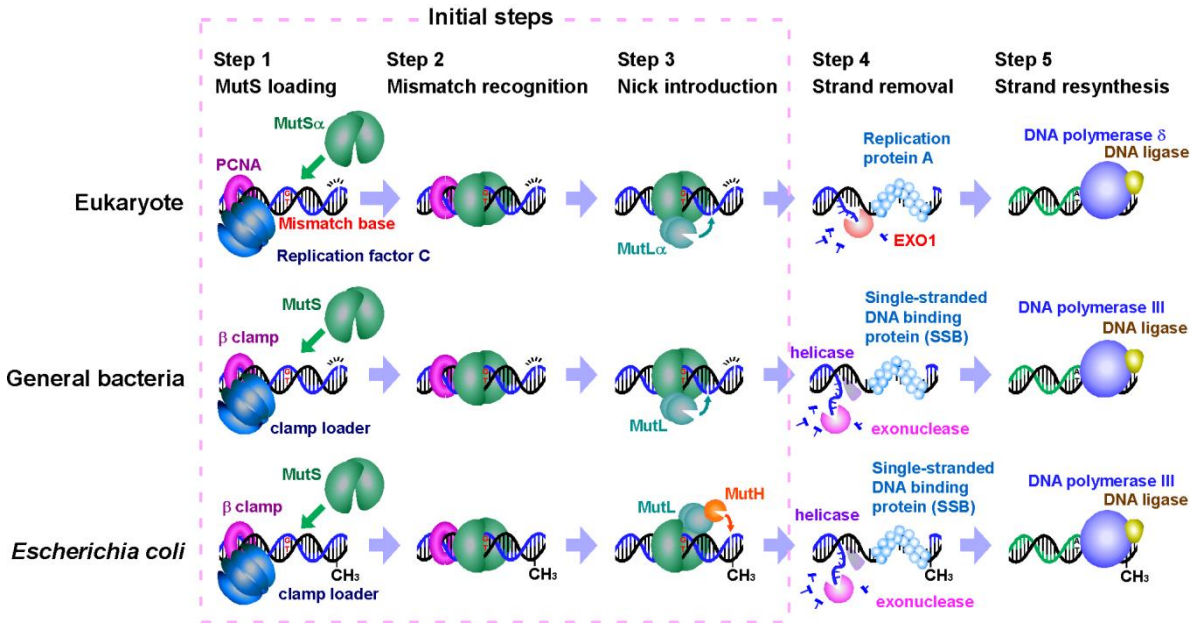

Figure G-1. MMR pathway models. During DNA replication, DNA polymerases misincorporate a base, thus generating a mispair. During the initial steps of a DNA mismatch repair, MutS binds to the DNA and searches for a mismatched base along the DNA strand (Step 1). When MutS recognizes a mismatch, it interacts with MutL on the damaged strand (Step 2). MutH (*E. coli*) or MutL (eukaryote and most bacteria) introduce a nick into the error-containing strand (Step 3). Single-stranded DNA-specific exonucleases (*E. coli* and most bacteria) or 5′→3′ exonuclease EXO1 (eukaryote) remove the DNA segment containing the mispair (Step 4). The single-stranded DNA region generated by removal of the error-containing DNA is immediately protected by a bacterial single-stranded DNA-binding protein or eukaryotic replication protein A (Step 4). Finally, DNA polymerases resynthesize the correct strand and a DNA ligase seals the nick (Step 5).

Table G-1. MMR components

Reactions	Organism				
	Thermus thermophilus	*Escherichia coli*	*Saccharomyces cerevisiae*	*Arabidopsis thaliana*	*Homo sapiens*
Mismatch recognition	MutS (TTHA1324)	MutS	MutSα (MSH2/MSH6) MutSβ (MSH2/MSH3)	MutSα (MSH2/MSH6) MutSβ (MSH2/MSH3)	MutSα (MSH2/MSH6) MutSβ (MSH2/MSH3)
Nick introduction	MutL (TTHA1323)	MutH (MutL activated)	MutLα (MLH1/PMS1) MutLβ (MLH1/MLH2) MutLγ (MLH1/MLH3)	MutLα (MLH1/PMS2) MutLβ (MLH1/MLH3)	MutLα (MLH1/PMS2) MutLβ (MLH1/PMS2) MutLγ (MLH1/MLH3)
Strand unwinding	UvrD (TTHA1427)	UvrD			
Strand removal					
5′ →3′ exonuclease	RecJ (TTHA1167)	RecJ ExoVII	EXO1	ATJG29630	EXO1
3′→5′ exonuclease	Unknown	ExoI ExoX			
Correct strand synthesis	DNA polymerase III δ, δ′, γ, and τ subunits (TTHA0788, 1860, 1952)	DNA polymerase III d, d′, g, and t subunits	RFC	RFC	RFC
	β subunit (TTHA0001)	β clamp	PCNA	PCNA	PCNA
	α subunit (TTHA0180)	α subuntis	DNA polymerase e	DNA polymerase e	DNA polymerase e

Strand discrimination is an essential feature of all MMR systems, but its molecular basis is not fully understood. The *E. coli*-type MMR is characterized by a lack of endonuclease activity in MutL. In *E. coli* type MMR, the nicking endonuclease activity is provided by MutH (Ban and Yang, 1998) (Table G-1). The MutH endonuclease recognizes the hemi-methylated dGATC sequence and cleaves the phosphodiester bond between G and A in the unmethylated strand (Längle-Rouault *et al*., 1987) (Fig. G-1, *E. coli* Step 3). This insertion of the nick by MutH is used to discriminate between the template strand and the newly synthesized strand. On the other hand, the strand discrimination in eukaryotic MMR has been argued. A recent study strongly suggests that strand discrimination in eukaryote requires an interaction between MutLα and a replication clamp, PCNA (Pluciennik *et al*., 2010; Pillon *et al*., 2011). In the presence of PCNA, MutLα cleaves the discontinuous strand 10-fold higher efficiently than continuous strand (Pluciennik *et al*., 2010). In MutH-less bacteria, the strand discrimination system has been unclear. In *Bacillus subtilis,* the C-terminal domain (CTD) of MutL possesses β clamp-interacting motif, and MutL colocalizes with β clamp in cells (Pillon *et al*., 2010; Simmons *et al*., 2008). However, there is no obvious evidence that β clamp serves as a strand discrimination signal. In *Pseudomonas aeruginosa*, it is reported that the MutL-β clamp interaction is not necessary for strand discrimination (Monti *et al*., 2012), suggesting that there is another mechanism involved in strand discrimination in most bacterial MMR.

In addition, the role of ATP hydrolysis in MMR process is still outstanding problem, although MutS homologs possess the ability to activate ATP hydrolysis activity. ATP binding are thought to be involved in mismatched base recognition by MutS (Fig. G-1, Step 2). It is reported that ATP binding causes the conformational changes in MutS (Fig. G-2). MutS (nucleotide-free or ADP-bound MutS) recognizes a mismatched base (Fig. G-2, Step 1 and 2), and then, the ADP in MutS is replaced with ATP (Antony and Hingorani, 2003; Antony and Hingorani, 2004; Zhai and Hingorani, 2010). The ATP hydrolysis activity of

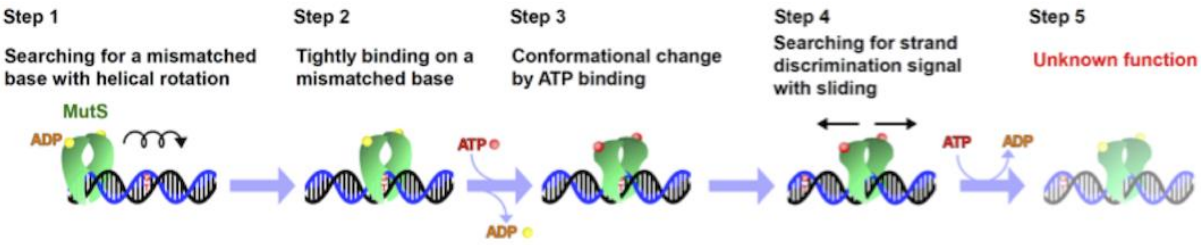

Figure G-2. Conformational and functional changes in MutS induced by adenine nucleotide binding. ADP-bound or nucleotide-free MutS binds on DNA more efficiently than ATP-bound one. ADP-bound MutS was able to search for a mismatched base with helical rotation along a DNA strand (Step 1) and then bind on a mismatched base tightly (Step 2). Mismatch-bound MutS immediately replaces ADP with ATP, and the ATP hydrolysis activity of MutS is inhibited (Antony and Hingorani, 2003; Antony and Hingorani, 2004; Zhai and Hingorani, 2010). Furthermore, ATP-binding induced the conformational changes in MutS, resulting in forming clamp-like formation (Step 3). Clamp-like MutS releases a mismatched base and slides along a DNA, postulating to find a strand discrimination signals (Step 4). The function of ATP hydrolysis by MutS released from a mismatched base is unclear (Step 5).

the mismatch-bound MutS is tightly suppressed, and ATP binding induces a MutS conformational change, thus resulting in the formation of a clamp-like structure to slide along the DNA strand (Biswas and Vijayvargia, 2000; Joshi *et al*., 2000) (Fig G-2, Steps 3 and 4). In *E. coli* type MMR, the ATP hydrolysis of MutS is necessary for the activation of MutH (Ban and Yang, 1998; Ban *et al*., 1999). However, in eukaryotic and general bacterial MMR, the role of ATP hydrolysis by MutS after the mismatch release is unclear (Fig. G-2, Step 5).

To verify the strand discrimination and the role of ATP hydrolysis by MutS in general bacterial MMR, I attempted partial *in vitro* reconstitution by using the recombinant proteins of *Thermus thermophilus* HB8. *Thermus thermophilus* HB8 has a small genome size (approximately 2.2 Mbp) and an extremely high optimum growth temperature of 75°C (Yokoyama *et al*., 2000). Proteins from this eubacterial strain are extremely stable and suitable for *in vitro* characterization. Therefore, we selected *T. thermophilus* HB8 for the systematic study of the structures and functions of all proteins from a single organism (Yokoyama *et al*., 2000). Our group has already investigated many DNA repair enzymes

form this strain, including the clamp loader complex, β clamp, MutS (Fukui *et al*., 2004), MutL (Fukui *et al*., 2008), DNA helicase, 5′ →3′ single-stranded DNA (ssDNA) specific exonuclease (ssExo) (Wakamatsu *et al*., 2010), ssDNA-binding protein (Inoue *et al*., 2011, Mikawa *et al*., 2009), and DNA ligase. These proteins are thought to be the most essential components of this bacterial MMR, except for 3′→5′ ssExo and DNA polymerase III (Table G-1).

In this work, I revealed that a novel 3′→5′ ssExo is involved in MMR, and the ATP hydrolysis by MutS is required for the nick introduction by MutL. In CHAPTER I, I describe the enzymatic analyses of 3′→5′ exonuclease and its cellular functions. This novel exonuclease was predicted to be involved in MMR in addition to double-stranded break (DSB) repair and oxidized base repair. The result that this novel 3'→5' ssExo was involved in MMR indicates that minimum components required for *in vivo* MMR reconstruction are completed in *T. thermophilus* (Table G-1). In CHAPTER II, although I tried to reconstruct the strand discrimination using recombinant MMR proteins, this assay was unsuccessful. This result suggests that as-yet unidentified factors could be involved in MMR of *T. thermophilus*. However, through the reconstruction analysis, I revealed that ATP hydrolysis by ttMutS triggers the nicking introduction by ttMutL.

CHAPTER I

A novel single-stranded DNA-specific 3′-5′ exonuclease, *Thermus thermophilus* exonuclease I, is involved in several DNA repair pathways

ABSTRACT

Single-stranded DNA-specific exonucleases are expected to be involved in a variety of DNA repair pathways corresponding to their cleavage polarities; however, the relationship between the cleavage polarity and the respective DNA repair pathways is only partially understood. To understand the cellular function of ssExos in DNA repair better, genes encoding ssExos were disrupted in *Thermus thermophilus* HB8, which seems to have only a single set of 5′→3′ and 3′→5′ ssExos unlike other model organisms. Disruption of the *tthb178* gene, which was expected to encode a 3′→5′ ssExo, resulted in significant increases in the sensitivity to H_2O_2 and frequency of the spontaneous mutation rate but scarcely affected the sensitivity to UV irradiation. In contrast, disruption of the *recJ* gene, which encodes a 5′→3′ ssExo, showed little effect on the sensitivity to H_2O_2 but caused increased sensitivity to UV irradiation. *In vitro* characterization revealed that TTHB178 possessed 3′→5′ ssExo activity, which degraded ssDNAs containing deaminated and methylated bases but not those containing oxidized bases or abasic sites. Consequently, I concluded that TTHB178 is a novel 3′→5′ ssExo that functions in various DNA repair systems in cooperation with or independently of RecJ. I named TTHB178 as *T. thermophilus* exonuclease I.

INTRODUCTION

ssDNA and double-stranded DNA (dsDNA)-specific exonucleases are essential for DNA replication, repair, and recombination. Functional defects of exonucleases are known to have a profound impact on human diseases, such as Aicardi-Goutieres syndrome, familial chilblain lupus, and ataxia telangiectasia-like disorder (Crow *et al*., 2006; Fukuda *et al*., 2001; Lee-Kirsch *et al*., 2007). The ssExos are categorised by their cleavage polarity; from 3′ to 5′ and from 5′ to 3′. A variety of DNA repair pathways require ssExos to process the intermediate DNA structures generated during the reactions (Burdett *et al*., 2001; Lombardo *et al*., 2003; Viswanathan *et al*., 2001). Because the diverse intermediate DNA structures are yielded depending on the repair pathway, living cells are considered to require several kinds of ssExos with different polarities. For example, a 5′→3′ ssExo is required for the early stage of double-strand break (DSB) repair. DSB is a potentially lethal lesion that is spontaneously generated in normal cells and also generated by external factors including UV-C (100-280 nm) (Rosenstein and Ducore, 1983). Bacterial DSB repair mainly occurs through homologous recombination (Cromie *et al*., 2001). In this mechanism, an ssExo with 5′→3′ polarity processes the termini of a dsDNA to a 3′-overhanging structure, generating an entry point for downstream enzymes.

Also, in MMR, which corrects a mismatched base generated during DNA replication, it is suggested that an ssExo is required for the excision of the ssDNA region containing the mismatched base. In *E. coli*, which has four ssExos (RecJ, ExoI, ExoX, and ExoVII described in Table I-1), each single ssExo deletion mutant showed no phenotype, but disruption of all four ssExos caused about 7-fold higher spontaneous mutation rate than wild-type (Friedberg *et al*., 1995). In bacterial MMR, the endonuclease (MutL of general bacteria and MutH of *E. coli* and its closely related species) introduces nicks into the 3′- and 5′-sides of the mismatched base (Fukui *et al*., 2008; Kadyrov *et al*., 2006; Kadyrov *et al*.,

2007; Kunkel and Erie, 2005; Modrich, 2006; Obmolova *et al*., 2000). Then, DNA helicase (e.g., UvrD which translocates with 3' to 5' direction along ssDNA) unwinds dsDNA form the nick on the 5'-side of the mismatched base, generating ssDNA gap region and 5'-flap end. It is thought that ssExos degrading ssDNA with 5' to 3' direction are involved in degrading liberated ssDNA to prevent form re-annealing of the ssDNA. Because nicks are also introduced into 3'-side of the mismatched base, it is suggested that DNA helicase translocating with 5' to 3' direction and 3'→5' ssExos are involved in MMR. In *E. coli* type MMR, it is known that ssDNA excision is carried out from the nick on the both 3'- and 5'-side (Friedberg *et al*., 1995; Pluciennik *et al*., 2009).

The type of ssExo polarity required for other DNA repair pathways is hardly understood. It also remains to be established how cells process intermediates in the repair of deaminated bases, such as xanthine, hypoxanthine, and uracil. Endonuclease V is known to hydrolyse the phosphodiester bond at the 3′-side of the deaminated lesion (Dalhus *et al*., 2009; Moe *et al*., 2003); however, the downstream reaction is unclear. ssExos might be involved in the downstream reaction. Furthermore, the role of ssExos is completely uncertain in the repair of other damages, such as oxidised bases, methylated bases, or abasic sites in DNA.

Whole genome sequencing revealed that *T. thermophilus* HB8 had 2,213 genes (Yokoyama *et al*., 2000). Our group has already investigated many DNA repair enzymes from *T. thermophilus* HB8 (Fukui *et al*., 2004; Morita *et al*., 2008; Tachiki *et al*., 1998; Yamagata *et al*., 2001), including a 5′→3′ ssExo, RecJ and RecJ-like (Wakamatsu *et al*., 2010 and 2011; Yamagata *et al*., 2002). From the result of sequence similarity search using already-known 5'→3' ssExo sequences as queries, it is suggested that, in *T. thermophilus*, there are no candidates for 5'→3' ssExos except for RecJ and RecJ-like protein (Table I-1). RecJ cleaves only ssDNA, whereas RecJ-like protein degrades ssRNA efficiently as well as ssDNA. Although RecJ cannot hydrolyze short ssDNA shorter than 3 nt, RecJ-like protein preferentially hydrolyzes short oligodeoxyribonucleotides and oligoribonucleotides (< 3 nt).

Furthermore, the growth rate of *recJ-like* deficient mutant recovers by the addition of the mononucleotides to the culture (Wakamatsu *et al*. 2011). These results indicate that RecJ-like protein participated in recycling short oligonucleotides to mononucleotides *in vivo*. Because there were no reports that exonucleases specialized in degrading short nucleotides were involved in strand removal in DNA repair such as DSB repair, I focused on RecJ as ssExo participating in DNA repair.

Sequence similarity search was also performed against genes of *T. thermophilus* using already-known 3'→5' ssExos as queries (Table I-1). The search result strongly suggested that *T. thermophilus* possesses a 3′→5′ ssExo, TTHB178. I found the DnaQ exonuclease motif in the *N*-terminal region of TTHB178 (Fig. I-1) that had been annotated as a function-unknown protein. Most of the exonuclease domains of 3′→5′ ssExos are categorised into the DnaQ superfamily (Moser *et al*., 1997; Zhang *et al*., 1998). The 3′→5′ exonuclease domains of the DnaQ superfamily share three conserved exonuclease motifs containing negatively charged amino acid residues (Bernad *et al*., 1989), which coordinate two divalent metal ions to catalyse the phosphodiester bond cleavage (Breyer and Matthews, 2000; Busam, 2008). Recent reports have described the expression of the *tthb178* gene under the control of a transcriptional regulator, cyclic AMP-receptor protein (CRP), in *T. thermophilus* HB8 (Shinkai *et al*., 2007), implying that *tthb178* plays a certain kind of biological role in the cell.

Table I-1. Distibution of single-stranded DNA-specific exonucleases (ssExos). ssExos were searched for using the amino acid sequences of following enzymes as queries in BLAST search: *E. coli* exonuclease I, *E. coli* exonuclease VII, *E. coli* exonuclease X, *E. coli* RecJ, *E. coli* RecD, *H. sapiens* EXO1, *H. sapiens* MRE11, *H. sapiens* TREX1, *H sapiens* TREX2, *H. sapiens* Altemis, *H. sapiens* WRN exonuclease, *H. sapiens* exo/endonuclease-G, *H. sapiens* PIF1, *H. sapiens* DNase III, *H. sapiens* Apoptosis enhancing exonuclease, and *S. cerevisiae* DIN7. The codes in parenthesis indicate accession numbers of each protein.

Species	3′ →5′ ssExo	5′ →3′ ssExo	Bi-polar ssExo
Thermus thermophilus HB8	TTHB178 (BAD71974)	RecJ (BAD70990) RecJ-like (BAD69941)	Not identified
Escherichia coli	exonuclease X (ACI82135) exonuclease I (AAA19938)	RecJ (AAA62789) RecD (AAG48658)	exonuclease VII (AAA24766)
Deinococcus radiodurans	DnaQ-like (NP_051628) DnaQ-like (NP_880692)	RecJ (ACX31683) RecJ-like (NP_294850)	exonuclease VII (Q9RXW9)
Bacillus subtilis	exonuclease I (CAA66997) DnaQ-like (O05231)	RecJ (O32044) RecJ-like (O31903) Putative 5′⟶3′ exonuclease (P54161)	exonuclease VII (P54521)
Pyrococcus furiosus	Not identified	RecJ (AAL82179) RecJ-like (AAL80523)	Not identified
Thermococcus kodakaraensis	Not identified	RecJ (YP_183665) RecJ-like (YP_182568)	Not identified
Saccharomyces cerevisiae	MRE11 (NP_013951) EXO1 (NP_014676)	PIF1 (NP_013650) PIF1-like (NP_011896) DIN7 (CAA94102)	Not identified
Homo sapiens	MRE11 (NP_005582) EXO1 (NP_006018) TREX1 (NP_057465) TREX2 (NP_542432) Apoptosis enhancing exonuclease (AAH20988) DNase III (CAB50866)	Altemis (NP_001029030) Exo/Endonuclease-G (NP_005098) PIF1 (NP_079325)	WRN exonuclease (AAR05448)

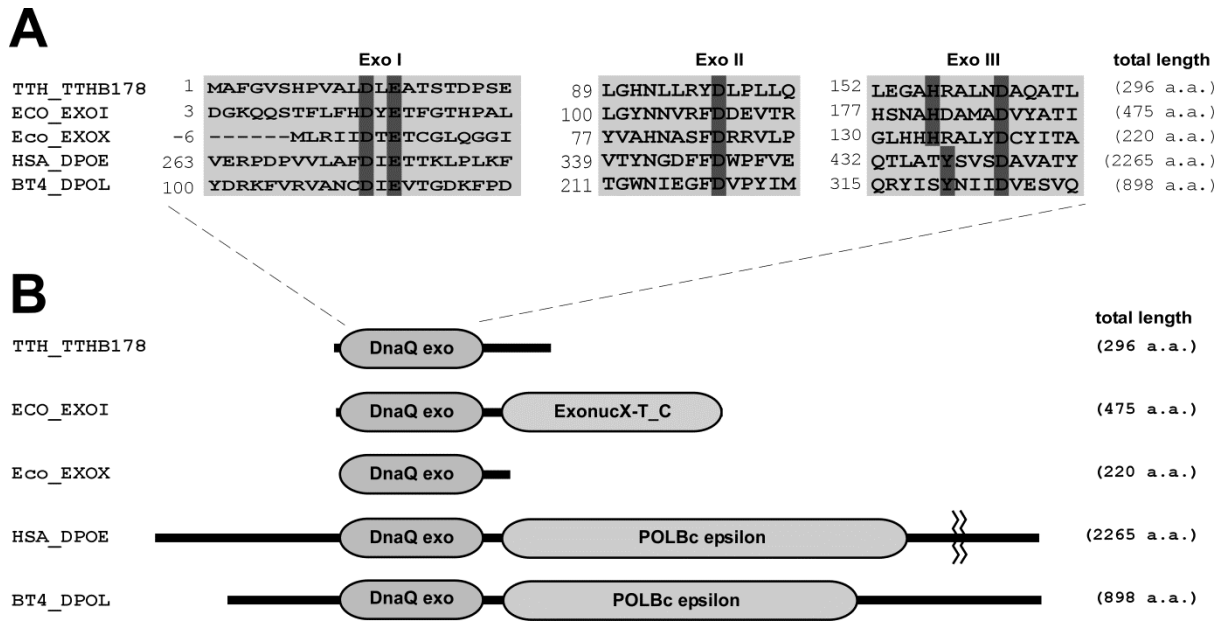

Figure I-1. Amino acid sequence alignments of TTHB178 and the proteins belonging to the DnaQ superfamily. (A) Exonuclease motifs I, II, and III of TTHB178 and exonucleases belonging to the DnaQ superfamily. The numbers to the left of the motifs indicate the distances from the protein *N*-termini. The predicted active site residues are highlighted in dark gray. (B) Schematic diagrams of TTHB178 and the other DnaQ superfamily proteins. DnaQ exo, ExonucX-T_C, and POLBc epsilon mean the exonuclease domain of the DnaQ superfamily, the SH3-like and helical domains of *E. coli* EXOI, and the DNA polymerase domain of type-B family DNA polymerases, respectively. Abbreviations: TTH_TTHB178, *T. thermophilus* HB8 TTHB178; ECO_EXOI, *E. coli* ExoI; ECO_EXOX, *E. coli* ExoX; HSA_DPOE, *H. sapiens* DNA polymerase ε; BT4_DPOL, bacteriophage T4 DNA polymerase.

As there seems to be no other candidate for the ssExos in *T. thermophilus* except for the proofreading domains of DNA polymerases, this organims is expected to have a single set of 3′→5′ ssExo (TTHB178) and 5′→3′ ssExo (RecJ). In the majority of the organisms, including *E. coli*, yeast, and humans, redundancy of the same polarity of ssExos makes it difficult to clarify the relationship between their cleavage polarities and their cellular functions (Table I-1). In contrast, *T. thermophilus* HB8 is suitable for investigating the difference in cellular functions between 3′→5′ and 5′→3′ ssExos, because gene disruption of an ssExo is expected to affect directly the phenotypes of the disruption mutants.

In this study, I investigated the phenotypes of the disruption mutants of the *tthb178* and *recJ* genes under DNA-damaging conditions. I also prepared the *tthb178* gene product, and examined its biochemical activity against various types of DNA *in vitro*. The results suggest that TTHB178 is a 3′→5′ ssExo that functions in several DNA repair pathways including MMR not only cooperatively with but also independently of RecJ.

EXPERIMENTAL PROCEDURES

Transcription analysis of tthb178—*T. thermophilus* HB8 cells were cultured overnight in TT-broth (0.8% polypeptone, 0.4% yeast extract, 0.2% NaCl, 0.4-mM $MgCl_2$, and 0.4-mM $CaCl_2$; pH 7.2) at 70°C, diluted 100-fold in fresh TT-broth, and the diluted culture was incubated at 70°C. At each time point, cells were harvested by centrifugation at 2,300 × *g* for 10 min at 4°C and stored at −20°C. Purification of mRNA was carried out by using an RNeasy mini kit (Qiagen, Hilden, Germany) according to the manufacturer′s protocol (Ishii *et al*., 2007). The cDNA was synthesised by reverse transcription-PCR using forward primer 5′-ACCTCTACGCCTTCCTCCTC-3′ and reverse primer 5′-CTCCTTGATTCTCTG GGCGG-3′. The amplified fragment was 332 bp.

Disruptions of tthb178 and recJ—The gene null mutants of *T. thermophilus* HB8 were constructed by using a previously reported procedure (Hashimoto *et al*., 2001). The plasmids for gene disruption were derivatives of the pGEM-T Easy vector (Promega Co., Madison, WI), constructed by inserting the thermostable kanamycin-resistance gene, *HTK* (Hoseki *et al*., 1999), flanked by approximately 500-bp upstream and downstream sequences of the *tthb178* and *recJ* genes (Fig. I-2A). The 500-bp DNA fragments from upstream and downstream of the *tthb178* gene were amplified by PCR using primer sets 5′-ACTCGGGCGGCACGATC-3′ and 5′-ATATGGTACCCGCCGTCAACGGGTACCG-3′, and 5′-ATATCTGCAGCATGTTGGTTACGCTGCA-3′ and 5′-GCGCCGCCTCCACCACCT-3′, respectively (the underlining indicates *Kpn*I and *Pst*I sites, respectively). The 500-bp DNA fragments from upstream and downstream of the *recJ* gene were also amplified by PCR using primer sets 5′-CGGGACCCTCTTGGGCCT-3′ and 5′-ATATGGTACCCGCCGTCAAC GGGTACCA-3′, and 5′-ATATCTGCAGCATGTTGGTTACGCTGCA-3′ and 5′-CGGGGGC CTCCACCACCC-3′, respectively (the underlining indicates *Kpn*I and *Pst*I sites,

respectively). The amplified fragments were digested with *Kpn*I and *Pst*I, respectively, to obtain fragments I and II. The *HTK* gene was also amplified by PCR from plasmid pUC18/*HTK* (Hoseki *et al*., 1999) by using 5′-ATATGGTACCCGTTGACGGCGGGATATG-3′ and 5′-ATATCTGCAGCGTAACCAACATGATTAA-3′ as primers (the underlining indicates *Kpn*I and *Pst*I sites, respectively). The amplified fragment was then treated with *Kpn*I and *Pst*I to obtain fragment III. Fragments I, II, and III were ligated into the pGEM-T Easy vector. For double gene knockout, the thermostable hygromycin-B-resistance gene was used for disrupting the *recJ* gene (Fig. I-2B). The hygromycin-B-resistance gene was amplified by PCR from plasmid pHG206 (Ooga *et al*., 2009) by using 5′-GAATTCGAGCTCGGTACCCG-3′ and 5′-ATATCTGCAGGAATTCGAGGTCGCTACCCG-3′ as primers (the underlining indicates *Kpn*I and *Pst*I sites, respectively). The amplified fragment was then digested with *Kpn*I and *Pst*I to obtain fragment IV. Fragments I and II from the *recJ* gene and fragment IV were ligated into pGEM-T Easy. The plasmid was transformed into *T. thermophilus* HB8 cells as previously described (Hashimoto *et al*., 2001). Disruptions of the *tthb178* and *recJ* genes were confirmed by PCR amplification using the isolated genomic DNAs as templates (Fig. I-3). The absence of the mRNA transcribed from *tthb178* and *recJ* was also confirmed by RT-PCR (Fig. I-4).

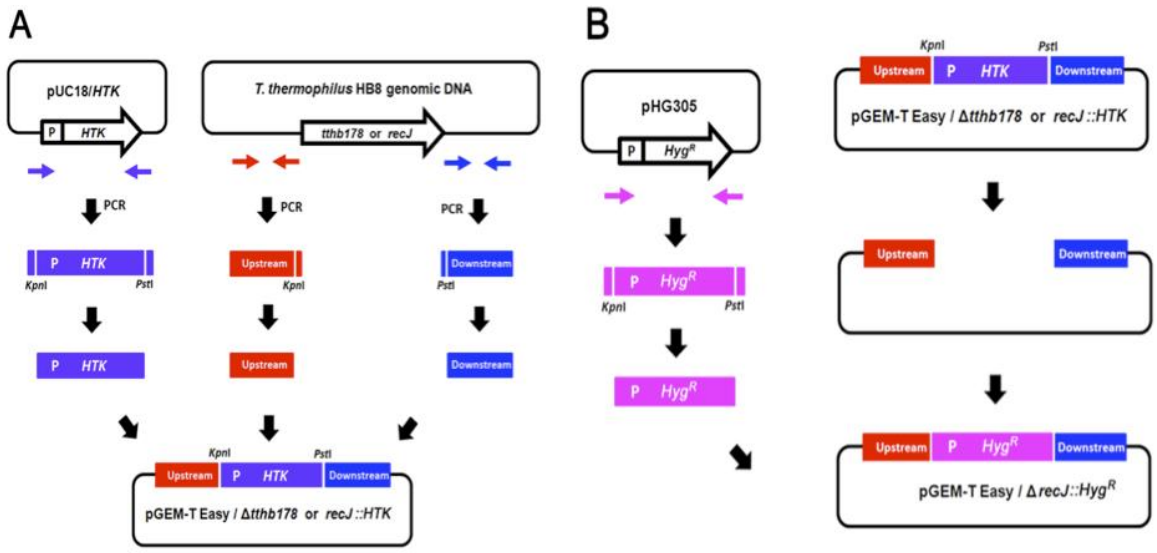

Figure I-2 Construction of plasmids for gene disruption. (A) Construction of plasmids for Δ*tthb178* and Δ*recJ* disruptions. The thermostable kanamycin-resistance gene, *HTK*, was amplified by PCR using pUC18/*HTK* plasmid as a template. The 500-bp DNA fragments from upstream and downstream of *tthb178* or *recJ* gene were amplified by PCR using *Thermus thermophilus* HB8 genomic DNA as a template. The DNA fragments were treated with KpnI and PstI, and then ligated into the pGEM-T Easy vector to obtain pGEM-T Easy/Δ*tthb178*::*HTK* and pGEM-T Easy/Δ*recJ*::*HTK* plasmids. (B) Construction of the plasmid for disruption of *recJ* by inserting the thermostable hygromycin-B-resistance gene, Hyg^R. The Hyg^R was amplified by PCR from pHG305 plasmid (accession number: AB470102). The amplified fragment was treated with KpnI and PstI, and then ligated into the corresponding site of pGEM-T Easy/Δ*recJ*::*HTK* to obtain pGEM-T Easy/ Δ*recJ*::Hyg^R plasmid.

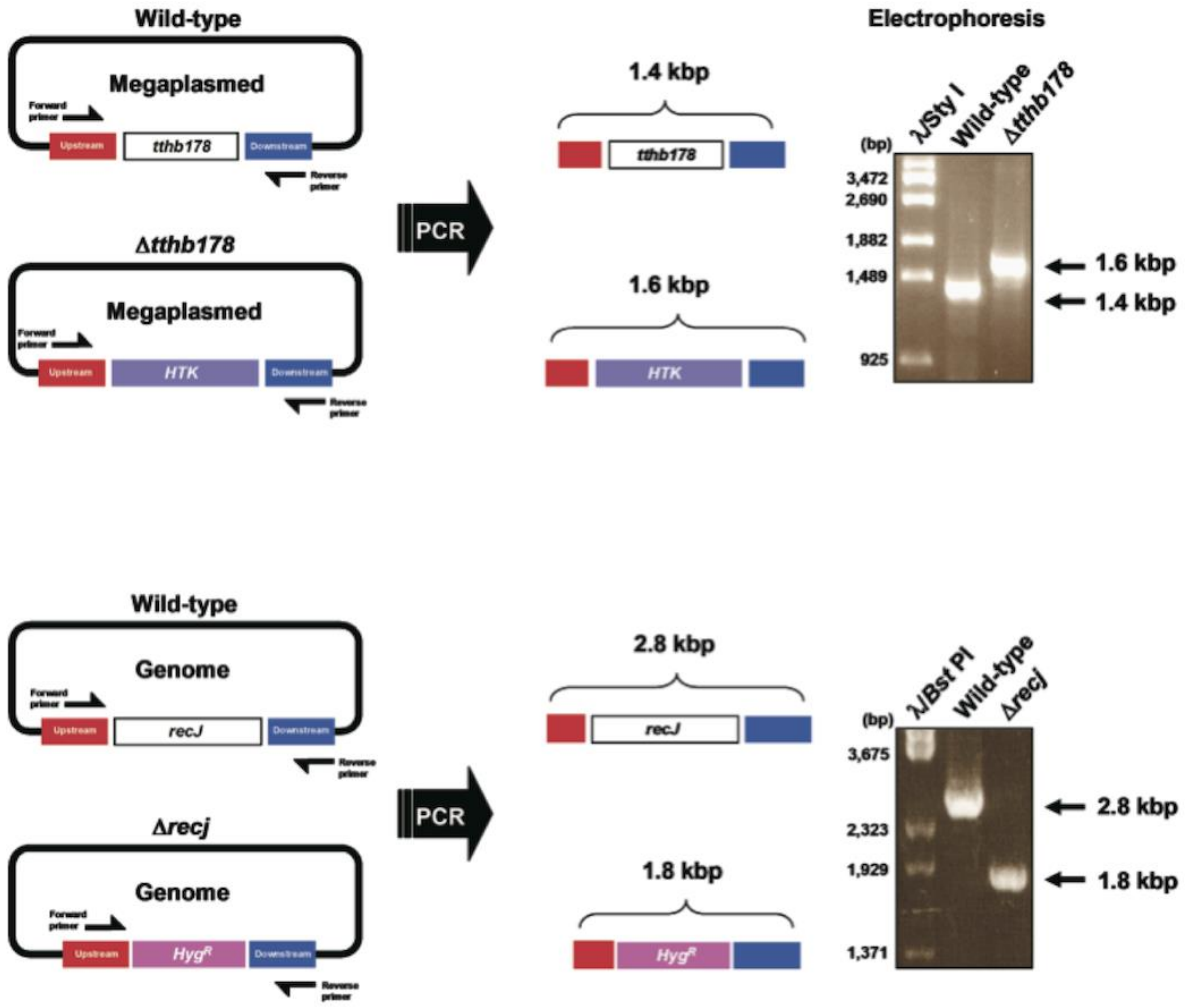

Figure I-3. The *tthb178* (A)- and *recJ* (B)-disruptions were confirmed by PCR. The coding region of each gene in the disruptant genomic DNA was amplified by PCR, using the wild-type genomic DNA as a control. On the basis of the lengths of amplified DNA products, I concluded that disruptions were carried out as desired.

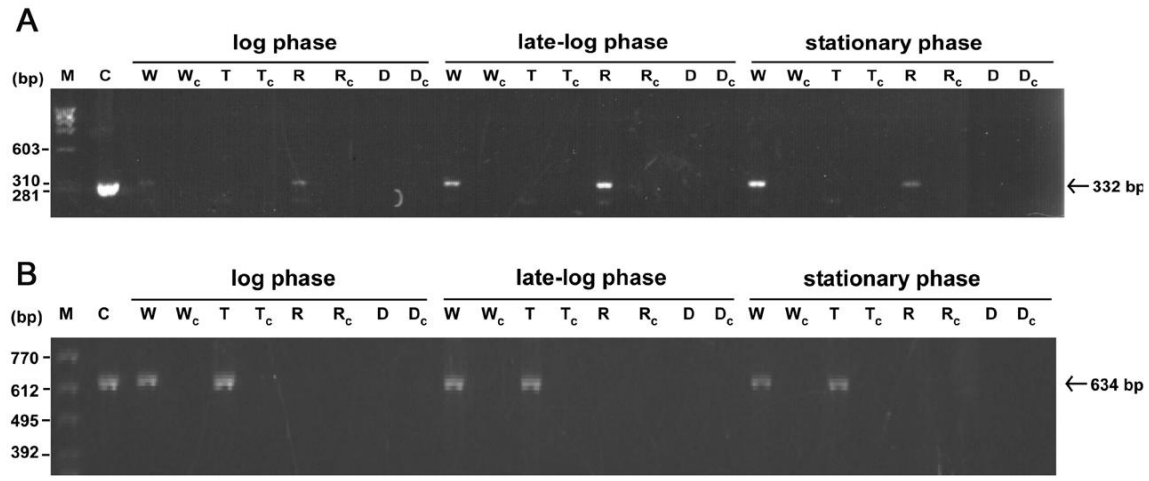

Figure I-4. The absence of mRNAs of *tthb178* and *recJ* was confirmed by RT-PCR according to the procedure described in Materials and Methods. The cDNAs of *tthb178* (A) and *recJ* (B) were synthesised using the primer sets 5′-ACCTCTACGCCTTCCTCCTC-3′ and 5′-CTCCTTGATTCTCTGGGCGG-3′, and 5′-TTGGAAAACGGGGTGGAGGTG-3′ and 5′-AAGAGGAGGAAGAGGGGCTCG-3′, respectively. The abbreviations used are: *M*, DNA size marker; *C*, a positive control using wild-type genomic DNA as a template; *W*, cDNA synthesised from wild-type total RNA; *T*, cDNA from *Δtthb178* total RNA; *R*, cDNA from *Δrecj* total RNA; *D*, cDNA from double disruptant total RNA; *subscript c*, a negative control without reverse transcriptase. The lengths of synthesised cDNAs of *tthb178* and *recJ* were designated to be 332- and 634-bp, respectively.

***Estimation of spontaneous mutation rates*—**The spontaneous mutation rate of *T. thermophilus* HB8 was estimated based on the frequency of streptomycin-resistant strains measured by means of the modified Luria-Delbrück fluctuation test (Luria and Delbruck, 1943). Cultured *T. thermophilus* HB8 wild type (WT) and disruptants in the mid-exponential growth phase (A_{660} = 1.0–1.5) were appropriately diluted in TT-broth and spread on TT-agar plates with or without 50 μg/ml streptomycin. The numbers of colonies formed, colony-forming units (CFUs), were counted after incubation at 70°C for 24 h. The surviving fractions were expressed as the average obtained from at least three independent experiments. The spontaneous mutation rates (%) were calculated according to the formula mutation rate (%) = $M/N \times 100$, where M is the counted CFUs on the TT-plates containing 50 μg/ml streptomycin and N is the mean of the CFUs on the TT-plates without streptomycin.

Examination of the sensitivities to UV irradiation and H_2O_2 addition*—T. thermophilus* HB8 cells in the mid-exponential growth phase were spread on TT-agar plates and irradiated with 254 nm UV light at the dose rate of 1.9 J m^{-2} s^{-1} for 40 s. The CFUs were counted after incubation at 70°C for 24 h, and the surviving fractions were expressed as the average obtained from at least three independent experiments.

The sensitivity to H_2O_2 addition was measured as follows. *T. thermophilus* HB8 cells in the mid-exponential growth phase were mixed with equal volumes of 0, 10, 20, and 100 mM H_2O_2. The cells were further incubated at 70°C for 20 min and spread on TT-agar plates. The CFUs were counted after incubation at 70°C for 24 h, and the surviving fractions were expressed as the average obtained from at least three independent experiments.

Overexpression and purification of TTHB178*—E. coli* Rosetta(DE3) (Novagen, Madison, WI) was transformed with pET-11a/*tthb178* (RIKEN BioResource Center, Tsukuba, Japan), and the transformed cells were cultured in L-broth containing 50 μg/mL ampicillin. When

the cell density reached 1×10^8 cells/ml, isopropyl-1-thio-β-D-galactopyranoside was added to the culture to induce *tthb178* gene expression. The cells were further cultured for 6 h and harvested by centrifugation at 9,000 × *g* under 4°C and stored at −20°C until use.

All the steps for TTHB178 purification except the heat treatment were performed at 4°C. The frozen cells were suspended in 50 mM Tris-HCl and 5 mM EDTA (pH 8.0; buffer A), and disrupted by sonication. The cell lysate was treated at 60°C for 10 min, and the supernatant was recovered after centrifugation at 34,000 × *g* for 1 h. $(NH_4)_2SO_4$ was gradually added to the solution to a final concentration of 1.5 M. The solution was applied to a Toyopearl Ether-650M column (bed volume of 20 mL; Tosoh Corp., Tokyo, Japan) equilibrated with 50 mM Tris-HCl, 1.5 M $(NH_4)_2SO_4$, 100 mM KCl, and 5 mM EDTA (pH 8.0; buffer B). The column was washed with buffer B and then eluted with a linear gradient of 1.5 to 0-M $(NH_4)_2SO_4$ in 50 mM Tris-HCl, 100 mM KCl, and 5 mM EDTA (pH 8.0). SDS-PAGE revealed that the target protein was eluted at 0.7 to 0.6 M $(NH_4)_2SO_4$. The fractions containing TTHB178 were dialysed twice against 5 L of buffer A. The dialyzed solution was diluted to 50 mL with buffer A and loaded onto a Toyopearl SuperQ-650M column (bed volume of 20 mL; Tosoh Corp.) equilibrated with buffer A. The column was substantially washed with buffer A, and the proteins were eluted with a linear gradient of 0 to 1 M KCl in buffer A. The target protein was eluted at 100 to 150 mM KCl. The fractions containing the target protein were dialyzed twice against 5 L of 10 mM K_3PO_4 and 5 mM EDTA (pH 7.4; buffer C). The dialyzed solution was diluted to 50 mL with buffer C and loaded onto a hydroxyapatite column, BioScale CHT5-I (bed volume of 20 mL; Bio-Rad Laboratories Inc., Hercules, CA) equilibrated with buffer C. The flow-through fraction was collected. The proteins were eluted with a linear gradient of 10 to 500 mM K_3PO_4 (pH 7.4) and 5 mM EDTA. Purified TTHB178 was concentrated to 10 mg/mL in 20 mM Tris-HCl, 100 mM KCl, and 60% glycerol (pH 8.0), and stored at −20°C. Peptide mass fingerprinting (Salzano *et al.*, 2008) confirmed that the purified protein was TTHB178.

***Size-exclusion chromatography*—**Size-exclusion chromatography was performed 25°C by using a Superdex 75 HR column (1 cm × 30 cm; GE Healthcare Biosciences) in an ÄKTA system (GE Healthcare Biosciences). The 100 μL of purified TTHB178 (0.75 mg/mL) was loaded onto the column and eluted at a flow rate of 0.5 mL/min with 20 mM Tris-HCl and 100-mM KCl (pH 8.0). The elution profile was monitored by recording the absorbance at 280 nm. The column was calibrated by using apoferritin (443 kDa), β-amylase (200 kDa), alcohol dehydrogenase (150 kDa), thyroglobulin (66.9 kDa), and cytochrome c (12.4 kDa).

***Dynamic light scattering experiment*—**The 2.0 mg/mL of *tth* ExoI was prepared in 20 mM Tris-HCl and 100 mM KCl, pH 7.5, and was passed through 0.02 μm Whatman Aodisc 13 Supported Membrane Filter. The 12 μL of the protein solution was loaded into a quartz cuvette, and then analyzed by dynamic light scattering instrument, DynaPro MSXTC/12/F with a gallium-arsentie diode laser, DynaPro-99-E-50 (Protein Solutions Inc., Sharlottesville, USA) at 20°C. The data was analyzed using the Dynamics version 6.3.18 (Proteins Solutions Inc.). The sample was analyzed a minimum of 10 times and the resulting data was analyzed to estimate apparent molecular weight assuming a globular protein in an aqueous solution. The hydrodynamic radius (R_h) value was calculated with the Stokes-Einstein equation (equation I-1) using the obtained translational diffudion coefficient (D_T):

$$R_h = k_B T / 6\pi\eta D_T \qquad \text{(Eq. I-1)}$$

where k_B is the Boltzman constant, T the absolute temperature, η the solvent viscosity, and R_h the hydrodynamic radius. Molecular mass of the protein in the solution was estimated from R_h using an empirical curve of known proteins (equation I-2).

$$\text{Molecular mass} = 3366.5\ R_h^{2.3398} \qquad \text{(I-Eq. 2)}$$

Mass analysis by using Fourier transform ion cyclotron mass spectrometer—The products of the exonuclease reaction were analysed by Fourier transform ion cyclotron mass spectrometer (FT-ICR MS) with electrospray ionization. In brief, 21 mer ssDNA (21f) (Table I-2) was reacted with 3 μM TTHB178 in 20 mM Hepes-KOH, 100 mM KCl, and 5 mM $MgCl_2$, pH 7.5, at 37°C for 0, 1, 5, and 10 min, respectively. Each reactant was mixed with ion-pairing agent, butyl dimethyl ammonium carbonate, pH 8.0 to a final 25 mM concentration. The mixture was loaded onto a self-made reverse-phase column using C18 Empore disk (3M Co., St. Paul, MN), after equilibration with 25 mM butyl dimethyl ammonium carbonate. The column was further washed with 5% acetonitrile containing 25 mM butyl dimethyl ammonium carbonate, and then the products were eluted with 50% acetonitrile. A basic additive, piperidine (pH 9) and imidazole (pH 8) for mass analysis of nucleic acids under negative mode were added to each eluent to a final concentration of 25 mM, respectively. The resulting solution was subjected to an APEX IV, FT-ICR MS shielded with 9.4 T magnet (Bruker Daltonics Inc., MA, USA) by electrospray ionization under 2 μL/min flow rate as describe in a previously report (Fukui *et al*., 2007).

Table I-2. Sequenses of oligonucleotides used in this study. Abbreviations used are: *mG*, O^6-methylguanine; *mT*, O^4-methylthymine; *oxoG*, 8-oxoguanine; *rAP*, reduced abasic site; *AP*, abasic site; *Ura*, uracil; *Hyp*, hypoxanthine; and *Xan*, xanthine.

Name	Length	Sequence
10f	10 mer	GGCCAGGTGG
21f	21 mer	ATGACAACTAAAGCAACACCC
21r	21 mer	GGGTGTTGCTTTAGTTGTCAT
21rna	21 mer	ATGACAACTAAAGCAACACCC
21sr	21 mer	CCTAGCGGCTGCCACCTGGCC
28sr	28 mer	GGGCACCATGCGGGCGGCCAAAATGCCC
40sr	40 mer	CGGGCGGCCTCCCCTCCACCCTAGC- -GGCTGCCACCTGGCC
50sf	50 mer	GGCCAGGTGGCAGCCGCTAGGGTG- -GAGGGGAGGCCGCCCGCATGGTGCCC
O6m	18 mer	GCCCGGCCA*mG*CTGCAGTT
O4m	18 mer	GCCCGGCCA*mT*CTGCAGTT
8OG	21 mer	TACTGTTGA*oxoG*TTGGTTGTGGG
rAP21	21 mer	TACTGTTGA*rAP*TTGGTTGTGGG
AP21	21 mer	TACTGTTGA*APG*TTGGTTGTGGG
Ura21	21 mer	TACTGTTGA*Ura*TTGGTTGTGGG
Hyp30	30 mer	GCTCGTAGAGCGGTC*Hyp*TAGTCAAGATACCG
Xan30	30 mer	GCTCGTAGAGCGGTC*Xan*TAGTCAAGATACCG

Exonuclease assays—Single-stranded oligonucleotides were synthesised (BEX Co., Tokyo, Japan), and their 5′-termini were radiolabelled with [γ-^{32}P]ATP using T4 polynucleotide kinase (Takara Bio, Shiga, Japan) at 37°C for 1 h. The substrates with 3′-overhanging, Y, and gapped flap structures were yielded by hybridising 50sf with 40sr, 50sf with 28sr, and 50sf with 28sr and 21sr (Table I-2), respectively. In the case of 3′-end labelling, an oligonucleotide (Table I-2; 21r; 5′-GGGTGTTGCTTTAGTTGTCAT-3′) was radiolabelled with [α-^{32}P]cordycepin-5′-triphosphate (PerkinElmer Life and Analytical Sciences, Boston, MA) by using terminal deoxynucleotidyl transferase (Promega Co., Fitchburg, WI). The radiolabelled substrates were incubated with 3 μM TTHB178 in 20 mM Hepes-KOH, 100 mM KCl, and 5 mM $MgCl_2$ (pH 7.5). The total reaction volume was 10 μL. The reaction temperatures and times were as indicated in the figure legends. The reactions were stopped by the addition of an equal volume of phenol, $CHCl_3$, and isoamyl alcohol (25:24:1) as well as 1 μL of 100 mM EDTA. The mixture was centrifuged at 15,000 × *g* at 4°C for 10 min, and the aqueous phase was mixed with an equal volume of sample buffer (5 mM EDTA, 80% deionised formamide, 10-mM NaOH, 0.1% bromophenol blue, and 0.1% xylene cyanol). The samples were analysed by electrophoresis through denaturing 25% polyacrylamide gels with 1 × TBE buffer (89 mM Tris-borate and 2 mM EDTA), and the gels were dried and placed in contact with an imaging plate. The substrates and products were detected and analysed with a BAS2500 image analyser (Fuji Photo Film, Tokyo, Japan). In the kinetic analysis, 10-nM radiolabelled substrates were mixed with 0.1, 1, 5, 10, 50, 100, 300, 500, or 1000 μM of non-labelled substrates and then reacted with 100 nM TTHB178 for 30 or 5 min at 37 or 60°C, respectively. The values of the initial rates were calculated based on the amount of undegraded substrates according to a previously described procedure (Perrino *et al*., 2008; Sharma and Rao, 2009; Yamagata *et al*., 2001). The k_{cat} and K_M values were determined by fitting the data to the Michaelis-Menten equation using Igor 4.03 (WaveMetrics, Lake Oswego, OR).

RESULTS

Sequence comparison between TTHB178 and DnaQ superfamily exonucleases

The *tthb178* gene encoded a protein that comprised 296 amino acid residues and whose *N*-terminal region showed significant sequence similarity to DnaQ superfamily exonucleases such as *E. coli* ExoI and ExoX (Lehman and Nussbaum, 1964; Viswanathan and Lovett, 1999), and the proofreading domains of the DNA polymerases. These regions contained exonuclease motifs I to III, which included conserved Asp, Glu, and His residues (Fig. I-1A). The DnaQ superfamily exonucleases had a wide variety of protein lengths and showed sequence diversities except for the exonuclease motifs (Fig. I-1B). Among them, the length of TTHB178 was comparable to that of *E. coli* ExoX; however, their *C*-terminal regions showed no detectable sequence similarity. Furthermore, multiple sequence alignment program, ClustalW2 (Larkin *et al.*, 2007; http://www.ebi.ac.uk/Tools/msa/clustalw2/), revealed that sequence similarity between TTHB178 and ExoI was slightly higher than it between TTBH178 and ExoX.

Expression of tthb178 *in T. thermophilus* HB8 cells

Unlike *recJ*, *tthb178* has been annotated as a hypothetical protein, and there was no evidence for the *in vivo* expression of *tthb178* before the recent report on the CRP-dependent expression of *tthb178* in cells (Shinkai *et al.*, 2007). I first performed time course-transcription analysis of the *tthb178* gene in *T. thermophilus* HB8 cells by using reverse transcription-PCR. Transcription of *tthb178* was detected from the mid-log phase to the late stationary phase (Fig. I-5). The gene was more actively transcribed in the late stationary phase (No. 6 in the figure) than in the mid-log phase (No. 3) or stationary phase (Nos. 4 and 5). The result strongly suggested that *tthb178* is not a pseudo-gene and is required for a cellular function in *T. thermophilus* HB8.

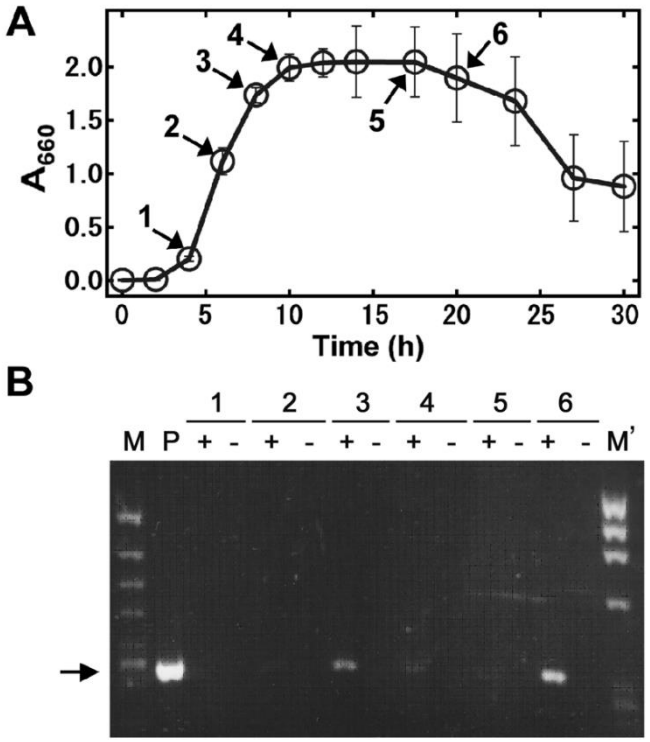

Figure I-5. Transcription of *tthb178* in *T. thermophilus* HB8 cells. (A) The growth curve of WT *T. thermophilus* HB8. The absorbance at 660 nm was monitored and plotted against the cultivation time. The data represent the average of three independent experiments, and each bar indicates the standard deviation. (B) The result of the RT-PCR analysis. Electrophoresis was carried out on 2% agarose gel. The numbers above the lanes correspond to those in (A). The plus (+) and minus (−) signs mean the addition and non-addition of reverse transcriptase during the RT-PCR, respectively. M, M′, and P mean the ϕ174/*Hinc*II DNA size marker, λ/*Hind*III DNA size marker, and the *tthb178* fragment amplified by PCR using genomic DNA as a template, respectively. The arrow indicates the amplified fragments of *tthb178*.

Phenotypes of tthb178 and recJ disruptants

To investigate the cellular functions of ssExos *in vivo*, I generated a *tthb178* disruptant (Δ*tthb178*), *recJ* disruptant (Δ*recJ*), and *tthb178-recJ* double disruptant (Δ*tthb178*-Δ*recJ*). All the disruptants grew in rich medium, indicating that these two genes were not essential under the condition examined. However, all of them exhibited a relatively long lag time prior to the exponential growth compared with the WT (Fig. I-6A). These disruptants also showed lower maximum cell density than the WT during the stationary phase (Fig. I-6A). Furthermore, the disruptants aggregated in the log phase whereas the WT did not (data not shown). Elongated cells of the disruptants were observed in the late log, stationary, and death phases, unlike in the case of the WT (data not shown). These results suggested that *T. thermophilus* HB8 requires TTHB178 as well as RecJ for optimal growth under conditions without external DNA-damaging stress.

To examine the possible involvement of TTHB178 and RecJ in DNA repair processes in *T. thermophilus* HB8, I first measured the spontaneous mutation rate of the disruptants to a streptomycin-resistant strain (Melancon *et al*., 1988). The spontaneous mutation rates of Δ*tthb178* and Δ*recJ* were approximately 4-fold and 3-fold higher than that of the WT, respectively (Fig. I-6B). Interestingly, Δ*tthb178*-Δ*recJ* showed about 10-fold higher mutation rate than the single-disruption cells (Fig. I-6B). The streptomycin-resistant strains obtained here must have mutations within the rRNA gene (Melancon *et al*., 1988; Moazed and Noller, 1987), and such spontaneous mutagenesis can be accelerated by defects in several DNA repair systems such as MMR. Therefore, the observed increase in mutation frequency suggested that both TTHB178 and RecJ are involved in DNA repair.

I then examined the growth phenotypes of these disruptants under DNA-damaging conditions. The disruption of *tthb178* did not affect the sensitivity to UV-C irradiation at 254 nm (Fig. I-6C). On the other hand, Δ*recJ* exhibited 3-fold higher sensitivity to UV-C than the WT and Δ*tthb178* (Fig. I-6C). The major damages caused by UV-C irradiation are

cyclobutane pyrimidine dimers, pyrimidine-pyrimidone (6-4) photoproducts, and DSBs (Bonura and Smith, 1975; Bourre *et al*., 1989; Bradley, 1981; Franklin and Haseltine, 1986; Weinfeld *et al*., 1989). The observed increase in the sensitivity indicated that RecJ is intimately involved in the repair of these lesions whereas TTHB178 is not. Nevertheless, it should be noted that the survival ratio of UV-C-irradiated Δ*tthb178*-Δ*recJ* was lower than that of Δ*recJ* (Fig. I-6C). This result raised the possibility that TTHB178 also participates in the repair pathway for those lesions in the cell strain lacking the *recJ* gene product.

In contrast, the disruption of *tthb178* caused drastic increase in the sensitivity to H_2O_2, whereas the disruption of *recJ* did not (Fig. I-6D). In addition, Δ*tthb178*-Δ*recJ* exhibited a similar survival ratio to Δ*tthb178*. Reactive oxygen species generated from H_2O_2 are responsible for the oxidation and deamination of bases, which result in transversion and transition mutations, respectively (Akagawa and Suyama, 2002; Weiss, 2006). Therefore, the increased sensitivity of Δ*tthb178* to H_2O_2 suggested that TTHB178 is involved in the repair pathway for such damaged bases. Thus, our *in vivo* experiments indicated that the *tthb178* and *recJ* genes are required for several DNA repair pathways in *T*. *thermophilus* HB8.

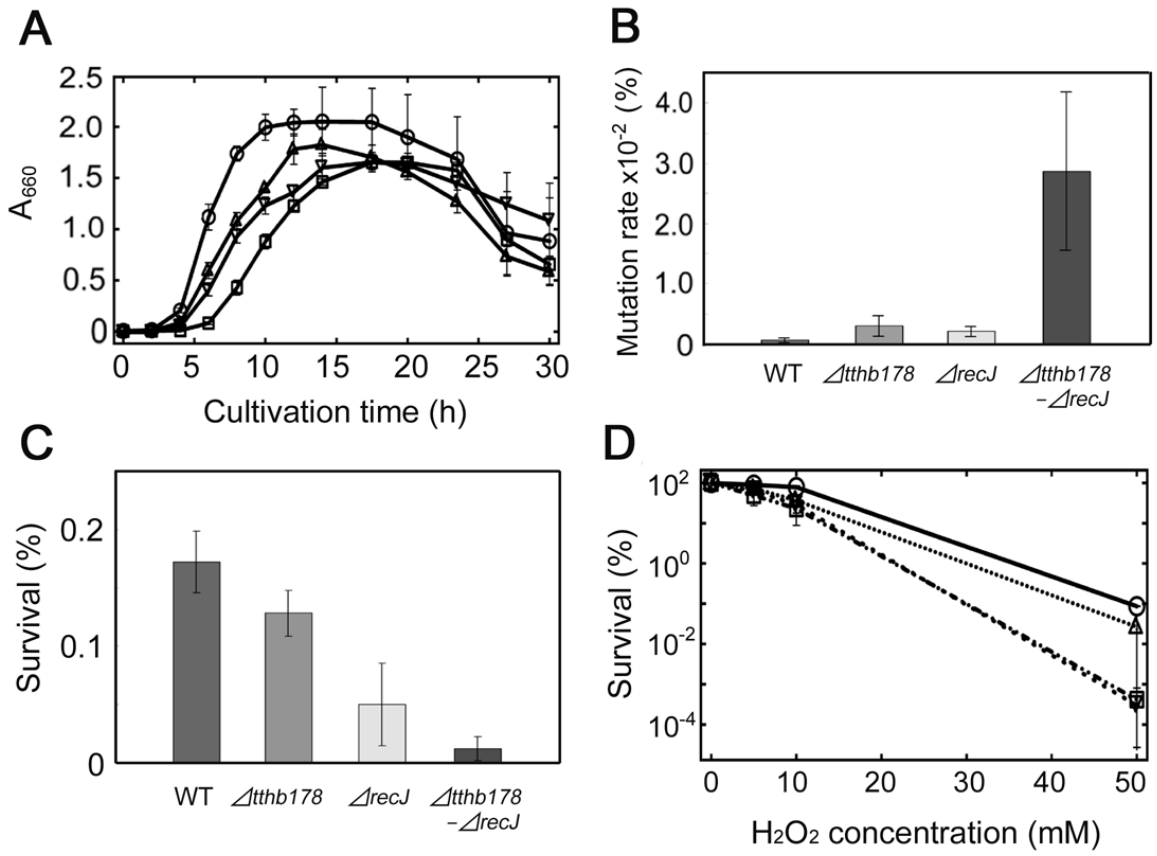

Figure I-6. Effects of the disruptions of the *tthb178* and *recJ* genes on the growth of *T. thermophilus* HB8. (A) Growth curves of the WT (*circles*), Δ*recJ* (*triangles*), Δ*tthb178* (*inverted triangles*), and the double disruptant (*squares*). Growth was monitored by measuring the absorbance at 660 nm. (B) Spontaneous mutation rates of each strain to the streptomycin-resistant strain. (C) Sensitivity to 254 nm UV-C irradiation. The survival ratios are shown as a bar graph. (D) Sensitivity to H_2O_2. The survival ratios were plotted against the H_2O_2 concentration. The symbols are the same as in (A). In all panels, the data represent the averages of at least three independent experiments, and each bar indicates the standard deviation.

Exonuclease activity of TTHB178

In order to characterize TTHB178 biochemically, I overexpressed TTHB178 in *E. coli* and purified it to homogeneity (Fig. I-7A). Size-exclusion chromatography was performed to examine the self-association ability of TTHB178. The result showed that TTHB178 was eluted with a single peak corresponding to an apparent molecular mass of 62 kDa (Fig. I-7B). Because the molecular mass of TTHB178 was calculated to be 33 kDa according to its amino acid sequence, this result implied that TTHB178 exists in a dimeric state in solution. The observed shoulder of the main peak might represent the slight tendency of TTHB178 to form a larger complex in the solution. Dynamic light scattering experiment was also performed to evaluate the dimerization ability of TTHB178. The measurement gave an R_h value of 3.6 nm, suggesting that the molecular mass of the particle in the TTHB178 solution is about 66 kDa (Fig. I-7C). Thus, the result of dynamic light scattering experiment also supports the dimerization of TTHB178.

To test the prediction that TTHB178 has 3′→5′ exonuclease activity, the activity was examined by using ssDNA as a substrate. The ssDNA reacted with TTHB178 was subjected to FT-ICR MS analysis. FT-ICR MS is a powerful tool for the characterisation of nuclease activity because it achieves precise and simultaneous identification of the length, nucleotide content, and nature of the 5′-termini and 3′-termini of all products (Fig. I-8A). As the reaction time increased, the shorter products became obvious, and all of them were the b-series ions which lack the 3′-terminal region of the substrate DNA (Fig. I-8B and C). This result strongly indicated that TTHB178 possesses exonuclease activity that degrades ssDNA from the 3′-end to the 5′-end and that TTHB178 hydrolyses a phosphodiester bond at the 3′-side of the phosphate.

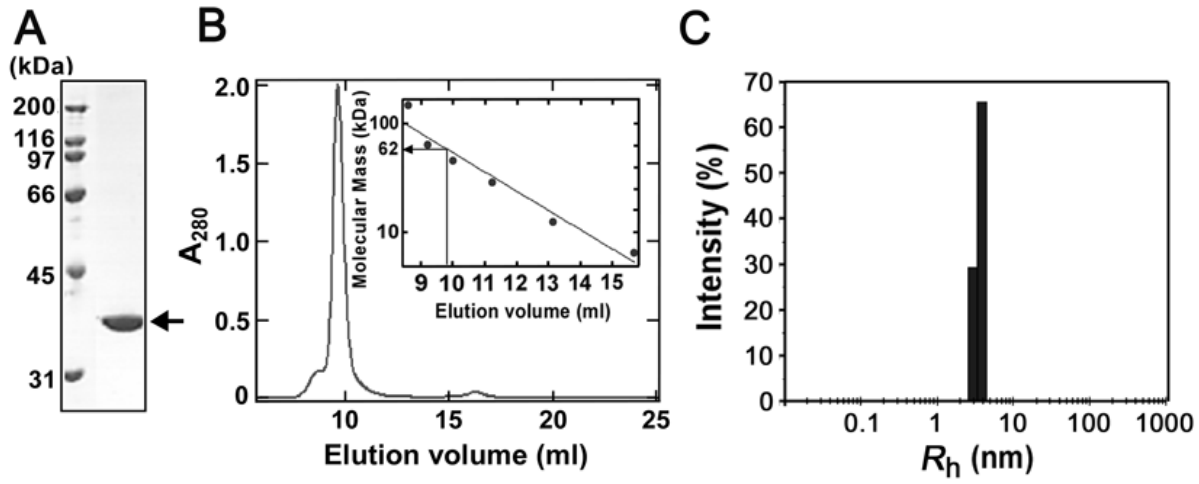

Figure I-7. Preparation of recombinant TTHB178. (A) Recombinant TTHB178 was purified as described in the Materials and Methods section and then subjected to SDS-PAGE. The 3 μg of protein was loaded on the gel. The calculated molecular mass of TTHB178 is 33 kDa. The arrow indicates the band of TTHB178. (B) Size-exclusion chromatography. TTHB178 (0.75 mg/ml) was loaded onto a Superdex 75 HR column. The apparent molecular mass of the main peak was estimated to be approximately 62 kDa, from the calibration curve shown in the inset. Apoferritin (443 kDa), β-amylase (200 kDa), alcohol dehydrogenase (150 kDa), thyroglobulin (66.9 kDa), and cytochrome c (12.4 kDa) were used as molecular size markers. (C) Dynamic light scattering measurement. R_h was calculated on the basis of the observed D_T as described in Materials and Methods.

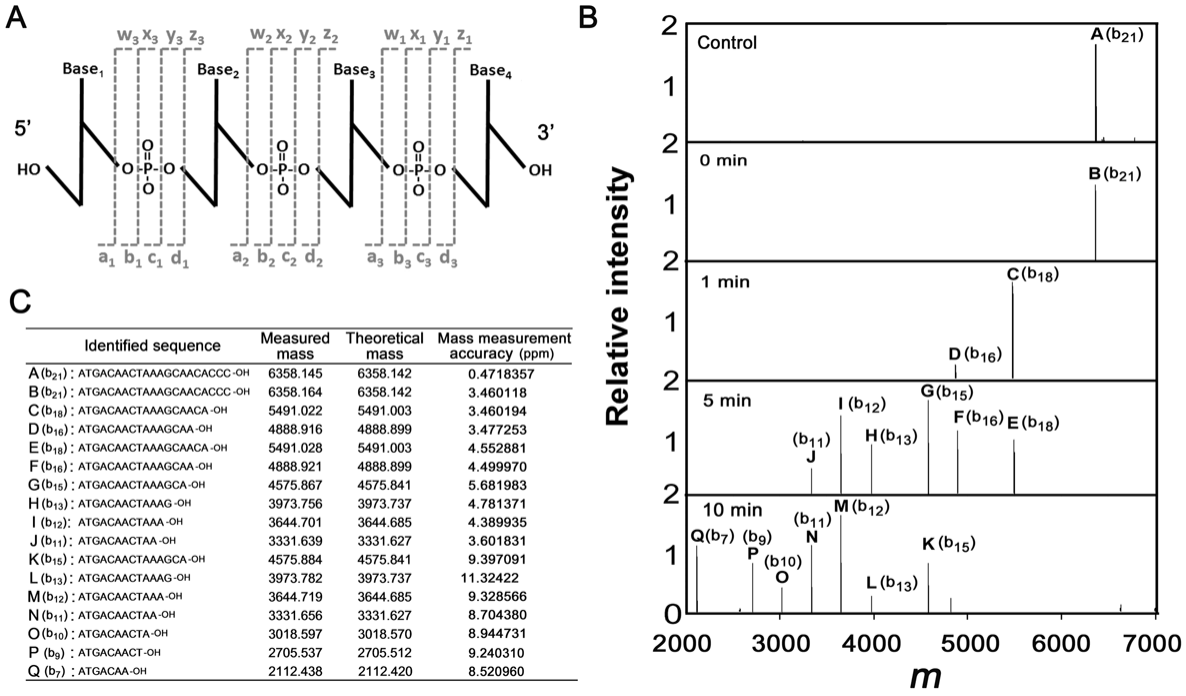

Identified sequence	Measured mass	Theoretical mass	Mass measurement accuracy (ppm)
A (b_{21}) : ATGACAACTAAAGCAACACCC-OH	6358.145	6358.142	0.4718357
B (b_{21}) : ATGACAACTAAAGCAACACCC-OH	6358.164	6358.142	3.460118
C (b_{18}) : ATGACAACTAAAGCAACA-OH	5491.022	5491.003	3.460194
D (b_{16}) : ATGACAACTAAAGCAA-OH	4888.916	4888.899	3.477253
E (b_{18}) : ATGACAACTAAAGCAACA-OH	5491.028	5491.003	4.552881
F (b_{16}) : ATGACAACTAAAGCAA-OH	4888.921	4888.899	4.499970
G (b_{15}) : ATGACAACTAAAGCA-OH	4575.867	4575.841	5.681983
H (b_{13}) : ATGACAACTAAAG-OH	3973.756	3973.737	4.781371
I (b_{12}): ATGACAACTAAA-OH	3644.701	3644.685	4.389935
J (b_{11}): ATGACAACTAA-OH	3331.639	3331.627	3.601831
K (b_{15}) : ATGACAACTAAAGCA-OH	4575.884	4575.841	9.397091
L (b_{13}) : ATGACAACTAAAG-OH	3973.782	3973.737	11.32422
M (b_{12}) : ATGACAACTAAA-OH	3644.719	3644.685	9.328566
N (b_{11}) : ATGACAACTAA-OH	3331.656	3331.627	8.704380
O (b_{10}) : ATGACAACTA-OH	3018.597	3018.570	8.944731
P (b_9) : ATGACAACT-OH	2705.537	2705.512	9.240310
Q (b_7) : ATGACAA-OH	2112.438	2112.420	8.520960

Figure I-8. Analysis of the exonuclease activity by using FT-ICR MS. (A) The nomenclature scheme used for oligonucletide ions (McLuckey, 1992). The four possible cleavages are indicated by the lower case letters a, b, c, and d for ions containing the 5′-OH group and w, x, y, and z for ions containing the 3′-OH group. The numerical subscripts indicate the number of bases from the respective termini. FT-ICR MS can achieve the simultaneous identification of these ions. (B) The deconvoluted mass spectra of the product ssDNAs of TTHB178. The 21 mer ssDNA (21f) was reacted with 3 μM TTHB178 at 37°C. The product ssDNAs were purified as described in the Materials and Methods, and then analysed by using FT-ICR MS. The reaction time is shown in the panel. (C) The measured and theoretical masses of each peak (named A to Q) are listed, and the corresponding sequences are also shown as the ′identified sequence′. The measured mass coincided with the theoretical mass about 10-ppm mass measurement accuracy.

The 3′→5′ exonuclease activity of TTHB178 was also confirmed by electrophoretic analyses using 5′-end-labelled ssDNAs as substrates. As shown in Fig. I-9A, TTHB178-digested products exhibited a ladder pattern of DNA fragments on the gel, which suggested that TTHB178 degrades ssDNA from the 3′-end to the 5′-end. I confirmed that the elution profile of the observed exonuclease activity from Superdex 75 HR column was exactly matched with that of TTHB178 (Fig. I-10), indicating that the observed activity is derived from TTHB178.

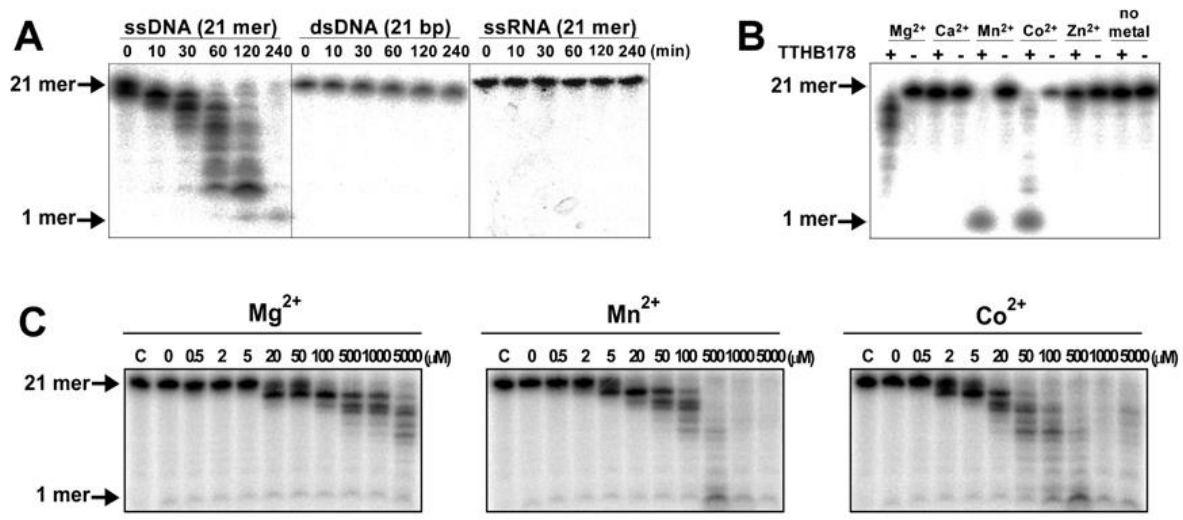

Figure I-9. Analyses of TTHB178 exonuclease activity by using 5′ radiolabelled substrates. (A) Substrate specificity of TTHB178 exonuclease activity. TTHB178 (3 μM) was incubated with 10-nM 5′-end-labelled 21-mer ssDNA (21f), 21 bp dsDNA (21f + 21r), or 21 mer ssRNA (21rna) in the presence of 5-mM Mg^{2+} at 37°C. The reaction time is shown at the top of the panels. (B) Dependence of the exonuclease activity on divalent metal ions. The 10-nM 5′-end-labelled ssDNA (21f) was incubated with 3-□M TTHB178 at 37°C for 2 h. The reaction mixture contained 5 mM of the respective divalent metal ions. (C) Dependence of the exonuclease activity on the concentrations of Mg^{2+}, Mn^{2+}, and Co^{2+}. The 10 nM 5′-end-labelled ssDNA (21f) was incubated with 3-μM TTHB178 at 37°C for 2 h in the presence of various concentrations of divalent cations. The concentrations of the divalent metal ions are indicated at the top of the panels.

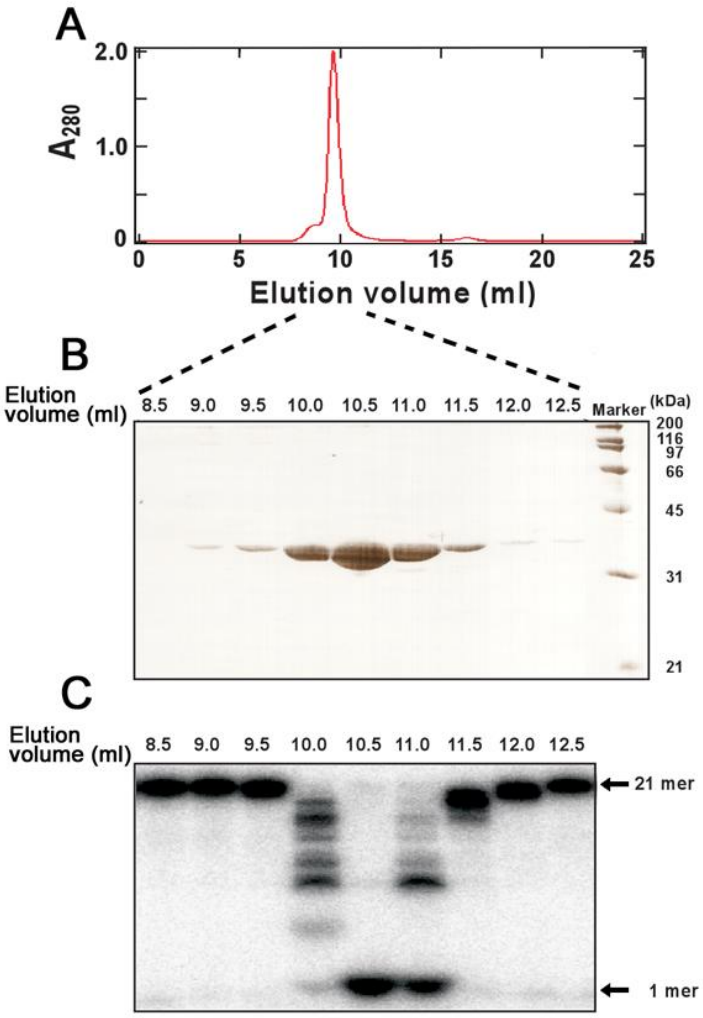

Figure I-10. The elution profile of the exonuclease activity. (A) Elution profile of TTHB178 from Superdex 75 HR column was monitored by the absorbance at 280 nm. (B) The eluted fractions were subjected to SDS-PAGE. The peptide mass fingerprinting mass spectrometry revealed that the detected bands were TTHB178. (C) Exonuclease activity of the each fraction. The 2 μL of each fraction was reacted with 21 mer ssDNA at 37°C for 60 min.

The results also showed that TTHB178 specifically cleaves an ssDNA (Fig. I-9A). No activity against ssRNA and dsDNA was observed in spite of the prolonged reaction time (up to 4 h). It was also shown that the activity required divalent cations such as Mg^{2+}, Mn^{2+}, or Co^{2+} (Fig. I-9B and C). Our previous study showed that the intracellular concentrations of Mn (0.16 mM) and Co ions (not detected) are significantly lower than that of Mg ions (35 mM) in *T. thermophilus* HB8 cells (Kondo *et al*., 2008). The concentrations of Mn^{2+} and Co^{2+} were thought to be insufficient for the activation of TTHB178 exonuclease activity *in vivo*. Therefore, the assays for exonuclease activity were carried out in the presence of Mg^{2+}.

The steady-state kinetic parameters of the TTHB178 exonuclease activity were determined (Table I-3) based on the reduction rate of undegraded substrates (Perrino *et al*., 2008; Sharma and Rao, 2009; Yamagata *et al*., 2001). The reaction temperature did not affect the K_M values of the respective substrates, but the k_{cat} values at 60°C were higher than those at 37°C. As the substrates became shorter, the K_M values became higher, showing the preferential binding of TTHB178 to longer ssDNAs. On the other hand, the k_{cat} values of longer ssDNAs were lower than those of the shorter ones. Therefore, the k_{cat}/K_M values, the index of the efficiency of an enzyme, were not affected by the lengths of the substrates. The k_{cat}/K_M values were fourfold to tenfold higher at 60°C than at 37°C, which indicated that the observed digestion of ssDNA was certainly performed by a protein from a thermophile (i.e., *T. thermophilus* HB8) and not by a contaminated protein from a host cell.

Table I-3. Steady-state kinetic parameters of the TTHB178 exonuclease activity for ssDNAs.

Length (mer)	Temperature (°C)	k_{cat} (s^{-1})	K_M (μM)	k_{cat}/K_M ($M^{-1}s^{-1}$)
10	37	0.71 ± 0.23	280 ± 83	$2.6 \times 10^3 \pm 0.19$
	60	7.5 ± 0.023	480 ± 16	$16 \times 10^3 \pm 0.49$
21	37	0.40 ± 0.15	350 ± 31	$1.1 \times 10^3 \pm 0.49$
	60	5.3 ± 2.10	440 ± 120	$12 \times 10^3 \pm 3.70$
28	37	0.23 ± 0.12	260 ± 105	$0.83 \times 10^3 \pm 0.20$
	60	1.9 ± 0.48	290 ± 58	$7.0 \times 10^3 \pm 2.40$
40	37	0.17 ± 0.016	240 ± 45	$0.72 \times 10^3 \pm 0.066$
	60	2.3 ± 0.10	320 ± 47	$7.5 \times 10^3 \pm 1.40$
50	37	0.19 ± 0.046	130 ± 52	$1.7 \times 10^3 \pm 0.58$
	60	1.0 ± 0.41	160 ± 39	$6.4 \times 10^3 \pm 0.87$

DNA structure and lesion specificity of the exonuclease activity

I further tested the specificity of the TTHB178 exonuclease activity to the structure and lesion of substrate DNA. The 3′-overhanging, Y, and gapped flap structures were used as substrates. These are possible intermediate DNA structures generated during the processes of several DNA repair pathways (Friedberg, 1995). The results indicated that TTHB178 can digest the ssDNA regions of the three substrates (Fig. I-11A-C). The Y and gapped flap structures mimicked the intermediate structures, which were generated by the unwinding of nicked dsDNAs by a DNA helicase. Furthermore, TTHB178 hardly degraded the ssDNA whose 3′-terminus was radiolabelled with [α-^{32}P]cordycepin-5′-monosphate (Fig. I-11D). The cordycepin-labelled ssDNA had 3′ -H instead of 3′-OH at its 3′-terminus. The 3′-OH group of the substrate would be essential for the TTHB178 activity.

I also examined the exonuclease activity for ssDNA substrates containing various kinds of damaged bases. As a result, TTHB178 degraded ssDNAs containing hypoxanthine, xanthine, uracil, O^4-methylguanine, and O^6-methylthymine (Fig. I-12A-D). At 37°C, the degradation stopped at the positions of hypoxanthine and xanthine in the respective substrates, but the degradation proceeded beyond these non-canonical bases at 60°C. In contrast, only slight activity was observed even at 60°C when the substrate contained 8-oxoguanine or an abasic site (Fig. I-12E and F). Base on these results, it is considered that TTHB178 can be involved in the excision step of the DNA repair pathways for deaminated and methylated bases.

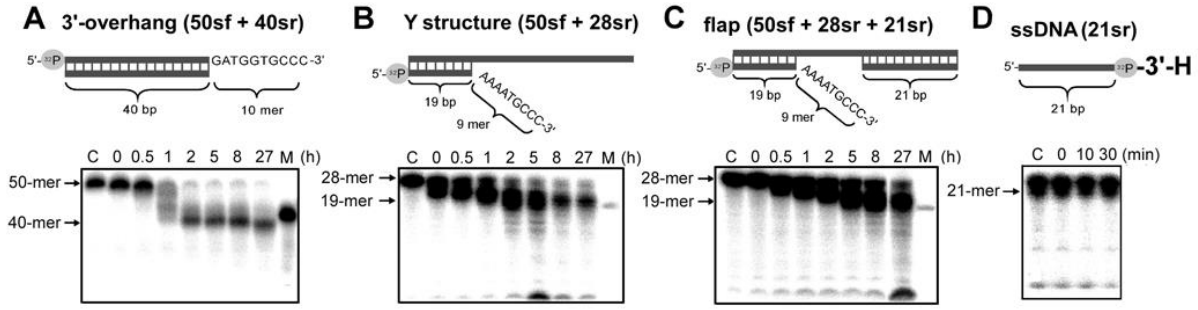

Figure I-11. Exonuclease activity of TTHB178 against various DNA structures. (A–C) The 3′-overhanging (50sf + 40sr) (A), Y structure (50sf + 20sr) (B), and gapped flap structure (50sf + 21sr + 28sr) (C) DNAs were reacted with 3 μM TTHB178 for various reaction periods. The reaction time is indicated at the top of the panels. Assays for the Y structure and gapped flap structure were carried out at 20°C to stabilise the short dsDNA region of the substrates. As TTHB178 showed relatively weak activity at 20°C compared with that at 37°C or 60°C, the assays were performed for a prolonged reaction time. The assay for 3′-overhanging DNA was carried out at 37°C. ′C′ means the substrate incubated without TTHB178 for 27 h. (D) Activity for an ssDNA with a 3′-H terminus. The substrate 21 mer ssDNA (21r) was 3′-end-labelled with [α-^{32}P] cordycepin-5′-triphosphate and reacted with 3 μM TTHB178 at 37°C. The reaction time is indicated at the top of the panel. ′C′ means the substrate incubated without TTHB178 for 30 min. In all the panels, the digested products were analysed by electrophoresis through denaturing 8% and 25% polyacrylamide gels. ′*M*′ means the 40- (in A) and 19-mer (in B and C) of marker DNAs.

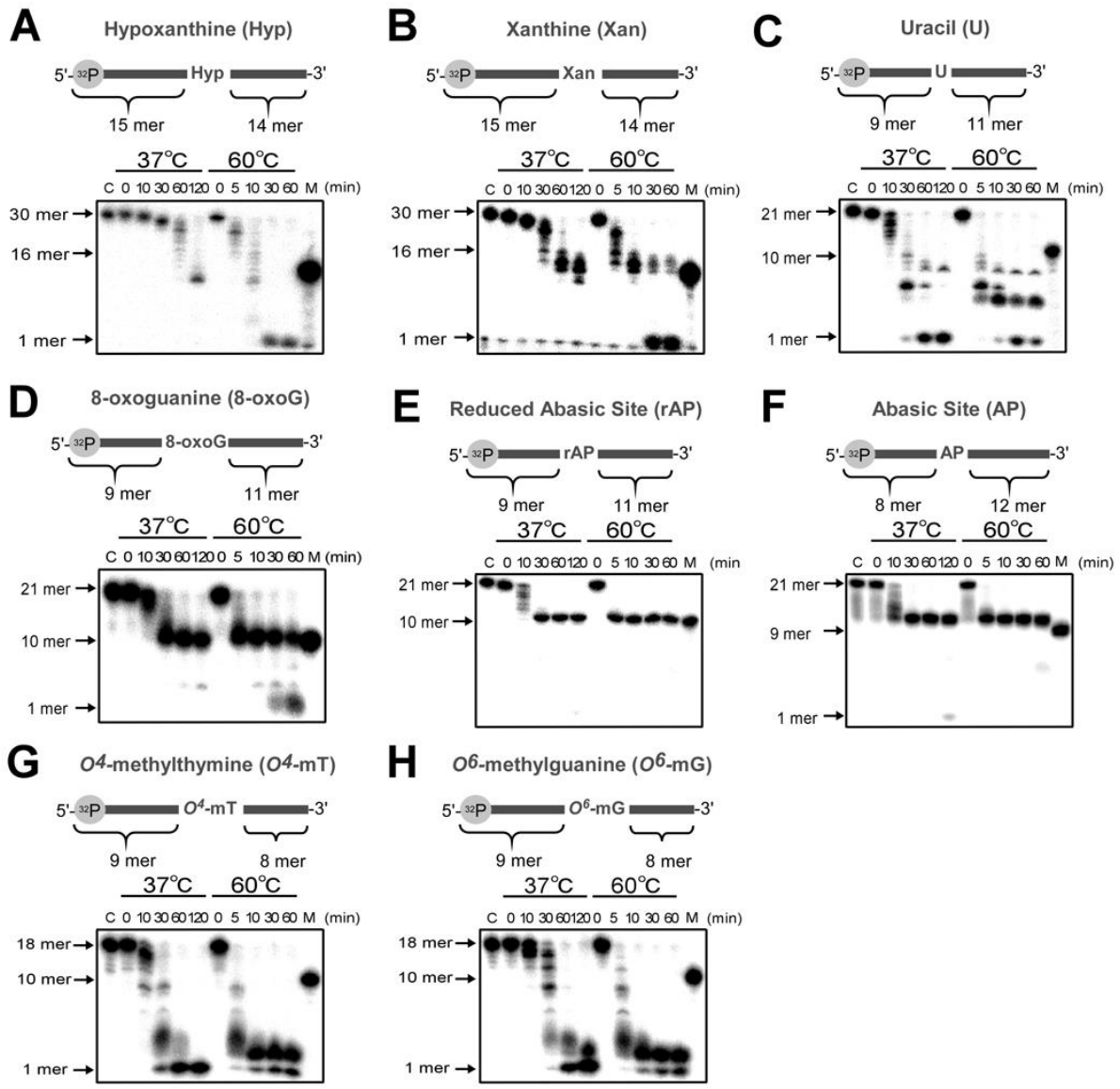

Figure I-12. Excision assay for ssDNAs containing various kinds of damaged bases. The 5′-end-labelled ssDNA containing a damaged base was reacted with 3 μM TTHB178 at 37°C or 60°C. The respective substrates contained hypoxanthine (A), xanthine (B), uracil (C), 8-oxoguanine (D), a reduced abasic site (E), an abasic site (F), O^4-methylthymine (G), and O^6-methylguanine (H). In all the panels, *′C′* means the substrate incubated at 60°C for 60 min without TTHB178. *′M′* indicates the 16- (in *A* and *B*), 10- (in *C*, *D*, *E*, *G*, and *H*), and 9-mer (in *F*) marker DNAs. The reaction time is shown at the top of the panels. ′M′ means

DISCUSSION

My study showed that TTHB178 possessed 3'→5' exonuclease activity. This result supports my prediction that TTHB178 is a member of DnaQ superfamily exonuclease. In terms of size, TTHB178 (296 a.a.) was more similar to ExoI (475 a.a.) and ExoX (220 a.a.) of *E. coli* than to proofreading domains of DNA polymerases belonging to DnaQ superfamily (Fig. I-1). However, the sequence similarity between TTHB178 and ExoI or ExoX (22% and 21%, respectively) was not enough to conclude that TTHB178 is a homolog of ExoI or ExoX. Detailed enzymatic analysis showed that TTHB178 had similarity and difference in the enzymatic features compared with ExoI and ExoX. First, TTHB178 exonuclease activity was specific for ssDNA, but not ssRNA (Fig. I-9). Such a strict specificity is similar to *E. coli* ExoI and ExoX (Lehman, 1960; Lehman and Nussbaum, 1964; Viswanathan and Lovett, 1999). Second, the observation that the "intermediate" products were decreased at 60°C suggests that the degradation of ssDNA by TTHB178 is processive, although it was unclear how processive it is. ExoI has high processivity, whereas ExoX was not (Han *et al*., 2006; Viswanathan and Lovett 1999; Thomas and Olivera 1978). Third, the finding that TTHB178 did not degrade AP site (Fig. I-12E and F) indicated that TTHB178 does not possess DNA deoxyribophosphodiesterase activity, which is in contrast to ExoI (Piersen *et al*., 2000; Sandigursky and Franklin, 1992; Sandigursky and Franklin, 1994). Finally, TTHB178 existed as a homodimer (Fig. I-7), and not a monomer like ExoI, ExoX and the other ssExos in DnaQ superfamily (Korada *et al*., 2013; Prasher et al., 1983; Wang *et al*., 2013). The C-terminal region of TTHB178 was hardly homologous to those of other DnaQ superfamily proteins. This raises the possibility that the C-terminal region might be involved in the dimer formation. Hence, TTHB178 is considered to be a novel ssDNA-specific 3'→5' exonuclease. Because TTHB178 is the first characterized 3'→5' exonuclease of *T. thermophilus*, I named TTHB178 as *T. thermophilus* exonuclease I (*Tth*

ExoI).

Tth ExoI preferably bound to the longer ssDNAs (Table I-3). However, the values of k_{cat}/K_M for all substrates examined were similar to each other, because the k_{cat} values for longer ssDNA were smaller than those for shorter ones. The k_{cat}/K_M value of TTHB178 was similar to that of RecJ (Yamagata *et al*., 2001). These results suggest that long and short ssDNAs are used equally efficiently as substrates of *Tth* ExoI. In addition, *Tth* ExoI degraded ssDNA regions in structured DNAs resembling intermediate structures generated during DNA repair pathways (Fig. I-11). This leads to the notion that *Tth* ExoI participates in DNA repair pathways.

The most important result was that the deletion of *tthb178* resulted in a phenotype that is thought to be associated with defects in DNA repair systems. As described in Introduction, sequence similarity search using already-known ssExos as queries strongly suggests that *T. thermophilus* has a single set of 3'→5' and 5'→3' ssExo, which is *Tth* ExoI and RecJ, respectively (Table I-1). Hence, *T. thermophilus* is suitable to verify the relationship between DNA repair pathways and ssDNA degradation polarity by investigating the difference of the phenotype of *ssExo* gene disruptants against DNA damaging agents. Δ*tthb178* as well as Δ*recJ* showed about 3-fold higher spontaneous mutation rate than WT (Fig. I-6B). DNA mismatches generated by misincorporation of nucleotides during DNA replication are responsible for spontaneous mutation (Luria and Delbruck 1943). The observed increases in spontaneous mutation rate support the notion that RecJ and *Tth* ExoI function to prevent fixation errors occurring during DNA replication in *T. thermophilus*. However, the spontaneous mutation rate of Δ*tthb178*-Δ*recJ* double disruptant was 10-fold higher than that of Δ*tthb178* or Δ*recJ* (Fig. I-6B). This can be explained by the following: even if one of the two ssExos is disrupted, the other could partly compensate for the disruption, but if both ssExos are disrupted, MMR would be dysfunctional. Because it has been known that, in *E. coli*, disruption of ssExo genes causes slightly increase of spontaneous

mutation rate, the necessity of ssExos in MMR has been obscure (Burdett et al., 2001; Viswanathan and Lovett 1998). However, in this study, Δ*tthb178*-Δ*recJ* double disruptant showed about 30-fold higher mutation rate than WT (Fig. I-6B). This increase was larger than that arises from deficiency of MMR genes, *mutS* or *mutL*: disruption of *mutS* or *mutL* resulted in a considerable increase in the frequency of spontaneous mutation about 10-fold higher than WT (Fukui *et al*., 2008b). Therefore, I concluded that, in *T. thermophilus*, ssExos were necessary for MMR. Because both *Tth* ExoI and RecJ did not degrade dsDNA, it is thought that these ssExos could not unwind dsDNA, strongly suggesting that a DNA helicase is also required for MMR in *T. thermophilus* (Fig. I-13A).

Unlike spontaneous mutation analysis, Δ*tthb178* showed higher sensitivity to H_2O_2 than WT and Δ*recJ* (Fig. I-6D). In addition, Δ*tthb178*-Δ*recJ* double disruptant showed similar sensitivity to Δ*tthb178*. The oxidative stress by H_2O_2 causes not only base oxidation but also base deamination (Akagawa *et al*., 2002). These results raise the possibility that *Tth* ExoI is involved in repair pathways for removal of the damaged bases but RecJ is not. *In vitro* experiments showed that *Tth* ExoI hardly degraded the ssDNA containing oxidation base (8-oxoguanine) but did ssDNA containing deaminated bases such as uracil, hypoxanthine, and xanthine (Fig. I-12A and B). Therefore, it is likely that the observed sensitivity to H_2O_2 was mainly owing to defects in the repair of deaminated bases in DNA. The repair pathway of deaminated bases has not yet been revealed even in *E. coli*, but endonuclease V (TTHA1347) was reported to participate in the repair of deaminated bases by nicking 3'-side of DNA strand containing a deaminated base~~s~~ (Moe *et al*., 2003; Weiss, 2001; Weiss, 2006). Based on my results and previous studies, I propose a model of deaminated bases (Fig. I-13B). In this model, *Tth* ExoI functions cooperatively with endonuclease V by removing the damaged strand. The reason why no sensitivity to H_2O_2 was observed for □*recJ* can be explained by this model because endonuclease V nicks 3'-side of a deaminated base in the strand. It should be noted that a DNA helicase with 5'→3' polarity depicted in

this model has not been identified, although the nicked dsDNA must be unwound for degradation by *Tth* ExoI. In the case of repairing oxidized base (8-oxoguanine), it is known that the oxidized base is/can be repaired mainly by specific DNA glycosylases involved in BER (Back *et al*., 2006; Michaels *et al*., 2002; Seeberg *et al*., 1995). There has been no report describing the involvment of ssExos in BER. Moreover, the exonuclease assay revealed that *Tth* ExoI cannot process abasic site (5′-deoxyribose-5-phosphate residue) generated by DNA glycosylases, and a previous study also showed that RecJ has no 5′-deoxyribose-5-phosphatase activity (Piersen *et al*., 2000). Thus, my study suggests that *Tth* ExoI and RecJ do not play a crucial role in BER in *T. thermophilus*.

Tth ExoI might also be involved in repair of methylated bases in DNA. *Tth* ExoI degraded ssDNA containing methylated bases (Fig. I-12G and H). In *T. thermophilus*, TTHA1564, annotated as O^6-methyguanine methylransferase, had no DNA methyltransferase activity, but interacted with UvrA, which functions in bacterial NER (Morita et al, 2008). Short ssDNA liberated by NER may be degraded by ssExos. The repair mechanism of methylated bases remains to be investigated.

My *in vivo* experiments also indicate that RecJ but not *Tth* ExoI plays a significant role in the repair of DNA damages caused by UV-C irradiation. UV-C irradiation mainly induces pyrimidine dimers, (6-4) photoproducts, and DSBs (Bourre *et al*., 1989). As pyrimidine dimers and (6-4) photoproducts are repaired mainly by nucleotide excision repair (NER) (Friedberg, 1995), our results indicate the possible involvement of RecJ in NER. However, it is believed that ssExos do not play a critical role in the NER pathway (Truglio *et al*., 2006). Instead, RecJ is suggested to be involved in the recovery of replication forks at blocking DNA lesions caused by UV irradiation (Courcelle and Hanawalt, 2001). My result also can be interpreted in the context of the rescue of arrested replication forks after UV-C irradiation. It should be mentioned that the double disruption of *tthb178* and *recJ* caused the more severe sensitivity to UV-C irradiation than the single disruption of *recJ*. It can be

speculated that *Tth* ExoI and RecJ participate in separate pathways for the repair of UV-induced damage and *Tth* ExoI-dependent pathway might be stimulated when RecJ-dependent one is inactive.

Unlike pyrimidine dimers or (6-4) photoproducts, DSBs directly result in cell death; therefore, I cannot exclude the possibility that the increase in the UV sensitivity of Δ*recJ* suggests the involvement of RecJ in DSB repair. DSB repair, in bacteria, is performed mainly by homologous recombination. In general, there are two pathways in bacterial homologous recombination: the RecBCD and RecF pathways (Dillingham *et al*., 2003; Ivancic-Bace *et al*., 2005). The RecBCD complex and another 5′→3′ ssExo process the termini of dsDNAs to generate the 3′-overhanging structure in the RecBCD and RecF pathways, respectively. Because *T. thermophilus* HB8 lacks the genes encoding RecBCD, the RecF pathway is expected to be dominant in this bacterium, and 5′→3′ exonuclease activity of RecJ may be required for the end-resection step in this pathway (Fig. I-13C).

In conclusion, the results of my *in vivo* and *in vitro* experiments suggest that 3′→5′ ssExo *Tth* ExoI participates in the excision step of MMR and the repair of deaminated bases while 5′→3′ ssExo RecJ is involved in the excision step of MMR and the repair of UV-C-induced damages. It is to be examined whether *Tth* ExoI plays other roles in addition to DNA repair. Interestingly, it was recently reported that phage infection induces the expression of *tthb178* in a CRP-dependent manner *in vivo* (Agari *et al*., 2010). Upon phage infection, *T. thermophilus* CRP upregulates the transcription of not only *tthb178* but also a variety of clustered regularly interspaced short palindromic repeat-associated genes, the so-called CRISPR-associated genes (Shinkai *et al*., 2007), which have been implicated as the components of a host defense system against invading foreign replicons (Sorek *et al*., 2008; Waters and Storz, 2009). The 3′→5′ exonuclease activity of *Tth* ExoI may also be utilised for the bacterial host defense system.

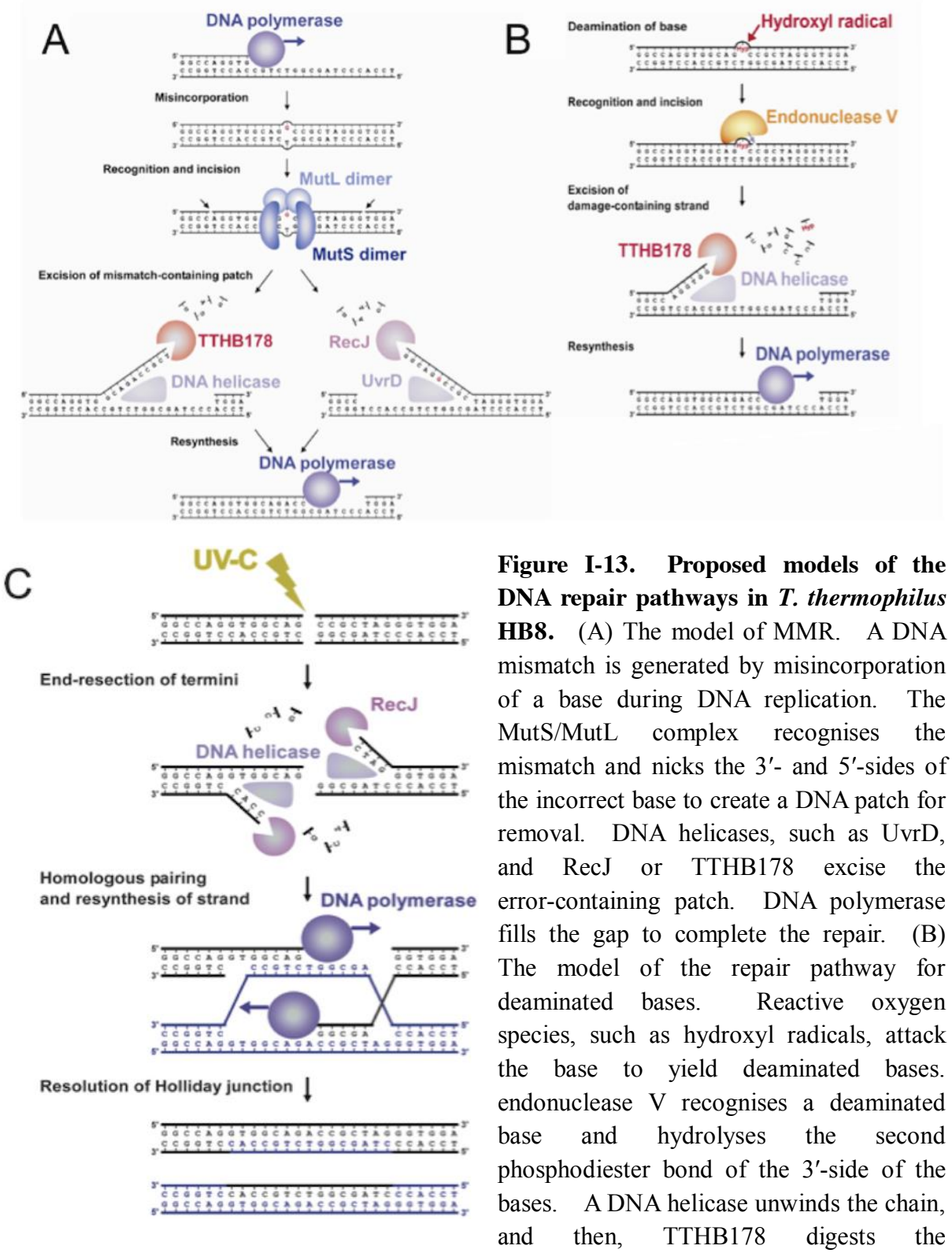

Figure I-13. Proposed models of the DNA repair pathways in *T. thermophilus* HB8. (A) The model of MMR. A DNA mismatch is generated by misincorporation of a base during DNA replication. The MutS/MutL complex recognises the mismatch and nicks the 3′- and 5′-sides of the incorrect base to create a DNA patch for removal. DNA helicases, such as UvrD, and RecJ or TTHB178 excise the error-containing patch. DNA polymerase fills the gap to complete the repair. (B) The model of the repair pathway for deaminated bases. Reactive oxygen species, such as hydroxyl radicals, attack the base to yield deaminated bases. endonuclease V recognises a deaminated base and hydrolyses the second phosphodiester bond of the 3′-side of the bases. A DNA helicase unwinds the chain, and then, TTHB178 digests the lesion-containing ssDNA. (C) The model of DSB repair. UV-C irradiation causes DSBs in DNA. RecJ processes the termini to the 3′-overhanging structure in cooperation with a DNA helicase. The homologous pairing and re-synthesis of the DNA strand yield Holliday junctions. The resolution of Holliday junctions completes the repair.

CHAPTER II

MutS stimulates the endonuclease activity of MutL in an ATP hydrolysis-dependent manner

ABSTRACT

In the initial steps of DNA mismatch repair, MutS recognizes a mismatched base and forms the complex with the latent endonuclease MutL on the mismatch-containing DNA in concert with other proteins. MutL then cleaves the error-containing strand to introduce an entry point for the downstream excision reaction. Because MutL has no intrinsic ability to recognize a mismatch and discriminate between newly synthesized and template strands, the endonuclease activity of MutL is strictly regulated by ATP-binding in order to avoid non-specific degradation of the genomic DNA. However, the activation mechanism for its endonuclease activity remains unclear. In this study, I found that co-existence of a mismatch, ATP, and MutS unlocks the ATP-binding-dependent suppression of MutL endonuclease activity. Interestingly, ATPase-deficient mutants of MutS were unable to activate MutL. Furthermore, wild-type MutS activated ATPase-deficient mutants of MutL less efficiently than wild-type MutL. I concluded that ATP hydrolysis by MutS and MutL is involved in the mismatch-dependent activation of MutL endonuclease activity.

INTRODUCTION

Biochemical and molecular biological analyses of eukaryotic MMR contribute the understanding the overview of MMR pathways (described in detail in GENERAL INTRODUCTION). One of the intriguing features of MMR is the strand discrimination between the template and newly synthesized strand. *In vitro* reconstruction studies of eukaryotic MMR suggested that strand discrimination is accomplished in the presence of RFC, PCNA, MutSα, and MutLα (Pluciennik *et al*., 2010, Pillon *et al*., 2011). Since PCNA is ring-shaped (clamp) protein comprising homotrimer and cannot bind on a circular DNA, the loading of PCNA requires clamp loader protein RFC (Bowman *et al*., 2004; Georgescu *et al*., 2008). Because RFC is only required for loading PCNA onto DNA, MutSα and PCNA are thought to be the core components for the introduction of the nick into the newly synthesized strand by MutLα. The important feature of PCNA is that two faces of the ring are asymmetric, and the interaction region between PCNA and other proteins exist in only one side (Krishna *et al*., 1994). Furthermore, PCNA is loaded on a DNA at a 3'-terminal of nicked site or primer-template junction with a specific orientation relative to the orientation of each DNA structure (Yao *et al*., 2000; Bowman *et al* 2004; Georgescu *et al*., 2008). Hence, PCNA-MutL interaction is able to serve as a signal of strand discrimination (Pluciennik *et al*., 2010; Lee and Alani 2006).

In bacterial MMR except for *E. coli* type, it has been discussed how strand discrimination is achieved. According to the reports that MutL possesses β clamp interacting motif in its CTD and colocalizes with β clamp in living cell, there is the possibility that β clamp-MutL interaction is required for strand discrimination (Pillon *et al*., 2010, Simmons *et al*., 2008). However, another possibility is that β clamp is unnecessary for bacterial MMR (Monti *et al*., 2012). To verify what serves as strand discrimination signal in general bacterial MMR, *in vitro* MMR reconstruction using recombinant proteins

provide valid insights into this issue. In the case of *T. thermophilus*, the counterparts of eukaryotic MMR proteins have been identified, and the expression plasmid vectors of these proteins are prepared. Consequently, *T. thermophilus* is suitable for investigating general bacterial MMR.

Although the conformational change induced by ATP binding of MutS homologues is required for MMR (Junop *et al*., 2001; Baitinger *et al*.,2003; Lebbink *et al*., 2006), the role of ATP hydrolysis by MutS homologues has been unclear in eukaryotic and general bacterial MMR. Structural and biochemical studies revealed that MutS homologs belong to the ABC ATPase superfamily (Fig. II-1A and C) (Gorbalenya and Koonin, 1990; Junop *et al*, 2001; Lamers *et al*, 2000; Obmolova *et al*, 2000). Binding to mismatched DNA induces ATP loading into MutS (Biswas and Vijayvargia, 2000; Joshi *et al*, 2000), and stabilizes of the ATP-bound form (Antony and Hingorani, 2003; Antony and Hingorani, 2004; Zhai and Hingorani, 2010). ATP binding induces a MutS conformational change, resulting in the formation of a clamp-like structure to slide along the DNA strand (Allen *et al*, 1997; Gradia *et al*, 1999). These reports indicate that ATP binding not hydrolysis plays an important role in MutS function in MMR process. In *E. coli*-type MMR, ATP hydrolysis by MutS is necessary for activation of MutH (Baitinger *et al*, 2003). However, in eukaryotic and general bacterial MMR, the role of ATP hydrolysis by MutS is unclear.

Additionally, in eukaryotic and general bacterial MMR, the role of ATP binding and hydrolysis by MutL homologues has also been argued. MutL homologues belong to the GHL ATPase superfamily (Ban *et al*, 1999; Dutta and Inouye, 2000) and contain the Bergerat ATP-binding fold in their N-terminal domain (NTD) (Fig. II-1B and D). The N-terminal ATPase domain of MutL tightly binds ATP, and ATP binding provokes the conformational change and dimerization of the NTD of MutL (Ban *et al*., 1999). ATP binding on the NTD of MutL causes stimulation or inhibition of the MutL endonuclease activity (Fukui *et al*., 2008; Mauris *et al*., 2009). It is suggested that the ATP-binding-dependent suppression of

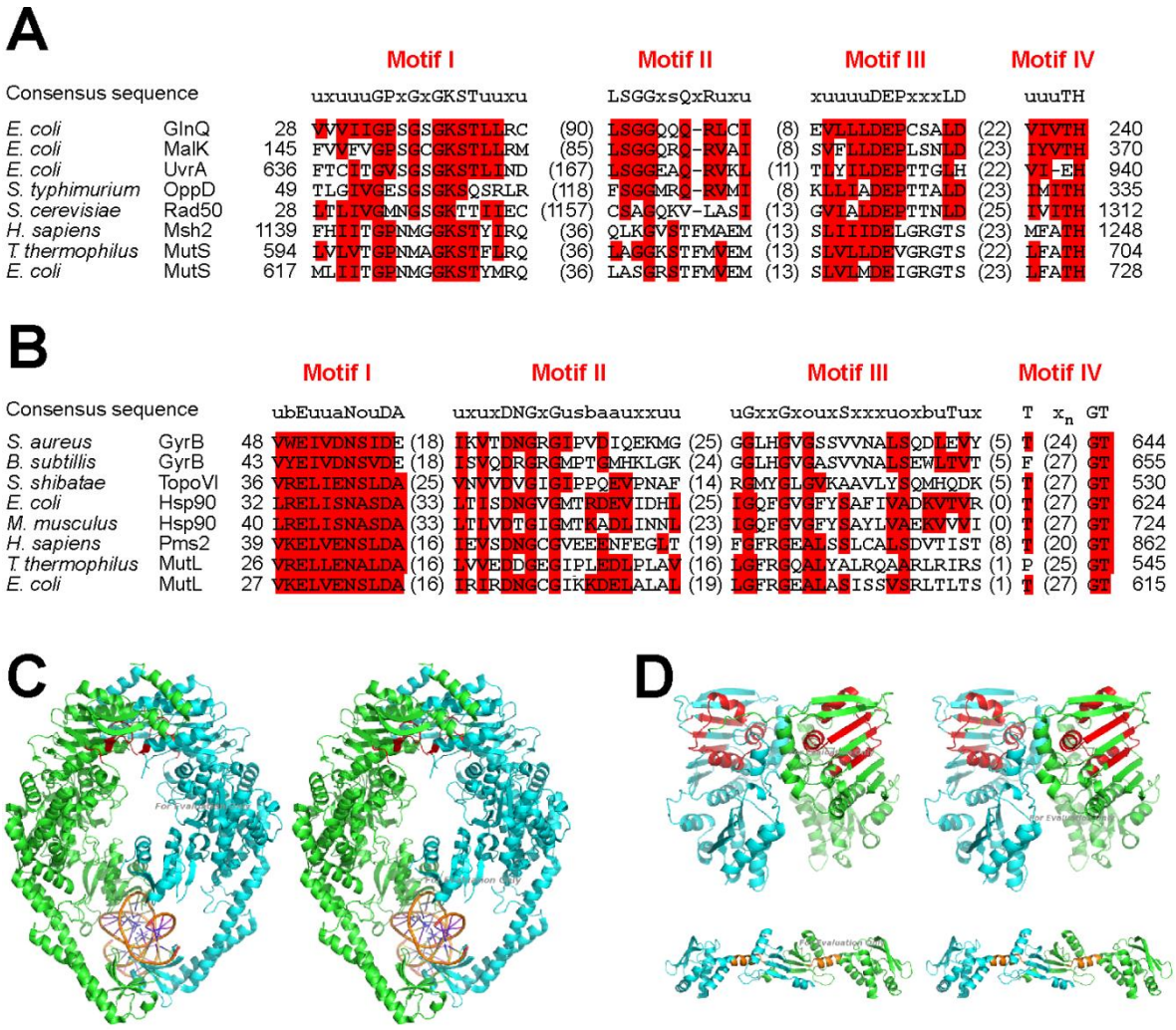

Figure II-1. Amino acid sequence alignments of the ATPase superfamilies. Red box indicates the conserved sequence motifs of ABC (A) and GHL (B) ATPase superfamilies. The numbers on the left and right show the distances form the N-termini for each protein and the full lengths of each protein, respectively. The numbers in parentheses show the number of residues that are omitted for the sake of clarity. The NCBI Entrez GI numbers of the sequences are as follows: (A) 378257190 (*E. coli* GlnQ), 146701 (*E. coli* MalK), 315138613 (*E. coli* UvrA), 383496438 (*Salmonella typhimurium* OppD), 1255968 (*S. cerevisiae* Rad50), 4557761 (*H. sapiens* Msh2), 55981293 (*T. thermophilus* MutS), 16130640 (*E. coli* MutS), and 16761683 (*S. typhimurium* MutS), (B) 540541 (*Staphylococcus aureus* GyrB), 2558946 (*B. subtilis* GyrB), 3024756 (*Sulfolobus shibatae* TopoVI), 209778366 (*E. coli* Hsp90), 40556608 (*Mus musculus* Hsp90), 4505913 (*H. sapiens* PMS2), 55981292 (*T. thermophilus* MutL), and 16131992 (*E. coli* MutL). (C) Stereo view of the crystal structure of *E. coli* MutS with heterodupelx (PDB, 1W7A). (D) Stereo view of the crystal structure of *E. coli* MutL N-terminal domain (top) and *B. subtilis* MutL C-terminal domain (bottom). The regions of ATPase and endonuclease motifs are colored red and orange, respectively.

the endonuclease activity protects lesion-less DNA from non-specific degradation in the cell, because MutL possesses non-specific endonuclease activity and degrades lesion-less DNA *in vitro* (Duppatla *et al*, 2009; Fukui *et al*, 2008; Iino *et al*, 2011; Kadyrov *et al*, 2006; Kadyrov *et al*, 2007; Pillon *et al*, 2010). However, whether ATP binding of MutL stimulates or inhibits the endonuclease activity has been unclear.

In order to achieve mismatch-specific DNA incision, it is expected that interactions with other MMR proteins unlock the ATP-binding-dependent suppression of MutL endonuclease activity and ATP enhances the nick introduction. In general bacterial MMR, MutL interacts with other MMR proteins such as the β clamp, clamp loader, and MutS (Amin *et al*., 2001; Li *et al*., 2008; Mendillo *et al*., 2009; Pillon *et al*., 2011; Simmons *et al*., 2008; Umar *et al*., 1996). Interactions between the β clamp, MutS, and MutL are important to recruit and stabilize the MutS-MutL complex (López de Saro *et al*., 2006; Simmons *et al*., 2008). Furthermore, in eukaryotic-type MMR, the interaction between MutLα and PCNA (an eukaryotic counterpart of β clamp) is thought to be necessary for discrimination between newly synthesized and template strands (Pluciennik *et al*., 2010). Because these MMR proteins are involved in the upstream processes of nick introduction by MutL (Fig. G-1), it can be expected that the ATP-bound form of MutL is activated by these proteins.

In this chapter, I tried to unmask the mechanism of strand discrimination of general bacterial MMR using recombinant proteins of *T. thermophilus*. Furthermore, I examined the effects of these MMR proteins on the activation of ttMutL, and investigated the roles of ATP binding and hydrolysis of ttMutS and ttMutL proteins in regulation of ttMutL endonuclease activity. As a result, I clarified how the endonuclease activity of MMR is controlled to achieve mismatch-specific incision in a *mutH*-less organism.

EXPERIMENTAL PROCEDURES

Construction of MutS and MutL mutants—The pET3a/*ttha1324* (ttMutS) and pET11a/*ttha1323* (ttMutL) plasmid were obtained from RIKEN BioResource Center (Tsukuba, Japan). pET3a/*ttha1324* was used as a template to generate the overexpression plasmids for ttMutS K597M and E671A by QuickChange mutagenesis (Stratagene, La Jolla, CA). The primers used to generate the expression plasmid for ttMutS K597M were 5′-CCCAACATGGCGGGGATGTCCACCTTCCTCCGC-3′ and 5′-GCGGAGGAAGGTG GACATCCCCGCCATGTTGGG-3′, and the primers for the expression plasmid of ttMutS E671A were 5′-GTCCTCCTGGACGCGGTGGGCCGGGGC-3′ and 5′-GCCCCGGCCCAC CGCGTCCAGGAGGAC-3′. The pET11a/*ttha1323* was used as a template to generate the overexpression plasmids for MutL E28A and D57A by QuickChange mutagenesis (Stratagene). The primer sets used to generate the expression plasmids for MutL E28A and D57A mutants were 5′-GGACGCCGTGCGGGCGCTTCTGGAAAACGCC-3′ and 5′-GGCGTTTTCCAGAAGCGCCCGCACGGCGTCC-3′, and 5′-GCTTGTGGTGGAGGC CGACGGGGAGGGGATC-3′ and 5′-GATCCCCTCCCCGTCGGCCTCCACCACAAGC-3′, respectively. A DNA fragment expressing the *T. thermophilus* MutL C-terminal domain (CTD) was generated by PCR using pET-11a/*ttha1323* as a template. The forward and reverse primers used for the amplification were 5′-ATATCATATGGCCCTCCCCGAGCCCA AGCCCCTC-3′ and 5′-ATATAGATCTTTAAGGTTCTCGGGGTAGAGGTG-3′, respectively. The forward and reverse primers contained NdeI and BglII sites, respectively (underlined). The amplified *T. thermophilus* MutL CTD gene fragment was ligated into the NdeI and BamHI site of pET-HisTEV (Novagen, Madison, WI, USA) to obtain the expression plasmid for histidine-tagged *T. thermophilus* MutL CTD.

Overexpression and purification of proteins—*E. coli* Rosetta2(DE3) pLysS (Novagen) was

transformed with pET11a/*ttha1952* (DNA polymerase III γ and τ subunit), pET11a/*ttha0788* (DNA polymerase III δ subunit), pET11a/*ttha1860* (DNA polymerase III δ′ subunit), pET11a/*ttha0001* (DNA polymerase III β clamp), pET3a/*ttha1324*, pET3a/*ttha1324-k597m* (MutS K597M), pET3a/*ttha1324-e671a* (MutS E671A), pET11a/*ttha1323*, pET11a/*ttha1323-e28a* (MutL E28A), pET11a/*ttha1323-d57a* (MutL D57A), or pET-HisTEV/*ttha1323-ctd*. The transformants were cultured to early log-phase (1×10^8 cells/mL) in L-broth containing 50 μg/mL ampicillin, and then isopropyl-1-thio-β-D-galactopyranoside was added to induce expression of the target gene. The cells were further cultured for 6 h, and harvested by centrifugation at 9000 × g for 10 min at 4°C, then stored at –20°C until use.

mRNAs of *T. thermophilus* DNA polymerase III γ and τ subunits were transcribed from the same gene *ttha1952* (*dnaX*) by programmed transcriptional slippage (Larsen *et al.*, 2000). To purify the DNA polymerase III γ and τ subunits, stored cells were suspended in 50 mM Tris-HCl and 50 mM KCl, pH 8.0, then disrupted by sonication. The cell lysate was heat-treated at 65°C for 10 min, and the supernatant was recovered by centrifugation at 34,500 × g at 4°C for 60 min. Ammonium sulfate was gradually added to the crude extract to a final concentration of 1.5 M, and the solution was incubated at 4°C overnight. The precipitate was recovered by centrifugation at 7,600 × g for 30 min at 4°C, and dissolved in 50 mM Tris-HCl (pH 8.0). The solution was loaded onto a TOYOPEARL SuperQ-650M column (bed volume of 20 mL; Tosoh Corp., Tokyo, Japan) equilibrated with 50 mM Tris-HCl (pH 8.0). The column was washed with 200 mL 50 mM Tris-HCl (pH 8.0), and the proteins were eluted with a linear gradient of 0–1 M KCl in 200 mL 50 mM Tris-HCl (pH 8.0). The fractions containing DNA polymerase III γ and τ subunits were diluted to 50 mL with 10 mM potassium phosphate buffer (pH 7.0) and loaded onto a hydroxyapatite column (bed volume of 20 mL; nacalai tesque, Kyoto, Japan) equilibrated with 10 mM potassium phosphate buffer (pH 7.0). The proteins were eluted with a linear gradient of 10–500 mM potassium phosphate (pH 7.0) (200 mL). The fractions containing DNA polymerase III γ

and τ subunits were applied to TOYOPEARL Heparin (bed volume 10 mL; Tosoh Corp.) equilibrated with 50 mM Tris-HCl (pH 7.5). The column was washed with 50 mM Tris-HCl (pH 7.5) and the DNA polymerase III γ and τ subunits were eluted with a linear gradient of 0–1 M KCl in 200 mL Tris-HCl (pH 7.5). The fractions containing DNA polymerase III γ and τ subunits were detected by SDS-polyacrylamide gel electrophoresis (SDS-PAGE). DNA polymerase III γ and τ subunits were concentrated to 80 μM with a Vivaspin concentrator (GE Healthcare Biosciences) by centrifugation at 6,000 rpm for 10 min, immediately frozen in liquid nitrogen, and stored at –80°C.

To purify DNA polymerase III δ and δ′ subunits, stored cells expressing δ and δ′ subunits were mixed, and suspended in 20 mM Tris-HCl (pH 7.5), then disrupted by sonication. The cell lysate was heat-treated at 55°C for 10 min, and the supernatant was recovered by centrifugation at 34,500 × g at 4°C for 60 min. Ammonium sulfate was gradually added to the crude extract to the final concentration of 1.5 M, and the solution was applied to a TOYOPEARL Ether-650M column (bed volume of 20 mL; Tosoh Corp.) equilibrated with 20 mM Tris-HCl and 1.5 M ammonium sulfate, pH 7.5. The column was washed with 20 mM Tris-HCl and 1.5 M ammonium sulfate, pH 7.5, and then eluted with a linear gradient of 1.5–0 M ammonium sulfate in 200 mL 20 mM Tris-HCl (pH 7.5). The fractions containing DNA polymerase III δ and δ′ subunits were detected by SDS-PAGE, and dialyzed twice against 5 L 20 mM Tris-HCl (pH 7.5). The dialyzed solution was diluted to 50 mL with 20 mM Tris-HCl (pH 7.5), and loaded onto a TOYOPEARL SuperQ-650M column (bed volume of 20 mL; Tosoh Corp.) equilibrated with 20 mM Tris-HCl (pH 7.5). The column was washed with 200 mL 20 mM Tris-HCl (pH 7.5), and the proteins were eluted with a linear gradient of 0–1 M KCl in 200 mL 20 mM Tris-HCl (pH 7.5). The fractions containing DNA polymerase III δ and δ′ subunits were diluted to 50 mL with 10 mM potassium phosphate buffer (pH 7.0) and loaded onto a hydroxyapatite column (bed volume of 20 mL; nacalai tesque) equilibrated with 10 mM potassium phosphate buffer (pH

7.0). The proteins were eluted with a linear gradient of 10–500 mM potassium phosphate (pH 7.0) (200 mL). The fractions containing DNA polymerase III δ and δ′ subunits were detected by SDS-PAGE and concentrated with a Vivaspin concentrator. Concentrated DNA polymerase III δ and δ′ subunits were applied to a Superdex 200 HR column (1 cm × 30 cm; GE Healthcare Biosciences) in an ÄKTA system (GE Healthcare Biosciences). The elution profile was monitored by recording the absorbance at 280 nm. DNA polymerase III δ and δ′ subunits were eluted at 0.5 mL/min with 20 mM Tris-HCl and 150 mM KCl, pH 8.0. DNA polymerase III δ and δ′ subunits were concentrated to 60 μM, immediately frozen in liquid nitrogen, and stored at –80°C.

To purify the β clamp, stored cells were suspended in 20 mM Tris-HCl and 100 mM KCl, (pH 7.5) (buffer A), then disrupted by sonication. The cell lysate was heat-treated at 70°C for 10 min and the supernatant was recovered by centrifugation at 34,500 × g at 4°C for 60 min. Ammonium sulfate was gradually added to the crude extract to a final concentration of 1.5 M, and the solution was applied to a TOYOPEARL Ether-650M column (bed volume of 20 mL; Tosoh Corp.) equilibrated with 20 mM Tris-HCl, 1.5 M ammonium sulfate, and 100 mM KCl (pH 7.5). The column was washed with 20 mM Tris-HCl, 1.5 M ammonium sulfate, and 100 mM KCl (pH 7.5), and then eluted with a linear gradient of 1.5–0 M ammonium sulfate in 200 mL buffer A. The fractions containing β clamp were dialyzed twice against 5 L buffer A. The dialyzed sample was diluted to 50 mL with buffer A and loaded onto a TOYOPEARL SuperQ-650M column (bed volume of 20 mL; Tosoh Corp.) equilibrated in buffer A. The column was subsequently washed with 200 mL buffer A, and the proteins were eluted with a linear gradient of 0.1–1 M KCl in 200 mL 20 mM Tris-HCl (pH7.5). The fractions containing β clamp were dialyzed twice against 5 L of 10 mM potassium phosphate buffer (pH 7.4). The dialyzed solution was diluted to 50 mL with 10 mM potassium phosphate buffer (pH 7.4) and loaded onto a hydroxyapatite column (bed volume of 20 mL; nacalai tesque) equilibrated in 10 mM potassium phosphate buffer (pH

7.4). The proteins were eluted with a linear gradient of 10–500 mM potassium phosphate (pH 7.4) (200 mL). The fractions containing β clamp were detected by SDS-PAGE and β clamp was concentrated with a Vivaspin concentrator. Concentrated β clamp was applied to a Superdex 200 HR column (1 cm × 30 cm; GE Healthcare Biosciences) in an ÄKTA system (GE Healthcare Biosciences). β clamp was eluted at 0.5 mL/min with 20 mM Tris-HCl and 100 mM KCl (pH 7.5). The fractions containing β clamp were concentrated to 300 □M, immediately frozen in liquid nitrogen, and stored at –80°C.

To purify wild-type (WT) ttMutS and its mutant derivatives, stored cells were suspended in buffer containing 20 mM Tris-HCl and 500 mM KCl (pH 7.5), and disrupted by sonication. The cell lysate was incubated at 70°C for 10 min and the supernatant was recovered by centrifugation at 34,500 × g at 4°C for 60 min. Ammonium sulfate was gradually added to the crude extract at final concentration of 1.5 M, and the solution was applied to a TOYOPEARL Ether-650M column (bed volume of 20 mL; Tosoh Corp.) equilibrated with 20 mM Tris-HCl, 1.5 M ammonium sulfate and 500 mM KCl (pH 7.5). The column was washed with 200 mL 20 mM Tris-HCl, 1.5 M ammonium sulfate and 500 mM KCl (pH 7.5), and eluted with a linear gradient of 1.5–0 M ammonium sulfate in 200 mL 20 mM Tris-HCl and 500 mM KCl (pH 7.5). The fractions containing target protein were dialyzed twice against 5 L buffer containing 20 mM Tris-HCl and 150 mM KCl (pH 8.0) (buffer B). The dialyzed solution was diluted to 50 mL with buffer B and loaded onto a TOYOPEARL SuperQ-650M column (bed volume of 20 mL; Tosoh Corp.) equilibrated in buffer B. The column was washed with 200 mL buffer B and the proteins were eluted with a linear gradient of 0.15–1 M KCl in 200 mL 20 mM Tris-HCl, pH7.5. The fractions containing target protein were concentrated with a Vivaspin concentrator. Concentrated protein was loaded onto a Superdex 200 HR column (1 cm × 30 cm; GE Healthcare Biosciences) in an ÄKTA system (GE Healthcare Biosciences). Target protein was eluted at 0.5 mL/min with 20 mM Tris-HCl and 500 mM KCl (pH 7.5). The fractions containing WT ttMutS or its mutant

derivatives were concentrated to 50 μM, immediately frozen in liquid nitrogen, and stored at –80°C.

To purify WT ttMutL and its mutant derivatives, I used potassium phosphate buffer to prevent protein self-assembly (Niedziela-Majka *et al*., 2011). Stored cells were suspended in buffer containing 50 mM potassium phosphate, 50 mM KCl, 1 mM EDTA, 2 mM β-mercaptoethanol, and 0.2 mM PMSF, pH 7.4 (buffer C), and disrupted by sonication. The supernatant was recovered by centrifugation at 34,000 × g at 4°C for 60 min. The supernatant was applied to TOYOPEARL SP-Sepharose (bed volume of 10 mL; Tosoh Corp.) equilibrated with buffer C. The column was washed with 200 mL buffer C. The flow-through and wash fractions containing target protein were applied to TOYOPEARL Heparin (bed volume 10 mL; Tosoh Corp.) equilibrated with buffer C. The column was washed with 200 mL buffer C, and then target protein was eluted with a linear gradient of 50–1000 mM KCl in 200 mL buffer C. The fractions containing target protein were detected by SDS-PAGE, and target protein was concentrated with a Vivaspin concentrator. Concentrated protein was applied to Superdex 200 HR column (1 cm × 30 cm; GE Healthcare Biosciences) in an ÄKTA system (GE Healthcare Biosciences). Target protein was eluted at 0.5 mL/min with 50 mM potassium phosphate and 500 mM KCl (pH 7.4). The fractions containing WT ttMutL or its mutant derivatives were concentrated to 20 □M, immediately frozen in liquid nitrogen, and stored at –80°C.

To purify the His-tag fused ttMutL CTD, stored cells were suspended in buffer containing 20 mM Tris-HCl and 50 mM NaCl (pH 7.2) (buffer D), and disrupted by sonication. The supernatant was recovered by centrifugation at 34,000 × g at 4°C for 60 min. The supernatant was applied to TOYOPEARL SuperQ 650-M (bed volume of 10 mL; Tosoh Corp) equilibrated with the buffer D. The column was washed with 200 mL buffer D, and then the flow-through and wash fractions containing target protein were applied to Ni-NTA His-Bind Resin (bed volume 5 mL; Merck KGaA, Darmstadt, Germany) equilibrated

with buffer D containing 50 mM imidazole. The column was washed and target protein was eluted with a linear gradient of 50–500 mM imidazole in 200 mL buffer D. The fractions containing target protein were detected by SDS-PAGE and target protein was concentrated with a Vivaspin concentrator. Concentrated protein was applied to Superdex 200 HR column (1 cm × 30 cm; GE Healthcare Biosciences) in an ÄKTA system (GE Healthcare Biosciences). Target protein was eluted at 0.5 mL/min with 50 mM potassium phosphate and 500 mM KCl (pH 7.4). The fractions containing His-tag fused ttMutL CTD was concentrated to 200 μM, immediately frozen in liquid nitrogen, and stored at –80°C.

Protein purity was assessed by 12.5% SDS-PAGE and gels were visualized by staining with Coomassie Brilliant Blue (Fig. II-2). The target proteins were identified by peptide mass fingerprinting (Salzano *et al*., 2008). Briefly, the protein band was excised from polyacrylamide gels, digested with trypsin, and analyzed by MALDI-TOF mass spectrometry (Bruker Daltonics). The mass spectra of the peptide fragments from the purified proteins were compared to theoretical mass spectra of the digests of the target proteins, using the MASCOT search tool.

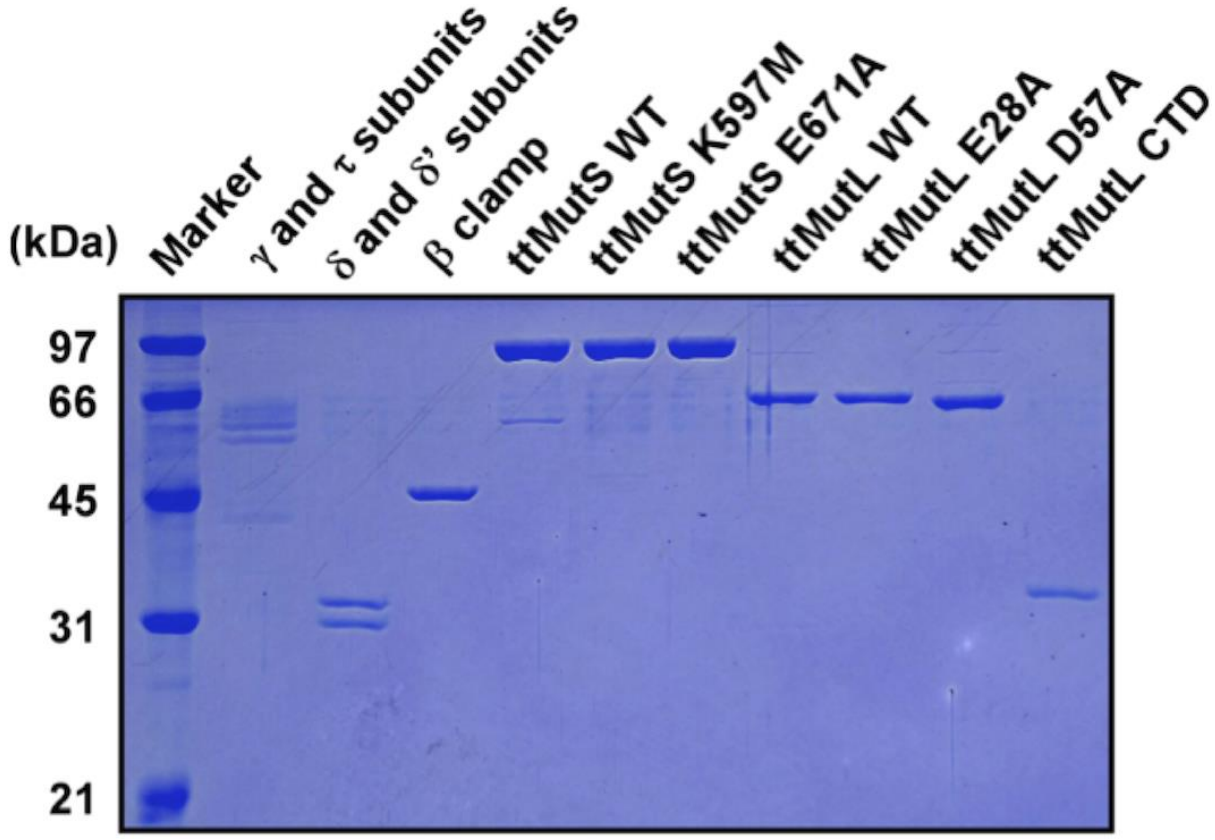

Figure II-2. Purified MMR proteins visualized by Coomassie brilliant blue staining. MMR proteins were purified according to the procedures described in Materials and Methods. Each protein (10 pmol) was subjected to SDS-PAGE on 12.5% acrylamide gel. The molecular weights theoretically calculated from the amino acid sequences of DNA polymerase III γ and τ subunits, δ subunit, δ′ subunit, β clamp, MutS, MutL, and MutL CTD are 58, 32, 29, 41, 91, 60, and 27 kDa, respectively. The major protein band on each lane was identified as the target protein by peptide mass fingerprinting with MALDI-TOF mass spectrometry. Peptide mass finger printing also revealed that the bands detected at lower molecular weights were degraded products of the target proteins.

Far-Western blotting analysis—Purified MMR proteins and BSA as negative control (1–40 pmol) were spotted onto a Protran nitrocellulose membrane (Whatman, Kent, UK). The membrane was blocked for 2 h at room temperature with buffer E (25 mM Tris-HCl, 150 mM KCl, and 1 mM EDTA, 0.1% Triton X-100, and 4% skim milk, pH 8.0), and then incubated with 0.5 μM γ and τ subunits, δ and δ′ subunits, β clamp, ttMutS, or ttMutL in buffer F (50 mM Tris-HCl and 150 mM NaCl, pH 7.5) at 25°C for 24 h. The membrane was washed 3 times with buffer E without skim milk for 5 min. Then, the membrane was incubated with rabbit anti-γ and -τ subunits, -δ and -δ′ subunits, -β clamp, -ttMutS, or -ttMutL antibody in buffer E for 60 min at 25°C, and then the membrane was washed and incubated with alkaline phosphatase-conjugated goat anti-rabbit antibody (Bio-Rad laboratories).

Immunoprecipitation analysis—*T. thermophilus* HB8 was cultured in TT-broth to stationary phase and harvested by centrifugation. Cells (1 g) were suspended in buffer F containing 1 mM PMSF and disrupted by sonication. The soluble cell lysate was recovered by centrifugation at 34,000 × g for 60 min at 4°C. Cell lysate (10 mL) was treated with 25 units/mL benzonase (Merck KGaA) for 60 min at 37°C to avoid nonspecific detection of DNA-bound proteins. Each antibody (100 μg) was cross-linked with Protein A sepharose (GE Healthcare Biosciences), added to 10 mL of cell lysate and incubated at 25°C for 12 h with end-over-end mixing. After incubation, antibody-conjugated Protein A sepharose was recovered and washed 5 times with 200 μL buffer F, and the interacting proteins were eluted with 50 μL buffer containing 100 mM glycine with 2 M urea, pH 2.9. The eluted proteins were electrophoresed on 12.5% polyacrylamide gel, and then electrotransferred to a polyvinylidene difluoride membrane (Bio-Rad laboratories Inc., Hercules, CA). The membrane was blocked for 60 min in buffer E. Next, the membrane was incubated with antibodies against MMR proteins at 25°C for 60 min. For the enhanced chemiluminescence detection system, the membrane was incubated with alkaline phosphatase-conjugated goat

anti-rabbit antibody (Bio-Rad laboratories Inc.) at 25°C for 60 min.

***Quantitative Western blotting*—**Cells from a single colony of *Thermus thermophilus* HB8 wild-type (WT), *mutS* null mutant strain (Δ*mutS*), or *mutL* null mutant strain (Δ*mutL*) (Fukui *et al*., 2008) were cultured in 3 mL TT-broth (0.4% tryptone, 0.2% yeast extract, 0.1% NaCl, 0.4 mM $MgCl_2$, and 0.4 mM $CaCl_2$, pH 7.5) at 70°C for overnight. One milliliter overnight culture was added to 100 mL TT-broth at 70°C. A 1.5-mL aliquot of the culture was removed at each time point and cells were harvested by centrifugation at 2,300 × g for 10 min at 4°C. Cells were suspended in buffer containing 50 mM Tris-HCl, 100 mM KCl, 1 mM EDTA, 1 mM DTT, and 10% glycerol, pH 7.5, and then disrupted by sonication. The cell extract was recovered by centrifugation at 20,000 × g for 1 h at 4°C, and the concentration of the extract was measured by the Bradford method.

WT protein samples (100 μg) were separated by 12.5% SDS-PAGE. As quantification standards, various amounts of purified recombinant proteins were mixed with 100 μg proteins prepared from Δ*mutS* or Δ*mutL*, and electrophoresed on the same gel. The proteins were electrotransferred to a polyvinylidene difluoride membrane (Bio-Rad laboratories Inc., Hercules, CA). The membrane was treated with blocking solution containing 25 mM Tris-HCl, 150 mM KCl, and 1 mM EDTA, 0.1% Triton X-100, and 4% skim milk, pH 8.0 (buffer A) at 25°C for 60 min. The membrane was washed with buffer A without skim milk, and then incubated with polyclonal rabbit anti-ttMutL antibody (MBL Co., Nagoya, Japan) or anti-ttMutS antibody (Oriental Yeast Co., Tokyo, Japan) at 25°C for 60 min. For the enhanced chemiluminescence detection system, the membrane was incubated with alkaline phosphatase-conjugated goat anti-rabbit antibody (Bio-Rad laboratories Inc.) at 25°C for 60 min. The intensities of stained ttMutS or ttMutL bands were quantified by ImageJ (http://rsb.info.nih.gov/ij/). The amounts of ttMutS and ttMutL in cellular extracts were determined by referencing the standard curve. The concentration of ttMutS or ttMutL in the

cell was determined by referencing the single-cell volume of *T. thermophilus* ($2.11 \times 10^{-12} \pm 1.35 \times 10^{-12}$ mL) (Kondo *et al.*, 2008).

Preparation of 120-base pair double-stranded DNA − The 3′ -biotinylated 120 nt oligonucleotides were synthesized (BEX Co., Tokyo, Japan) (Table II-1). The 5′ -terminal of 120-2T was radiolabeled with [γ-^{32}P] ATP using T4 DNA polynucleotide kinase (TAKARA Bio) at 37°C for 60 min. The radiolabeled 120-2T was annealed with non-radiolabelled 12-1A or 120-1G, generating 120-bp homoduplex or heteroduplex, respectively. To block both termini of the double-stranded DNA, excess streptavidin was added to the annealed DNA solution and incubated at 37°C for 60 min. For nick introduction, 50 μL of 10 nM 120-bp DNA was incubated with 5 units of Nb. Bpu10I at 37°C for 1 h, and then the sample mixture was heat-treated with 80°C for 20 min in order to inactivate Nb. Bpu10I.

Table II-1. The oligonucleotide sequences used in this study

Bold and italic sequence is EcoRI site. Because the 3rd base from 5′ at the EcoRI site in 120-1G is converted to G, the annealing of 120-2T and 120-1G results in 120-bp DNA resistant to EcoRI. Underlined sequence is Nb. *Bpu* 10I site. Nb. *Bpu* 10I introduces a nick in only one strand containing the sequence GC↓TCAGG.

Name	Sequence
120-2T	CGA GCT CGG TAC CCG GGG ATC CGA TAT C***GA ATT C***AC TAG TAG ATC CTC TAG AGT CGA CCT GCA GGC ATG GAA GCT TTC CCT ATA CCT TAG CGC TCA GGA GCT TGG CGT AAT CAT GGT CAT (Biotin)-3′
120-1A	ATG ACC ATG ATT ACG CCA AGC TCC TGA GCG CTA AGG TAT AGG GAA AGC TTG GAT GCC TGC AGG TCG ACT CTA GAG GAT CTA CTA GT***G AAT TC***G ATA TCG GAT CCC CGG GTA CCG AGC TCG (Biotin)-3′
120-1G	ATG ACC ATG ATT ACG CCA AGC TCC TGA GCG CTA AGG TAT AGG GAA AGC TTG GAT GCC TGC AGG TCG ACT CTA GAG GAT CTA CTA GT***G AGT TC***G ATA TCG GAT CCC CGG GTA CCG AGC TCG (Biotin)-3′

Preparation of plasmid DNA for endonuclease assay—The construction of plasmid DNA substrate containing a GT mismatch is described in Fig. II-3A. pUC119 was used as a template to generate a small DNA fragment containing the Nb. Bpu10I using following primers; 5′-TC*GAATTC*ACTGGCCGTC-3′ (forward primer) and 5′-TTT*GGCGCC*GCTAAG GCATTCGCCATTCAGGCTGC-3′ (reverse primer). The forward and reverse primer contained EcoRI and NarI sites (italics), respectively. The Nb. Bpu10I site is underlined in the reverse primer. The amplified fragment was ligated into the EcoRI and NarI sites of pUC119, generating pUC119-Bpu10I. After the error-free construction of pUC119-Bpu10I was confirmed by DNA sequencing, the plasmid was transformed into *E. coli* JM109. The cells from a single colony of transformed *E. coli* JM109 were precultured in 5 mL L-broth containing 50 μg/mL ampicillin at 37°C overnight. The overnight culture was diluted 100-fold with fresh L-broth containing 50 μg/mL ampicillin, and then cultured at 37°C until the culture reached the exponential growth phase (OD_{600} = 0.05). At this point, 0.5 mL M13KO7 helper phage solution (1×10^{11} p.f.u./mL) was added to the culture and incubated at 37°C for 90 min. Subsequently, 500 μL 70 mg/mL kanamycin was added to the culture, and cells infected by M13KO7 helper phage were cultured at 37°C overnight. Cells were removed by centrifugation at 9,000 × g for 20 min at 4°C, and 29.2 mg/mL NaCl and 40 mg/mL PEG6000 was added to the recovered supernatant. The mixture was incubated at 4°C for 1.5 h, and the precipitate was recovered by centrifugation at 9,000 × g for 30 min at 4°C. The pellet was dissolved in 10 mM Tris-HCl and 1 mM EDTA, pH 7.4 (TE buffer), followed by addition of 5% PEG6000 and 625 mM NaCl. The mixture was incubated at 25°C for 5 min, and the precipitation was recovered by centrifugation at 5,800 × g for 10 min at 4°C. The pellet was dissolved in TE buffer and 0.4 g/mL CsCl was added. Phage particles were purified by density gradient centrifugation at 100,000 × g for 16 h at 20°C. The purified phage solution was diluted 10-fold with TE buffer and mixed with an equal volume of phenol/chloroform/isoamyl alcohol (25:24:1). The single-stranded DNA of

pUC119-Bpu10I was recovered by ethanol precipitation. Complementary strand synthesis was carried out by isothermal amplification using the isolated single-stranded plasmid DNA as a template. The 5′-terminus of primer 5′-CTAGAGTCGACCTGCGGGCATGCAAGCT TG-3′ was phosphorylated. The underlined sequence is a PstI site containing a mispaired G (bold). The synthesis reaction was performed at 37°C for 60 min in the presence of 100 μg/mL primer annealed single-stranded plasmid DNA, 1× NEBuffer2 (New England Biolabs, Ipswich, MA, USA), 0.25 mM each dNTP, 100 μg/mL BSA, 1 mM ATP, 3,500 unit/mL T4 DNA ligase (TAKARA Bio, Shiga, Japan), and 100 unit/mL T7 DNA polymerase (New England Biolabs). The covalently closed circular form (CCC) of pUC119-mis DNA was recovered by density gradient centrifugation using CsCl and ethidium bromide. The quality of the recovered CCC of pUC119-mis was tested by sensitivity against PstI and Nb. Bpu10I (Fig. II-3B).

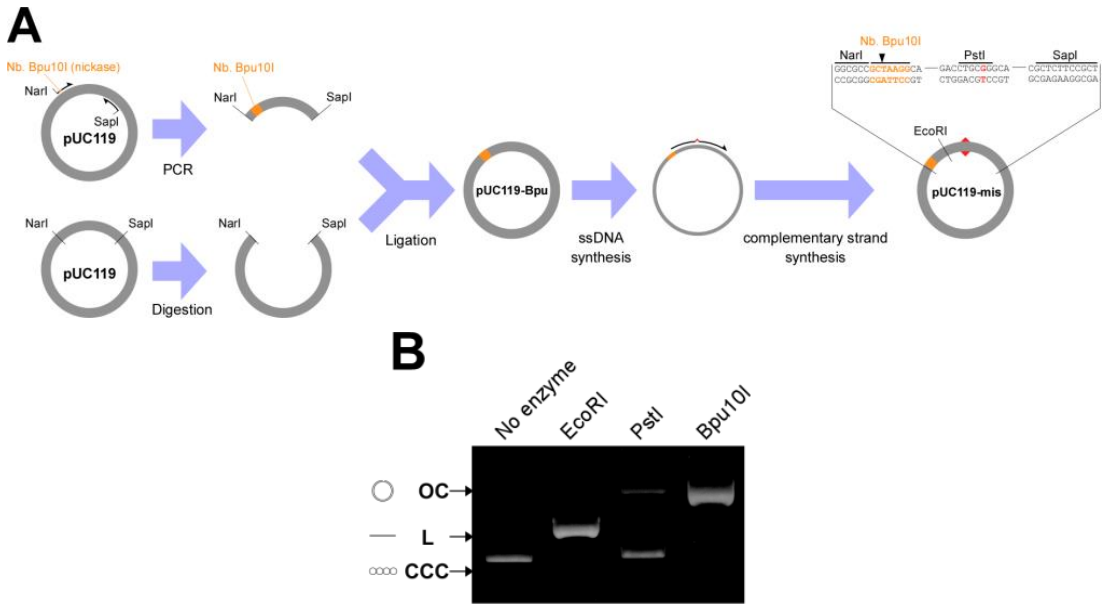

Figure II-3. The construction scheme for the GT-mismatch-containing plasmid DNA. (A) The method of construction is described in Materials and Methods. (B) The agarose gel electrophoresis of the covalently closed circular (CCC), linear (L), and open circular (OC) forms of pUC119-mis. pUC119-mis was treated with no enzyme, EcoRI, PstI or Nb. Bpu10I before electrophoresis.

Nicking endonuclease assay— In the assay using various concentrations of ttMutL, a 100 ng CCC form of DNA (pUc119-mis) in 10 μL buffer containing 50 mM HEPES-KOH, 1 mM DTT, 40 μg/mlL BSA, 4% glycerol, 0.1 mM EDTA, 5 mM $MgCl_2$, 5 mM $MnCl_2$, 0–8 μM ttMutL, and 750 μM ATP, pH 7.5 was incubated at 55°C for 10 min. In the assay using various concentrations of $MnCl_2$, a 100 ng CCC DNA in 10 μL buffer containing 50 mM HEPES-KOH, 1 mM DTT, 40 μg/mlL BSA, 4% glycerol, 0.1 mM EDTA, 5 mM $MgCl_2$, 0–10 mM $MnCl_2$, 500 nM ttMutL, and 750 μM ATP, pH 7.5 was incubated at 55°C for 10 min. In the assay using various concentrations of ATP, a 100 ng CCC DNA in 10 μL buffer containing 50 mM HEPES-KOH, 1 mM DTT, 40 μg/mlL BSA, 4% glycerol, 0.1 mM EDTA, 5 mM $MgCl_2$, 5 mM $MnCl_2$, 500 nM ttMutL, and 0–10 mM ATP, pH 7.5 was incubated at 55°C for 10 min. The final concentrations of ttMutL, $MnCl_2$, and ATP are indicated in the figure legends. In the time-course assay, 100 ng CCC DNA and 500 nM ttMutL or ttMutL CTD was incubated in buffer containing 50 mM HEPES-KOH, 60 mM KCl, 1 mM DTT, 40 μg/mL BSA, 4% glycerol, 0.1 mM EDTA, 750 μM ATP, 5 mM $MgCl_2$, and 5 mM $MnCl_2$, pH 7.5 at 55°C for 0 to 180 min. The reaction was terminated by addition of 5 μL stop solution containing 0.35% SDS, 0.3 mg/mL Proteinase K, 400 mM KCl, and 5 mM $MgCl_2$, and the mixture was incubated at 25°C for 15 min. The samples were electrophoresed on a 1% agarose gel in buffer containing 25 mM Tris-HCl, 25 mM boric acid, 0.5 mM EDTA, and 0.5 μg/mL ethidium bromide. The DNA bands were visualized by UV irradiation at 254 nm. In the assay for the effect of MMR proteins on the MutL endonuclease activity, a 150 ng CCC sample of DNA in 10 μL buffer containing 50 mM HEPES-KOH, 1 mM DTT, 40 μg/mL BSA, 4% glycerol, 0.1 mM EDTA, 750 μM ATP, 5 mM $MgCl_2$, and 5 mM $MnCl_2$, pH 7.5 was pre-incubated with 750 nM ttMutS, 40 nM DNA polymerase III δ and δ′ subunits, 60 nM γ and τ subunits, and/or 300 nM β clamp at 55°C for 10 min. Subsequently, 5 μL 1.5 μM ttMutL in the same buffer was added to the reaction mixture and incubated at 55°C for 10 min. Reaction conditions are detailed in each figure legend. In the time-course assay, 100

ng CCC DNA and 500 nM MutL or MutL CTD was incubated in buffer containing 50 mM HEPES-KOH, 60 mM KCl, 1 mM DTT, 40 μg/mL BSA, 4% glycerol, 0.1 mM EDTA, 750 μM ATP, 5 mM $MgCl_2$, and 5 mM $MnCl_2$, pH 7.5 at 55°C for 0 to 180 min. In the assay using various concentrations of ttMutL WT or mutants, 100 ng CCC DNA in 10 μL buffer containing 50 mM HEPES-KOH, 1 mM DTT, 40 μg/mL BSA, 4% glycerol, 0.1 mM EDTA, 750 μM ATP, 5 mM $MgCl_2$, and 5 mM $MnCl_2$, pH 7.5 was preincubated with or without 750 nM WT or K597M mutant of ttMutS at 55°C for 10 min. Subsequently, 5 μL of various concentrations of WT or E28A mutant of ttMutL in the same buffer was added to the reaction mixture and incubated at 55°C for 3 or 10 min. The final concentrations of WT and E28A mutant of ttMutL are indicated in the figure legends. To observe initial velocity, I stopped the reaction before linear form of plasmid DNA was generated. The reaction was terminated by addition of 5 μL stop solution containing 0.35% SDS, 0.3 mg/mL Proteinase K, 400 mM KCl, and 5 mM $MgCl_2$, and the mixture was incubated at 25°C for 15 min. The samples were electrophoresed on a 1% agarose gel in buffer containing 25 mM Tris-HCl, 25 mM boric acid, 0.5 mM EDTA, and 0.5 μg/mL ethidium bromide. The DNA bands were visualized by UV irradiation at 254 nm and quantified using ImageJ software.

Pull-down assay using plasmid DNA immobilized on sepharose beads—The preparation and immobilization of Singly-biotinylated OC or CCC form of plasmid DNA was carried out using the following procedures in (Higashi *et al*., 2012). The β clamp loading reaction was performed in 6 μL of reaction mixture containing 20 ng of Single biotinylated plasmid DNA (CCC or OC form) immobilized on sepharose beads was incubated with 300 nM β clamp, 60 nM γ and τ subunits, and/or 40 nM δ and δ′ subunits in the buffer containing 50 mM HEPES-KOH, 5 mM $MgCl_2$, 60 mM KCl, 4% glycerol, 40 μg/mL BSA, 1 mM DTT, and 750 μM ATP, pH 7.5 at 55°C for 10 min. The reaction mixture was diluted with 9 volume of the washing buffer containing 50 mM HEPES-KOH, 5 mM $MgCl_2$, 60 mM KCl, 4% glycerol,

and 40 μg/mL BSA and then centrifuged at 2,300 × g for 2 min. The supernatant was removed, and the DNA beads were washed with 60 μL of washing buffer containing 1 M KCl four times. DNA beads were suspended in SDS-PAGE sample buffer containing 31 mM Tris-HCl, 1% SDS, 5% glycerol, 700 mM β-mercaptoethanol, and 0.1% bromophenol blue and heat-treated at 95°C for 5 min. Samples were analyzed by Western blotting analysis described above.

Southern blotting analysis—A 150 ng of DNA substrate (pUC119-mis or nicked pUC119-mis) (Fig. II-4) in 10 μL buffer containing 50 mM HEPES-KOH, 1 mM DTT, 40 μg/mL BSA, 4% glycerol, 0.1 mM EDTA, 750 μM ATP, 5 mM $MgCl_2$, and 5 mM $MnCl_2$, pH 7.5 was pre-incubated with 750 nM ttMutS, 40 nM DNA polymerase III δ and δ′ subunits, 60 nM γ and τ subunits, and/or 300 nM β clamp at 55°C for 10 min. Subsequently, 5 μL 1.5 μM ttMutL in the same buffer was added to the reaction mixture and incubated at 55°C for 10 min. Reaction conditions are detailed in each figure legend. The reaction was terminated by addition of 5 μL stop solution containing 0.35% SDS, 0.3 mg/mL Proteinase K, 400 mM KCl, and 5 mM $MgCl_2$, and the mixture was incubated at 25°C for 15 min. The proteins in the reaction mixture were removed by addition of phenol/chloroform/isoamylalchol (25:24:1) mixture, and DNA was then recovered by ethanol precipitation. DNAs were digested by ScaI and/or PstI restriction enzyme and electrophoresed at 2.5 V/cm through 1% agarose gel in 50 mM sodium hydroxide and 1 mM EDTA.

DNA was transferred to a nitrocellulose membrane (Whatman) by traditional capillary transfer method with 10 × SSC (1.5 M sodium chloride and 150 mM sodium citrate). In nylon membrane, the membranes onto which immobilized DNA was dried up, and then crosslinking between membrane and DNA was carried out by UV irradiation with 120 mJ/cm^2. Membranes were pre-hybridized at 49˚C for 2 h in 500 mM sodium phosphate, 7% SDS, and 10 mM EDTA, pH7.2, then hybridized at 49˚C for 20 h in the same buffer

containing appropriate 5′-radiolabeled oligonucleotides (Table II-2). In nitrocellulose membrane, crosslinking between membrane and DNA was performed by UV irradiation with 120 mJ/cm^2, and pre-hybridization and hybridization was carried out at 49˚C for 20 h in 5 × SSC, 0.1% ficoll 400, 0.1% polyvinylpyrrolidone, 0.1% BSA, and 1% SDS, pH 7.2 with or without appropriate probes.

After hybridization, membranes were washed twice with 1 × SSC containing 0.1% SDS at 49˚C or 42˚C for 5 min, and then washed twice with 0.1 × SSC containing 0.1% SDS at 49˚C or 42˚C for 5 min. Membranes were dried up and placed in contact with an imaging plate to visualize and analyze the bands using BAS2500 imaging analyzer (Fuji Film). Membranes were stripped of probes by washing twice with 0.1 × SSC containing 0.5% SDS solution heated to boiling for 15 min. Membranes were then washed 0.1 × SSC containing 0.1% SDS, followed by pre-hybridized and hybridized.

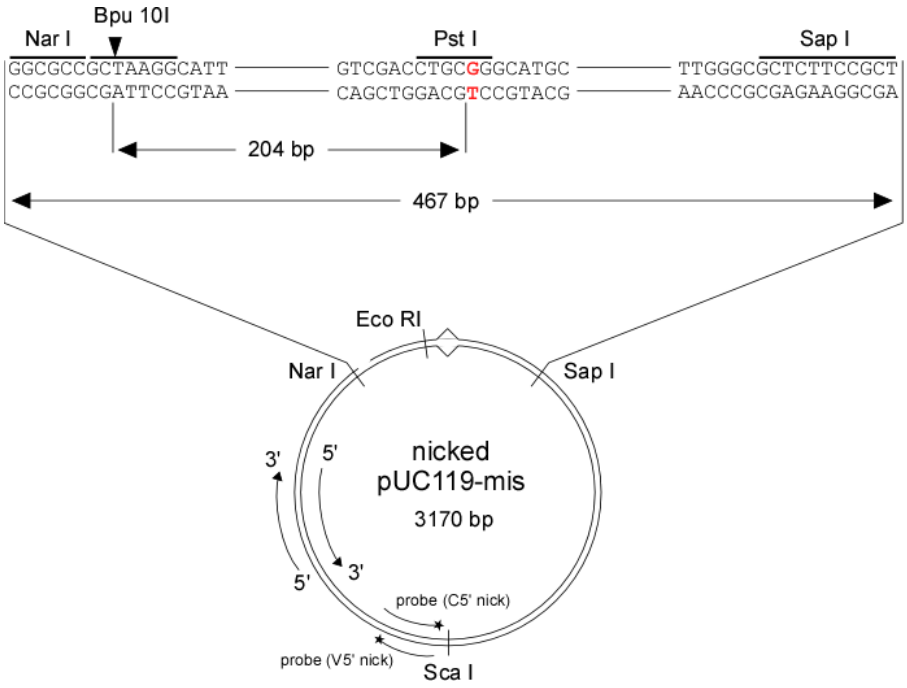

Figure II-4. The scheme of nicked pUC119-mis. The method of the construction was described in Fig. 4. For Southern blotting analysis, probes were created to hybridize with each strand. The sequences of probes were indicated in Table II-2.

Table II-2. The sequences of oligonucleotides using as probes.

Name	Sequence	*Position
V5′nick	5′-CGCCGCATACACTATTCTCAG-3′	2680–2700 in viral strand
C5′nick	5′-CTGAGAATAGTGTATGCGGCG-3′	2680–2700 in complementary strand

*The position number is counted from the first T in the sequence of TCGCGCGTTT.

Surface plasmon resonance analysis—Surface plasmon resonance (SPR) measurements were performed on a BIAcore 3000 (GE Healthcare Biosciences). The 9,000 response units of ttMutS were immobilized on a CM5 sensor chip (GE Healthcare Biosciences) using the amine coupling kit (GE Healthcare Biosciences). ttMutS was diluted to 200 μg/mL with 10 mM sodium acetate (pH 4.5), and injected over the sensor chip to generate the covalent bond between amine and ester group activated by1-ethyl-3-(3-dimethylaminopropyl)-carbodiimide and *N*-hydroxysuccinimide. Subsequently, 1 M ethanolamine hydrochloride (pH 8.5) was injected over the sensor chip to block the remaining activated ester group. In the preparation of the reference surface, amine coupling reaction was performed without ttMutS. Each concentration of full-length or the CTD of ttMutL was flowed over the immobilized ttMutS and blank surface in running buffer containing 10 mM HEPES-KOH, 150 mM NaCl, 50 mM EDTA, and 0.005% tween20, pH 7.2 at 30 μL/min at 25°C. After each measurement of the binding response, the sensor chip was regenerated with 25 mM NaOH and 500 mM NaCl at a flow rate of 30 μL/min for 10 sec. After subtracting the reference response units, the values of the dissociation constant (K_D) were determined by fitting the average response unit of the steady state (R_{eq}) to the following equation using Igor Pro 4.03 (Wavemetrics),

$$R_{eq} = R_{max}[S]/([S] + K_D) \qquad \text{(Eq. II-1)}$$

where R_{eq} and R_{max} correspond to $[ES]$ and $[E]0$, respectively, and $[S]$ is the free concentration of the full length or CTD of ttMutL. The R_{eq} value of each binding curve was determined by fitting the curve to the following equation using Igor 4.03,

$$R_t = R_{eq} - A(\exp^{-kt}) \qquad \text{(Eq. II-2)}$$

where R_t, A, and k are response units at each time point, an amplitude constant, and the

binding rate constant o the first-order reaction, respectively.

DNase I footprinting—The various concentrations of MutS were incubated with 10 nM 5′ -radiolabeled DNA substrate in 50 mM HEPES-KOH, 10 mM $MgCl_2$, 1 mM DTT, 40 μg/mL BSA, 4% glycerol, and 0.1 mM EDTA, pH 7.5 in the presence of 2 mM ADP and/or 2 mM ATP at 55°C for 10 min, followed by the addition of 0.01 U of DNase I (TAKARA Bio). The degradation by DNase I was stopped by the addition of equal volume of phenol/chloroform/isoamylalchol (25:24:1) mixture. The samples were loaded onto a 10% polyacrylamide gel and electrophoresed in the buffer containing 89 mM Tris-HCl, 89 mM boric acid, and 2.9 mM EDTA. The gels were dried and placed in contact with an imaging plate to visualize and analyze the bands with a BAS2500 imaging analyzer (Fuji Photo Film, Tokyo, Japan)

Trans-activation analysis—The 120-bp double-stranded DNA with a GT mismatch was obtained by hybridizing the single-stranded DNA, 120-2T with the complementary single-stranded DNA 120-1G (Table II-1). The GT mismatched double-stranded DNA (2.25 pmol 120-bp) was pre-incubated with 750 nM MutS in reaction buffer (10 μL) containing 50 mM HEPES-KOH, 1 mM DTT, 40 μg/mL BSA, 4% glycerol, 0.1 mM EDTA, 750 μM ATP, 5 mM $MgCl_2$, and 5 mM $MnCl_2$, pH 7.5, at 55°C for 10 min. A 5 μL 1.5 μM MutL in the same buffer containing 180 mM KCl and 48 fmol CCC DNA with or without a GT mismatch was then added to the reaction mixture and incubated at 55°C for 10 min. The reaction was terminated by addition of 5 μL termination mixture containing 0.35% SDS, 0.3 mg/mL proteinase K, 400 mM NaCl, and 5 mM $MgCl_2$. The samples were electrophoresed on a 1% agarose gel in buffer containing 25 mM Tris-HCl, 25 mM boric acid, 0.5 mM EDTA, and 0.5

μg/mL ethidium bromide. The DNA bands were visualized by UV irradiation at 254 nm.

ATPase assay–ATPase activity was assayed in 10 μL reaction mixture containing 50 mM HEPES-KOH, 5 mM $MgCl_2$, 1 mM DTT, 4% glycerol, 40 μg/mL BSA, 500 nM MutS or MutL, and 10 μM to 2 mM ATP and 22 nM γ-^{32}P-radiolabeled ATP, pH 7.5. Reactions were initiated by addition of hot and cold ATP, incubated at 70°C for 10 or 30 min, and terminated by addition of an equal volume of phenol/chloroform/isoamylalcohol (25:24:1) and 1 μL of 10 mM EDTA. Aqueous fractions were recovered by centrifugation, and then 0.5 μl of each samples were spotted onto a polyethyleneimine cellulose plate (Merck KGaA) and analyzed by thin-layer chromatography (TLC). Labeled intact ATP and released phosphate were separated by developing the TLC plate in 0.5 M formic acid and 0.25 M LiCl at room temperature for 5 min. The TLC plate was dried and placed in contact with an imaging plate to visualize and analyze the spots using BAS2500 imaging analyzer (Fuji Photo Film Co., Kanagawa, Japan). The initial rate was calculated by quantifying the proportion of released phosphate to unreacted ATP, and kinetic parameters were determined from the Michaelis-Menten equation.

RESULTS

The cellular concentrations of MutL and MutS

It was reported that the endonuclease activity of relatively low concentrations (500 nM) of MutL from *Thermus thermophilus* (ttMutL) and *Aquifex aeolicus* (aaMutL) was inhibited in the presence of ATP (Fukui *et al*., 2008). I showed that high concentrations of ttMutL were activated in the presence of ATP (Fig. II-5A). Thus, the difference in these results of the response of MutL to ATP was attributed to differences in MutL concentrations. Therefore, I first determined the intracellular concentration of ttMutL in *T. thermophilus* HB8.

T. thermophilus HB8 was cultured and harvested at each time point in the growth curve (Fig. II-6A). The cell lysates were Western blotted to detect endogenous ttMutS and ttMutL (Fig. II-6B and C, left panel). Referencing the standard curve generated by the same experiment with recombinant ttMutS and ttMutL proteins (Fig. II-6B and C, right panel), the intracellular concentrations of ttMutS and ttMutL were determined to be approximately 500 nM and 300 nM, respectively, at logarithmic growth phase (Table II-4). Protein concentrations gradually decreased as growth progressed (Fig. II-6B, C, and Table II-3). Previously, it was demonstrated that the intracellular concentrations of *E. coli* MutS and MutL are approximately 1000 nM and 600 nM, respectively. It was also reported that the concentrations of *E. coli* MutS and MutL decreased gradually as growth progressed (Feng *et al*, 1996). Therefore the concentrations of ttMutL and ttMutS were comparable to those of *E. coli* MutS and MutL. Because DNA replication and MMR frequently occur during logarithmic growth, the concentration of ttMutL at logarithmic phase will be adequate for the endonuclease assay. Therefore, in this study, I conducted endonuclease assays with 500 nM ttMutS and ttMutL.

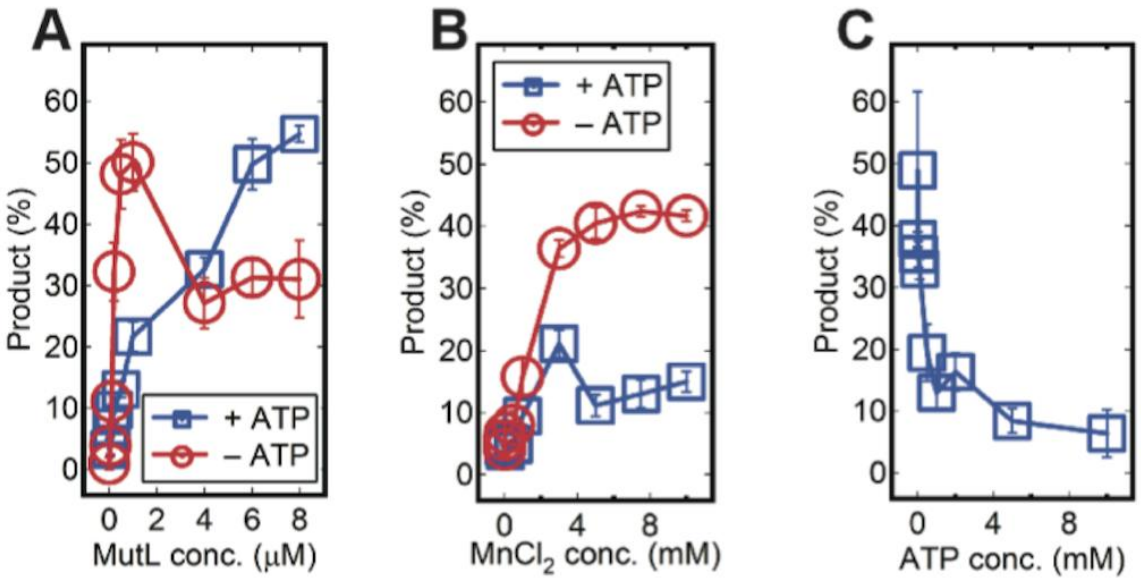

Figure II-5. The endonuclease activity in the presence of various concentrations of ttMutL, $MnCl_2$, or ATP. (A) The DNA products cleaved by 0, 0.05, 0.1, 0.2, 0.5, 1, 4, 6, and 8 μM ttMutL were shown. (B) The reaction was performed in the presence of 0, 0.025, 0.05, 0.5, 1, 3, 5, 7.5, or 10 mM $MnCl_2$. Red and blue indicate that the reactions were performed in the absence of ATP and presence of ATP, respectively. (C) The reaction was performed in the presence of 0, 0.01, 0.05, 0.1, 0.5, 1, 2, 5, or 10 mM ATP.

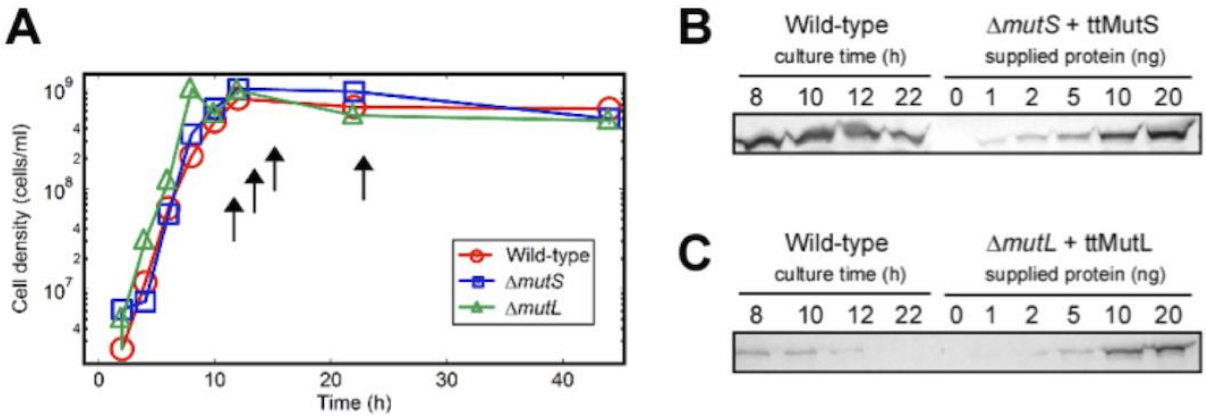

Figure II-6. Cellular concentrations of ttMutS and ttMutL were analyzed by quantitative Western blot analysis. (A) Growth curves of *T. thermophilus* HB8 WT (circle), Δ*mutS* (square), and Δ*mutL* (triangle) strains. Growth of each strain was monitored by counting the number of cells. Cells were harvested by centrifugation at 8, 10, 12, and 22 h after inoculation. (B) Harvested cells were Western blotted using anti-ttMutS antibody as described in the Materials and Methods. The indicated amount of purified recombinant ttMutS was mixed with cell lysate from the Δ*mutS* strain. The mixture was electrophoresed on the same gel to obtain a standard curve for estimation of the amount of endogenous ttMuS. (C) Western bloting with anti-ttMutL antibody was performed as in (B).

Table II-3. ttMutS and ttMutL concentrations in the cell

Protein	Culture time (h)	Concentration (nM)
ttMutS	8	505 ± 74.9
	10	329 ± 58.3
	12	169 ± 47.2
	22	133 ± 16.2
ttMutL	8	299 ± 54.9
	10	203 ± 21.1
	12	97.2 ± 29.4
	22	n.d.*

n.d.*, not detected

MutL endonuclease activity is inhibited by ATP

The endonuclease activity of ttMutL was analyzed by monitoring the conversion of a CCC form of plasmid DNA to its open circular (OC) or linear (L) form. To examine the ability of MutL to distinguish hom- and heteroduplexes, I used perfectly matched plasmid DNA (pUC119) and the GT mismatched plasmid DNA (pUC119-mis) as substrates. The construction of pUC119-mis is described in the Materials and Methods (Fig. II-3A). To determine the electrophoretic mobility of the OC form of plasmid DNA, the recognition site for nickase Nb. Bpu10I was introduced into pUC119-mis. The purified CCC form of pUC119-mis was treated with EcoRI, PstI, or Bpu10I, and then electrophoresed on 1% agarose gel (Fig. II-3B). Because pUC119-mis has a GT mismatch in the PstI site, the CCC form of pUC119-mis was resistant to digestion by PstI. The CCC form of pUC119-mis treated with EcoRI and Nb. Bpu10I was converted into L and OC forms, respectively. The CCC, L, and OC forms exhibited high, moderate, and low mobility, respectively.

ATP tightly inhibited the endonuclease activity of ttMutL (Fig. II-7A and B). In Fig. II-7A-C, the plasmid DNA containing a GT mismatch was used as a substrate. The inhibition was observed in the presence of various concentrations of ATP and $MnCl_2$ (Fig. II-5B and C). The nicked and linearized products generated by ttMutL were about 5-fold higher in the absence of ATP than in the presence of ATP (Fig. II-7C). With the perfectly-matched pUC119 substrate, the endonuclease activity of ttMutL was also inhibited in the presence of ATP (Fig. II-7D-F).

Addition of ATP did not suppress the endonuclease activity of ttMutL when $MnCl_2$ was substituted with $MgCl_2$ (Fig. II-7G-I). The necessity of manganese ion for ATP regulation suggests manganese ion may be a physiological cofactor for the endonuclease activity of ttMutL. This notion is also supported by previous findings that MutL homologs from *Homo sapiens*, *Saccharomyces cerevisiae*, *Bacillus subtilis*, *A. aeolicus* and *Neisseria gonorrhoeae* exhibit maximal endonuclease activity in the presence of $MnCl_2$ (Duppatla *et al.*, 2009; Iino

et al., 2011).

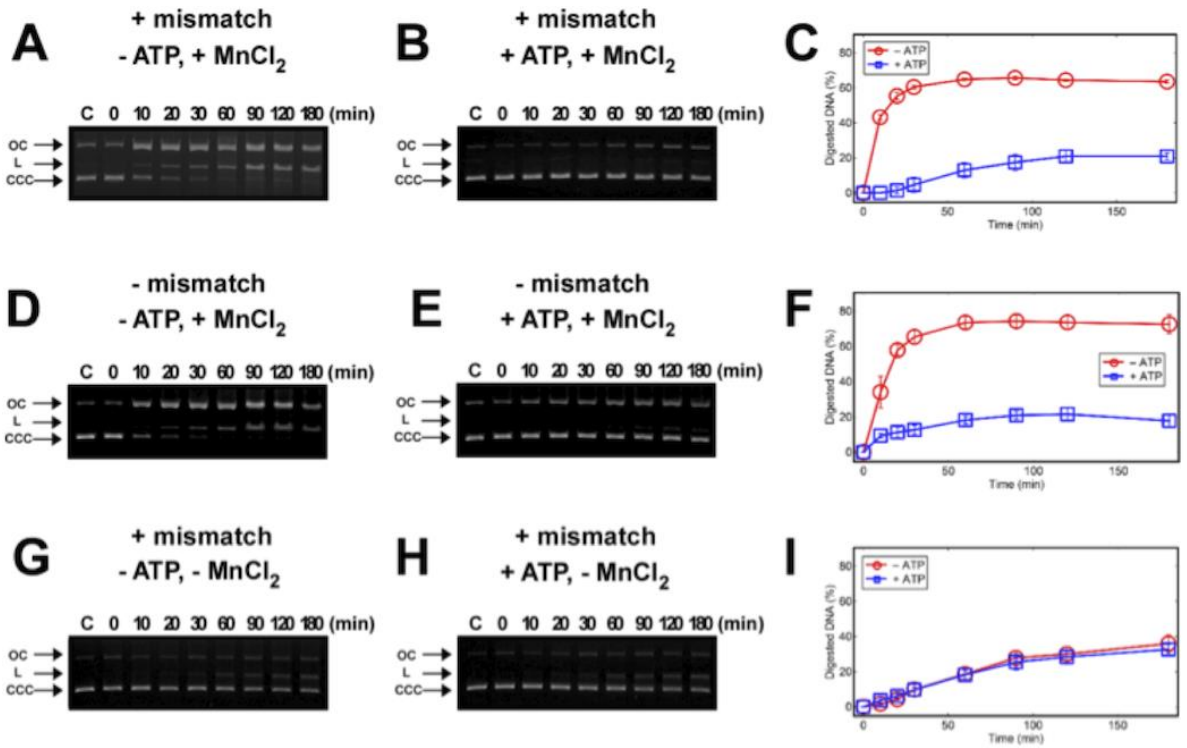

Figure II-7. ATP-dependent suppression of ttMutL endonuclease activity required $MnCl_2$. (A-C) Time-course assay for the endonuclease activity of ttMutL using pUC119-mis as a substrate in the presence of $MnCl_2$. (A) Reaction performed in the absence of ATP. (B) Reaction performed in the presence of ATP. (C) After subtracting the background, the percentage of total products (nicked and linearized DNA) was plotted against reaction time. Red and blue lines correspond to (A) and (B), respectively. (D-F) Time-course assay of ttMutL endonuclease activity using pUC119 as a substrate in the presence of $MnCl_2$. (D) Reaction performed in the absence of ATP. (E) Reaction performed in the presence of ATP. (F) After subtracting the background, the percentage of total products generated by ttMutL was plotted against reaction time. Red and blue lines correspond to (D) and (F), respectively. (G-I) Time-course assay of ttMutL endonuclease activity using pUC119-mis as a substrate in the absence of $MnCl_2$. (G) Reaction performed in the absence of ATP. (H) Reaction performed in the presence of ATP. (I) The percentage of total products is plotted against reaction time. Red and blue lines correspond to (G) and (H), respectively.

The interaction between MutL and the other MMR proteins

To characterize the activation mechanism for ATP-bound ttMutL, I tested the effects of other MMR proteins on ttMutL endonuclease activity. I selected clamp loader (DNA polymerase III γ, τ, δ, and δ′ subunits), β clamp, and ttMutS, because these proteins are expected to function upstream of nick introduction (Fig. G-1). Although the full clamp loader complex in a bacterial cell is composed of DNA polymerase III γ, δ, δ′, ψ, and χ subunits (Dong *et al*., 1993), *T. thermophilus* does not have the genes encoding DNA polymerase III ψ, and χ subunits. Therefore, DNA polymerase III γ, τ, δ, and δ′ subunits are sufficient for composing clamp loader complex in *T. thermophilus*.

Our far-Western blotting experiments suggested that, in *T. thermophilus*, ttMutL interacts with DNA polymerase III γ and τ subunits, β clamp, and ttMutS (Fig. II-8). These interactions were confirmed by co-immunoprecipitation analyses (Fig. II-9). The far-Western analyses support the interaction of the recombinant DNA polymerase III γ and τ subunits with the recombinant δ and δ′ subunits (Fig. II-8A and B), indicating the clamp loader complex was successfully reconstituted from recombinant subunits.

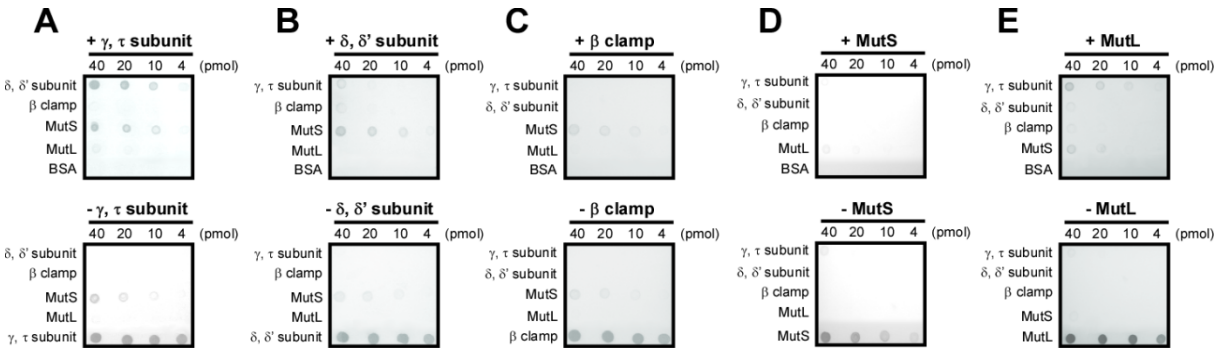

Figure II-8. The interactions among MMR proteins analyzed by far-Western blotting. Each MMR protein (1 to 40 pmol) (indicated at the left side of the panel) was spotted on nitrocellulose membranes, and incubated with (upper panels) or without (lower panels) each bait protein. Then, the membrane was immunostained with the antibody against the bait protein. The detected spots in lower panels indicate the non-specific. (A) DNA polymerase III γ and τ subunits were used as a bait protein. (B) DNA polymerase III δ and δ′ subunits were used as a bait protein. (C) β clamp was used as a bait protein. (D) ttMutS was used as a bait protein. (E) ttMutL was used as a bait protein.

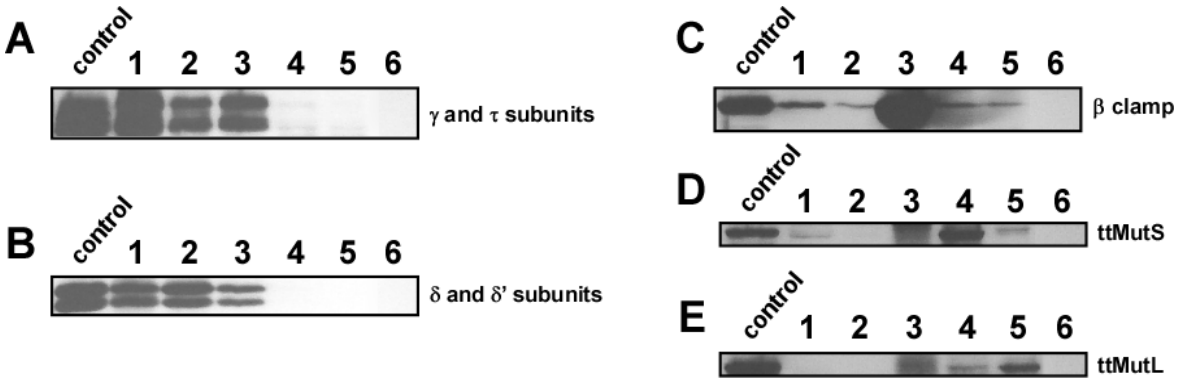

Figure II-9. The interactions among MMR proteins analyzed by immunoprecipitation. The protein mixtures immunoprecipitated with anti-γ and τ subunits, anti-δ and δ′ subunits, anti-β clamp, anti-ttMutS, or anti-ttMutL antibody were applied to lanes 1 through 5 of an SDS-polyacrylamide gel, respectively. Preimmune serum was used as a negative control for the immunoprecipitation (lane 6). Each purified recombinant protein (20 pmol) was applied to a control lane. Separated immunoprecipitates were electrotransferred to PVDF membrane, and then were Western blotted using anti-γ and -τ subunits antibody (A), anti-δ and -δ′ subunits antibody (B), anti-β clamp antibody (C), anti-ttMutS antibody (D), anti-ttMutL antibody (E).

The effect of MMR proteins on ttMutL endonuclease activity

To investigate the effect of MMR proteins on the endonuclease activity of ttMutL, each MMR protein was pre-incubated with substrate DNA, and then ttMutL was added to the reaction mixture. Without ttMutL, the other MMR proteins showed no detectable activity to generate nicked or linearized plasmid DNA (Fig. II-10A and B). When the reaction mixture contained a mismatch, ATP, and $MnCl_2$, ttMutS stimulated ttMutL endonuclease activity: the rate of accumulation of the products generated by ttMutL was 6-fold higher in the presence of ttMutS than in the absence of ttMutS (Fig. II-10C and D). No stimulation by ttMutS was observed when the reaction was performed without ATP (Fig. II-10E and F). The stimulating effect of ttMutS was also abolished by substituting $MnCl_2$ with $MgCl_2$ (Fig. II-10G and H). Furthermore, ttMutS did not induce ttMutL endonuclease activity when mismatch-free plasmid DNA was used as a substrate (Fig. II-10I-L), indicating that the ttMutS-dependent stimulation of ttMutL requires a mismatch. Unlike ttMutS, DNA polymerase III subunits (γ, τ, δ, δ′ subunits and β clamp) showed no effect on the endonuclease activity of ttMutL (Fig. II-10C-H).

In order to confirm whether recombinant clamp loader and β clamp were active or inactive form, I carried out the pull-down assay using DNA substrates immobilized on Sepharose beads (Higashi *et al*., 2012). This result showed that β clamp was loaded onto the DNA dependent on the clamp loader complex (Fig. II-11). Although it was reported that RFC recruits PCNA on the discontinuous DNA more efficiently than continuous one (Pluciennik *et al*., 2010; Produst *et al*., 1995; Yao *et al*., 2000), my experiment showed that the clamp loader of *T. thermophilus* loaded β clamp efficiently on the DNA regardless of discontinuity. Furthermore, the effect of β clamp and DNA on the ATP hydrolysis activity of the clamp loader was analyzed. It is known that clamp loader recruits clamps on to the DNA using ATP hydrolysis energy, and its ATP hydrolysis activity is activated in the presence of β clamp and DNA (Leu and O′Donnell 2001; Turner *et al*., 1999; Yao *et al*., 2000).

Consistent with the results of pull-down assay, the ATP hydrolysis activity was activated by β clamp, open circular, and covalently closed circular DNA (Fig. II-12). These results confirmed that the clamp loader and β clamp bound on the substrate DNA under the reaction condition used in the endonuclease activity assay.

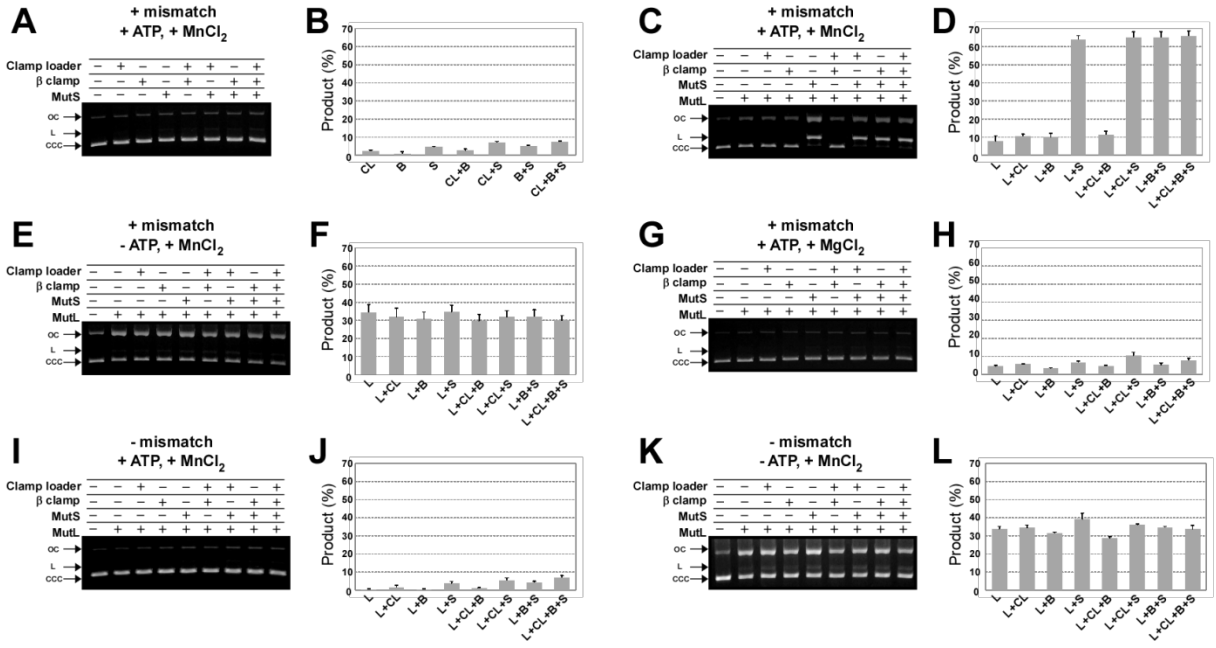

Figure II-10. The effect of MMR proteins on ttMutL endonuclease activity. (A to H) pUC119-mis was used as a substrate. (A) Endonuclease assay without ttMutL. Reaction performed in the presence of $MnCl_2$ and ATP. (B) The percentages of reaction products in (A) are shown in a bar graph. (C) The endonuclease assay was carried out in the presence of $MnCl_2$ and ATP. (D) The percentages of reaction products in (C) are shown. (E) The endonuclease assay was carried out without ATP in the presence of $MnCl_2$. (F) The percentages of reaction products in (E) are shown. (G) The endonuclease assay was carried out in the absence of $MnCl_2$ and in the presence of ATP. (H) The percentages of reaction products in (G) are shown. (I to L) pUC119 was used as a substrate. (I) The reaction was carried out in the presence of ATP. (J) The percentages of reaction products in (I) are shown in a bar graph. (K) The reaction was carried out in the absence of ATP. (L) The percentages of reaction products in (K) are shown. L, CL, B, and S indicate ttMutL, clamp loader, β clamp, and ttMutS, respectively. Error bars indicate standard deviations. The concentrations of ATP, $MgCl_2$, and $MnCl_2$ used in this study were 750 μM, 5 mM, and 5 mM, respectively.

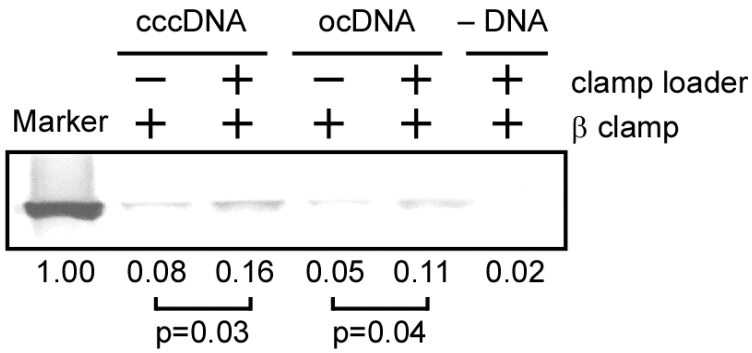

Figure II-11. β clamp loading assay using plasmid DNA immobilized on sepharose beads. Purified 2.25 fmol β clamp was electrophoresed on marker lane. Minus DNA means that β clamp loading reaction was performed using sepharose beads with no DNA. The intensities of stained β clamp bands were quantified by ImageJ software. Numbers below each lane represent quantified signals relative to marker lane. The p values for the effect of clamp loader are calculated.

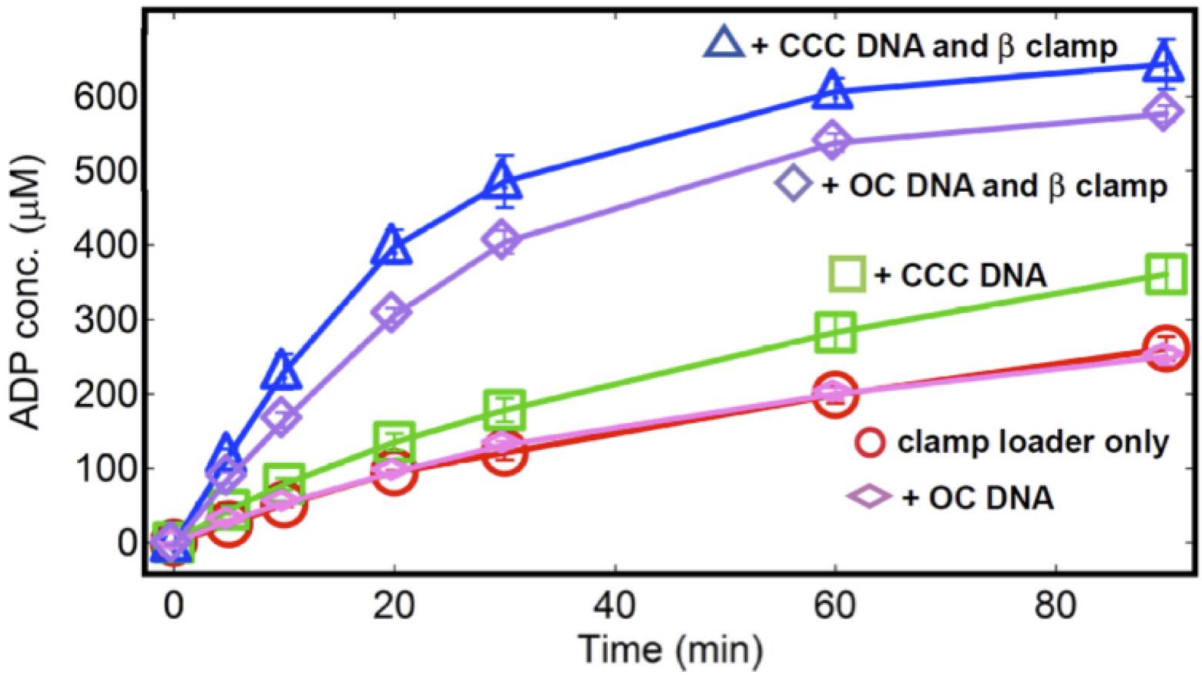

Figure II-12. The effects of β clamp and DNA on the ATPase activity of clamp loader. The concentrations of generated ADP were plotted against the reaction time. Each plot indicates the results of the ATPase assay in the absence of β clamp and DNA (○), in the presence of CCC DNA (□), in the presence of β clamp and CCC DNA (△), in the presence of OC DNA (◇), and in the presence of β clamp and OC DNA (◇). All data are shown after subtracting background value obtained from the assay with no clamp loader.

The strand discrimination in MMR of *T. thermophilus*

It was expected that, similar to eukaryotic MMR, the strand discrimination was achieved via the interaction between MutL and β clamp in general bacterial MMR. I tried to reconstruct the strand discrimination system by using the counterparts of the proteins used in the eukaryotic MMR reconstitution (Pluciennik *et al*., 2010). Interestingly, β clamp did not confer the strand specificity on ttMutL nicking activity (Fig. II-13). If the loading orientation of β clamp serves as the strand discrimination signal, nicks would be introduced by ttMutL into the complementary strand containing a pre-existing nick. However, ttMutL equally incised both viral and complementary strand. Furthermore, the nick introduction was observed depending on the presence of ttMutS in the reaction mixture, whereas β clamp and clamp loader showed no effect on the ttMutL endonuclease activity. These results suggest that the β clamp-ttMutL interaction does not serve as the strand discrimination signal and that another factor is involved in the strand discrimination in *T. thermophilus*.

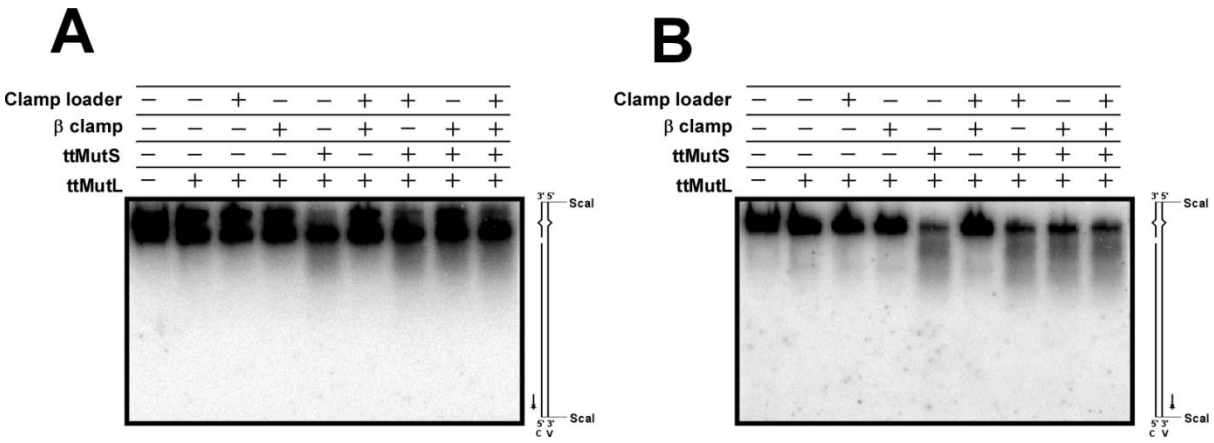

Figure II-13. The effect of a nick on ttMutL activation. Endonuclease activity was analyzed by Southern blotting using nicked pUC119-mis as a substrate. (A) The degraded products were determined using V5′nick probe hybridizing to the complementary strand (Table II-2). (B) The degraded products were determined using C5′nick probe hybridizing to the viral strand (Table II-2). The sheme of ScaI digested pUC119-mis containing a nick was shown in right of each panel. The characters of C and V indicates complementary and viral strand, respectively.

Activation of ttMutL required ATP hydrolysis by ttMutS and ttMutL

To determine whether ATP hydrolysis is required for the stimulation of ttMutL endonuclease activity, the endonuclease assay was performed in the presence of ADP or AMPPNP, a non-hydrolyzable analog of ATP. No stimulation by ttMutS was observed in the presence of ADP (Fig. II-14 A and K) or AMPPNP (Fig. II-14 B and K). On eukaryotic and bacterial MutS homologues, it has been reported that ADP-bound MutS binds to DNA and recognize the lesion whereas ATP-bound MutS is unable to recognize the lesion (Antony and Hingorani, 2003, Antony and Hingorani, 2004, Zhai and Hingorani, 2010). ATP-binding induces the conformational changes in MutS to form a clamp like formation to release from a mismatched base (Allen *et al*, 1997; Gradia *et al*, 1999). Because ATP-bound MutS forms the ring shape, ATP-bound MutS rarely binds on continuous DNA (Biswas and Vijayvargia R, 2000; Lamers et al., 2004). In the presence of AMPPNP alone, there was a possibility that AMPPNP-bound ttMutS was unable to bind to the DNA and to recognize a mismatched base. Hence, to reveal whether ATP hydrolysis by ttMutS and/or ttMutL is necessary for ttMutL activation, I investigated the endonuclease assay in the presence of both ADP and AMPPNP. As a result, stimulation of ttMutL by ttMutS was also rarely observed in the presence of both ADP and AMPPNP (Fig. II-14J), implying that the activation of the endonuclease activity requires ATP hydrolysis generated by ttMutS and/or ttMutL.

Since AMPPNP is not identical to ATP, I could not rule out the possibility that the difference observed with ATP and AMPPNP was due to the different binding modes of the each nucleotide to ttMutS and/or ttMutL. Then, I created the ATPase-deficient mutants of ttMutS and ttMutL by mutagenizing putative catalytic amino acid residues in order to further examine the effect of ATP hydrolysis on the stimulation of ttMutL endonuclease. In *E. coli* MutS and MutL, several amino acid residues have shown to be involved in catalysis (Ban *et al*., 1999; Junop *et al*., 2001; Lamers *et al*., 2000). The amino acid residues participating in ATP hydrolysis in ttMutS and ttMutL were predicted based on an alignment of ATPase motifs

(Fig. II-15) and mutagenized. The ttMutS mutant derivatives K597M and E671A showed k_{cat} values 3-fold and 12-fold lower than WT, respectively (Table II-4). ttMutL E28A exhibited no ATP hydrolysis activity. In contrast, k_{cat} value of D57A ttMutL was similar to that of WT (Table II-4). However, the K_M value of D57A was 780 μM, about 2-fold higher than that of WT (Table II-4). Because the concentration of ATP used for the endonuclease assay was 750 μM, the D57A mutant was only capable of half-maximum velocity of ATP hydrolysis.

Table II-4. Kinetics of ATPase activity
ATPase assays of MutS and MutL were performed at 70˚C for 10 and 30 min, respectively.

Protein name		K_M (μM)	k_{cat} (min^{-1})
ttMutS	WT	50.7 ± 9.87	9.19 ± 1.81
	K597M	53.9 ± 3.55	1.92 ± 0.120
	E671A	457 ± 267	0.522 ± 0.0912
ttMutL	WT	461 ± 138	0.614 ± 0.123
	E28A	n.d.*	n.d.*
	D57A	785 ± 202	0.564 ± 0.125

n.d.*, not detected

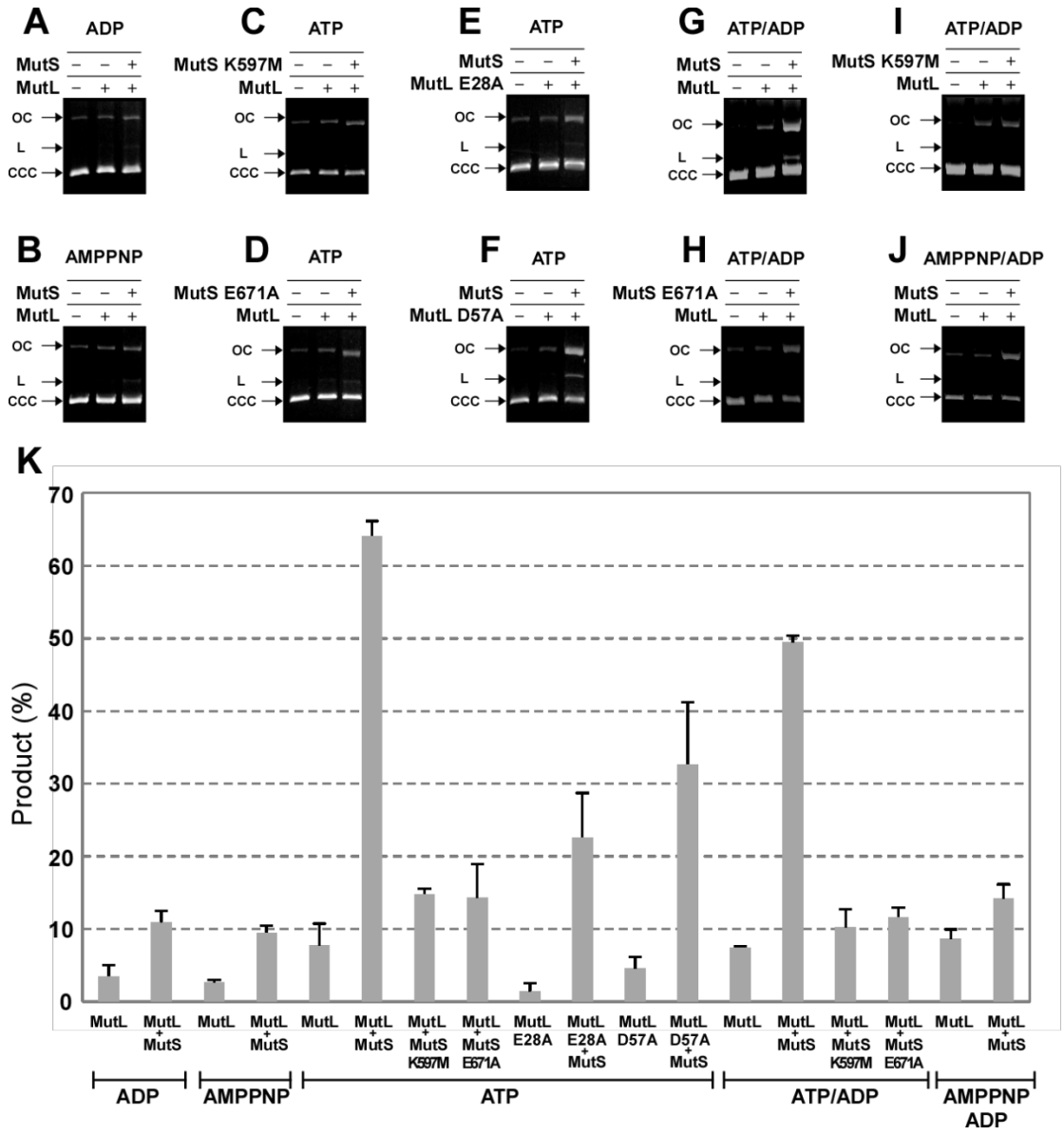

Figure II-14. The effect of ATP hydrolysis by ttMutS and MutL on the endonuclease activity of ttMutL. (A) The reaction was performed in the presence of ADP. (B) The reaction was performed in the presence of AMPPNP. (C-F) The reaction was performed in the presence of ATP. (C) ttMutS K597M was used for the reaction instead of ttMutS WT. (D) ttMutS E671A was used for the reaction instead of ttMutS WT. (E) ttMutL E28A was used for the reaction instead of ttMutL WT. (F) ttMutL D57A was used for the reaction instead of ttMutL WT. (G-I) The reaction was performed in the presence of both ATP and ADP. (H) ttMutS K597M was used for the reaction instead of ttMutS WT. (I) ttMutS E671A was used for the reaction instead of ttMutS WT. (J) The reaction was performed in the presence of both AMPPNP and ADP. (K) The percentages of reaction products in (A-J) and ttMutL WT-ttMutS WT in the presence of ATP are shown.

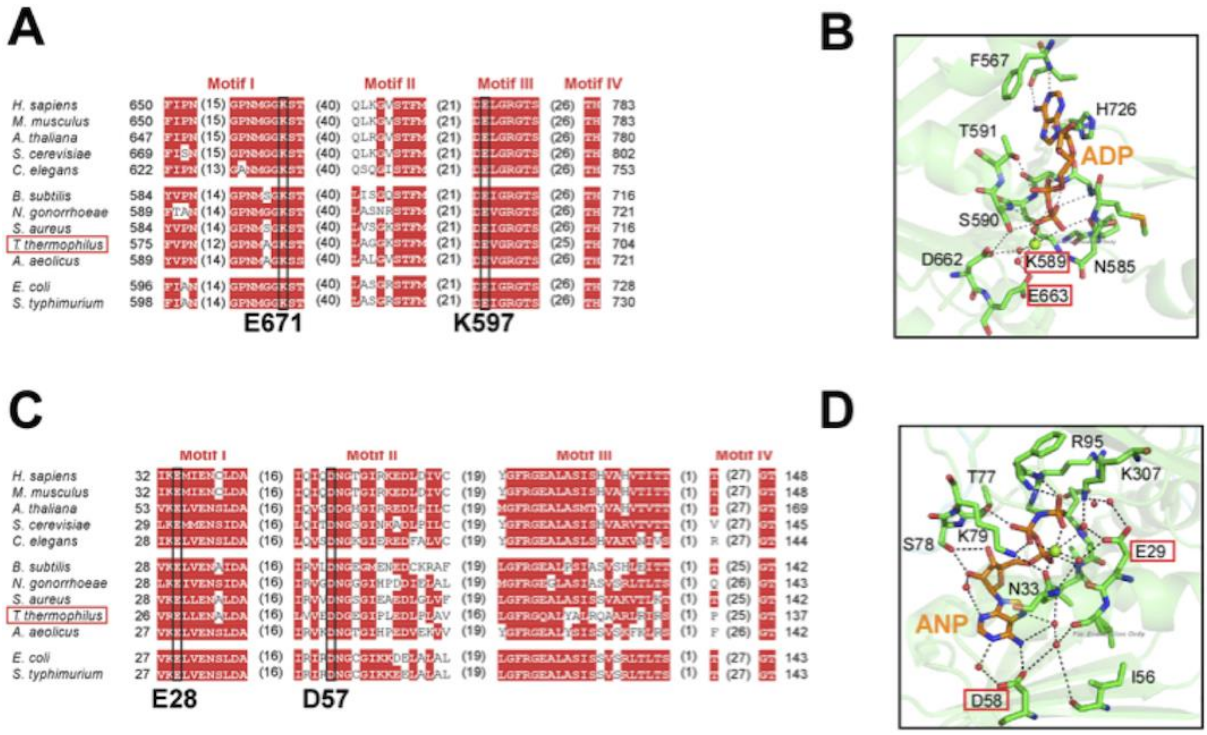

Figure II-15. Amino acid sequence alignment of the ATPase motifs in MutS and MutL homologues. Red box indicates the conserved sequence motifs of ABC (A) and GHL (C) ATPase superfamilies. The amino acids in the black box are target residues for ATPase-deficient mutants. The numbers on the left and right show the distances from the N-termini for each protein. The numbers in parentheses show the number of residues that are omitted for the sake of clarity. The NCBI Entrez GI numbers of the sequences are as follows: (A) 4505913 (*H. sapiens* PMS2), 121583910 (*M. musculus* PMS2), 18411951 (*Arabidopsis thaliana* PMS1), 46562124 (*S. cerevisiae* PMS1), 17562796 (*Caenorhabditis elegans* PMS2), 16078768 (*B. subtilis* MutL), 59801161 (*N. gonorrhoeae* MutL), 15926879 (*S. aureus* MutL), 55981292 (*T. thermophilus* MutL), 15606703 (*A. aeolicus* MutL), 16131992 (*E. coli* MutL), and 16767605 (*S. typhimurium* MutL), (B) 4504191 (*H. sapiens* Msh6), 6754744 (*M. musculus* Msh6), 332656720 (*A. thaliana* Msh6–1), 6320320 (*S. cerevisiae* Msh6), 17508447 (*C. elegans* Msh6), 255767391 (*B. subtilis* MutS), 59802243 (*N. gonorrhoeae* MutS), 379991612 (*S. aureus* MutS), 55981293 (*T. thermophilus* MutS), 15605835 (*A. aeolicus* MutS), 16130640 (*E. coli* MutS), and 16761683 (*S. typhimurium* MutS). (B) The ATP binding site of *Thermus aquaticus* MutS (PDB ID, 1FW6). (D) The ATP binding site of *E. coli* MutL (PDB ID, 1B63). The amino acids in red box correspond to the target amino acids for mutagenizing in *T. thermophilus* MutS and MutL. Red and green sphere indicate water and Mg^{2+} ion, respectively.

The stimulation of ttMutL endonuclease activity by K597M (Fig. II-14C and K) and E671A (Fig. II-14D and K) mutants of ttMutS was at the lower limit of detection. As described above that, in eukaryote and bacteria, ATP-bound MutS is unable to bind on circular DNA, there was the possibility that ATPase deficient mutants of ttMutS bound ATP and could not bind on DNA in the presence of ATP alone. To exclude this possibility, the endonuclease assay was carried out in the presence of both ATP and ADP (Fig. II-14G-I). In the presence of both ATP and ADP, the stimulation rate of ttMutL endonuclease by ttMutS WT was lower than in the presence of ATP alone (Fig. II-14K), suggesting competitive inhibition by ADP. In the presence of both ATP and ADP, the amount of endonucleolytic products by ttMutL in the presence of ttMutS WT was 4-fold higher than in the absence of ttMutS WT (Fig. II-14G and K). On the other hand, ATPase deficient mutants of ttMutS slightly stimulated endonuclease activity of ttMutL in the presence of ATP alone (Fig. II-14C, D, and K). Furthermore, in the presence of both ATP and ADP, ttMutL activation by ATPase deficient mutants of ttMutS was also slightly observed (Fig. II-14I-K). From these results, it is strongly suggested that ATP hydrolysis by ttMutS is essential for stimulation of endonuclease activity of ttMutL.

The ATPase-deficient ttMutL mutants were also activated by ttMutS WT (Fig. II-14E, F, and K). However, the efficiencies of ttMutS-dependent activation of the ttMutL mutants were 2-fold lower than that of ttMutL WT. The k_{app} value determined using WT of ttMutS and ttMutL was 7 and 3 times higher than that determined using mutants of ttMutS and ttMutL, respectively (Fig. II-16). Thus, ATP hydrolysis by ttMutS and ttMutL was involved in the activation of ttMutL. ATP hydrolysis by ttMutS more significantly contributed to the activation of ttMutL than the ATP hydrolysis by ttMutL under this experimental condition.

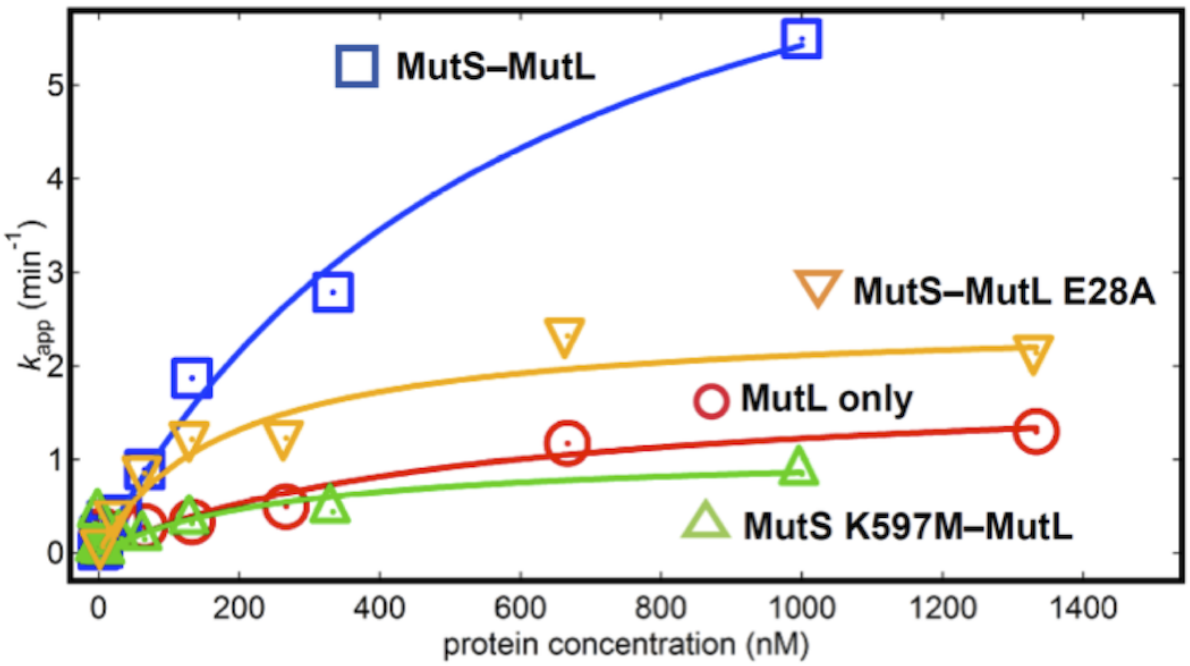

Figure II-16. The effect of ttMutS on the endonuclease activity of ttMutL. The velocity of generating OC form of plasmid DNA was plotted against concentrations of ttMutL WT or E28A mutant. Each plot indicates the results of the endonuclease assay using ttMutL WT without ttMutS (○), ttMutL WT with 500 nM ttMutS WT (□), ttMutL E28A with 500 nM ttMutS WT (▽), and ttMutL WT with 500 nM ttMutS K597M (△). The data were fitted to the Michaelis-Menten equation using Igor Pro 4.03, and the theoretical curves are shown. Because our method does not detect the incision reaction on the open circular form of plasmid DNA, accurate parameters were not determined.

No stimulation was detected in the N-terminal domain-deleted mutant of ttMutL

To analyze the function of the N-terminal ATPase domain of ttMutL, I constructed an NTD deletion mutant, leaving only the C-terminal domain (CTD) of ttMutL. It has been reported that the CTD contains endonuclease motifs and is sufficient for endonuclease activity (Duppatla *et al*., 2009; Fukui *et al*., 2008; Fukui *et al*., 2011; Kadyrov *et al*., 2006; Kolodner and Marsischky, 1999; Pillon *et al*., 2010) (Fig. II-17). I demonstrated that the ATP-dependent inhibition of ttMutL endonuclease was not observed with the ttMutL CTD (Fig. II-17 and 18), which supports our hypothesis that the ATP-bound NTD suppresses the endonuclease activity of the CTD via interdomain interaction. Interestingly, ttMutS was unable to activate ttMutL CTD even in the presence of a mismatch, ATP, and $MnCl_2$, indicating that the NTD of ttMutL is required for the activation of ttMutL by ttMutS (Fig. 17A and B). This result may indicate that ttMutS-dependent activation of ttMutL involves the interdomain interaction within ttMutL or that ttMutL NTD is required for interaction with ttMutS. Then, I investigated the interaction of ttMutS with the full-length and CTD of ttMutL by surface plasmon resonance. The results demonstrated that ttMutS was capable of interacting with full-length ttMutL and the CTD (Fig. II-19), although ttMutS interacted less stably with ttMutL CTD than with full-length ttMutL. These results suggest that interdomain interaction within ttMutL plays a significant role in ttMutS-dependent activation of the endonuclease. This notion has been proposed the previous report regarding the interdomain interaction in *A. aeolicus* MutL (Yamamoto *et al*., 2011).

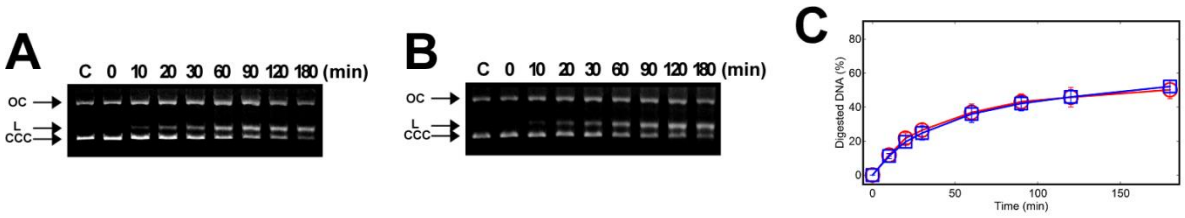

Figure II-17. The time-course assay of ttMutL CTD endonuclease activity for heteroduplex DNA in the presence of $MnCl_2$. (A) Reaction performed in the absence of ATP. (B) Reaction performed in the presence of ATP. (C) After subtracting the background, the percentage of total products (nicked and linearized DNA) was plotted against reaction time. Red and blue lines correspond to (A) and (B), respectively.

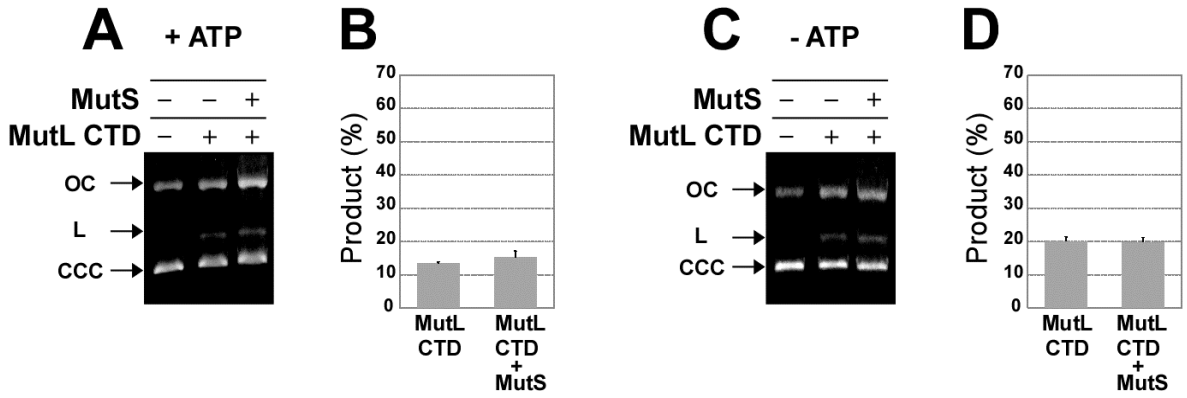

Figure II-18. ttMutL CTD was not activated by ttMutS. The endonuclease assay was performed using ttMutL CTD. (A) The reaction was carried out in the presence of ATP. (B) The percentages of reaction products in (A) are shown in a bar graph. (C) The reaction was carried out in the absence of ATP. (D) The percentages of reaction products in (C) are shown.

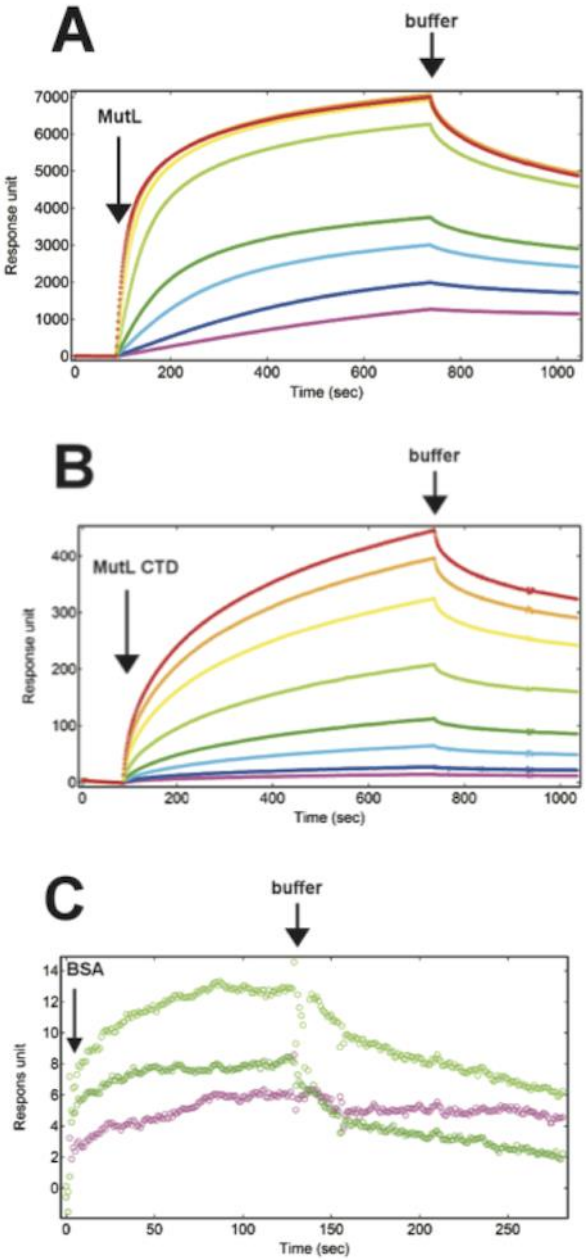

Figure II-19. The interaction between ttMutS and the full-length or CTD of ttMutL analyzed using SPR. SPR sensorgrams are shown after subtracting the response units of the reference surface. (A) The binding curves of the full-length ttMutL at 10 (purple), 20 (blue), 50 (light blue), 100 (green), 250 (light green), 500 (yellow), 750 (orange), and 1000 nM (red) are shown (upper panel). (B) The same experiment as (A) was performed using the CTD of ttMutL. (C) For the negative control, BSA was flowed over the same chip, on which ttMutS was immobilized. The binding curves of the BSA at 10 (purple), 100 (green), and 250 nM (light green) are shown.

***Trans*-activation by ttMutS**

To provide clue to understand the initial steps of general bacterial MMR (from the mismatch recognition until the nick introduction), I examined whether the stimulation of ttMutL endonuclease activity by ttMutS was required for the translocation of ttMutS or not. In *E. coli* MMR studies, *cis* and *trans* activation assays were employed to investigate the activation mechanism for MutH endonuclease (Junop *et al*., 2001). In the *cis* activation assay system, a mismatch and cleavable site reside on the same DNA molecule, whereas in the *trans* activation assay, they reside on separate DNA molecules. In previous *cis* experiments, I verified that ttMutS *cis*-activates the endonuclease activity of ttMutL (Fig. II-10). To further explore the activation mechanism for ttMutL endonuclease, I performed the *trans* activation assay, in which the mismatch is not on the cleavable plasmid DNA but on a separate double-stranded linear DNA molecule. In this experiment, I sought to determine whether ttMutS stimulates the endonuclease activity of ttMutL bound on a different DNA molecule.

To trap ttMutS on the linear mismatched DNA, I prepared a 120-bp GT mismatched DNA on which both 5′ -ends were blocked with biotin-streptavidin (See EXPERIMENTAL PROCEDURES). In a DNase I footprinting experiment, I confirmed that ttMutS was trapped on the 120-bp heteroduplex DNA (Fig. II-20A) but not on the 120-bp homoduplex DNA (Fig. II-20B). Then, ttMutS trapped by the 120-bp GT mismatched or perfectly-matched double-stranded DNA was added to the reaction mixture containing ttMutL and plasmid DNA substrate, and incision of the plasmid DNA was monitored (Fig. II-21A).

I performed the *trans*-activation assay with perfectly-matched plasmid DNA and found that ttMutS trapped on the 120-bp GT mismatched DNA was unable to stimulate ttMutL endonuclease activity against the homoduplex plasmid DNA (Fig. II-21B and C). As a control, 120-bp homoduplex DNA was used instead of heteroduplex DNA, and no activation

was observed (Fig. II-21D and E). These results show that ttMutS is capable of activating ttMutL endonuclease activity in *cis*, but not in *trans*.

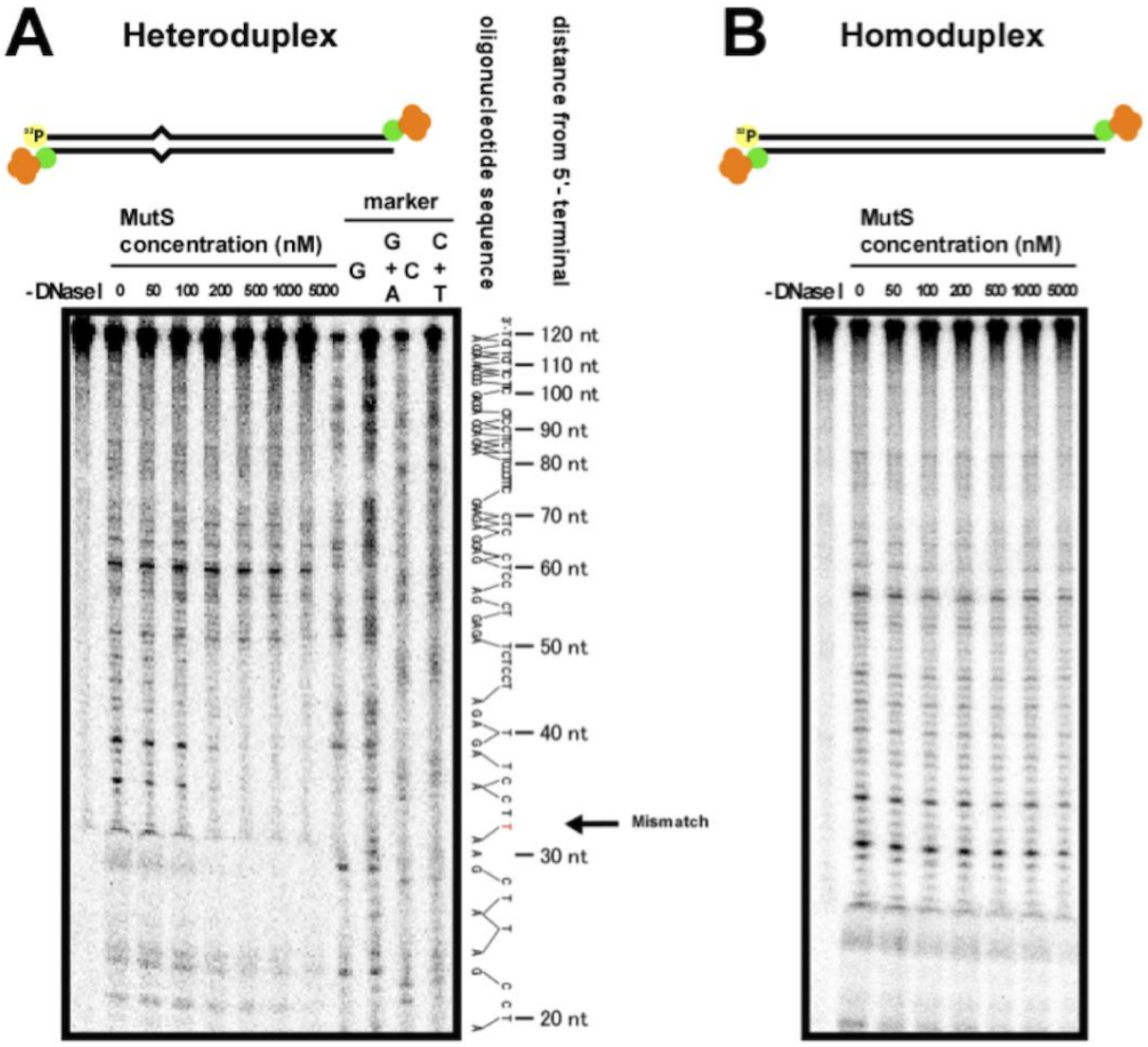

Figure II-20. Localization of ttMutS in the GT-mismatched (A) and perfectly-matched (B) DNA. DNase I footprinting was carried out using 120-bp double-stranded DNA on which the termini were blocked by streptavidin-biotin. To make DNA size marker, 5′-radiolabeled 120-2T single-stranded oligonucleotide was base-specifically modified and cleaved using the Maxam-Gilbert method. The concentrations of ttMutS are indicated at the top of the panels. The position of the mismatch in the G-T mismatched duplex is indicated by an arrow.

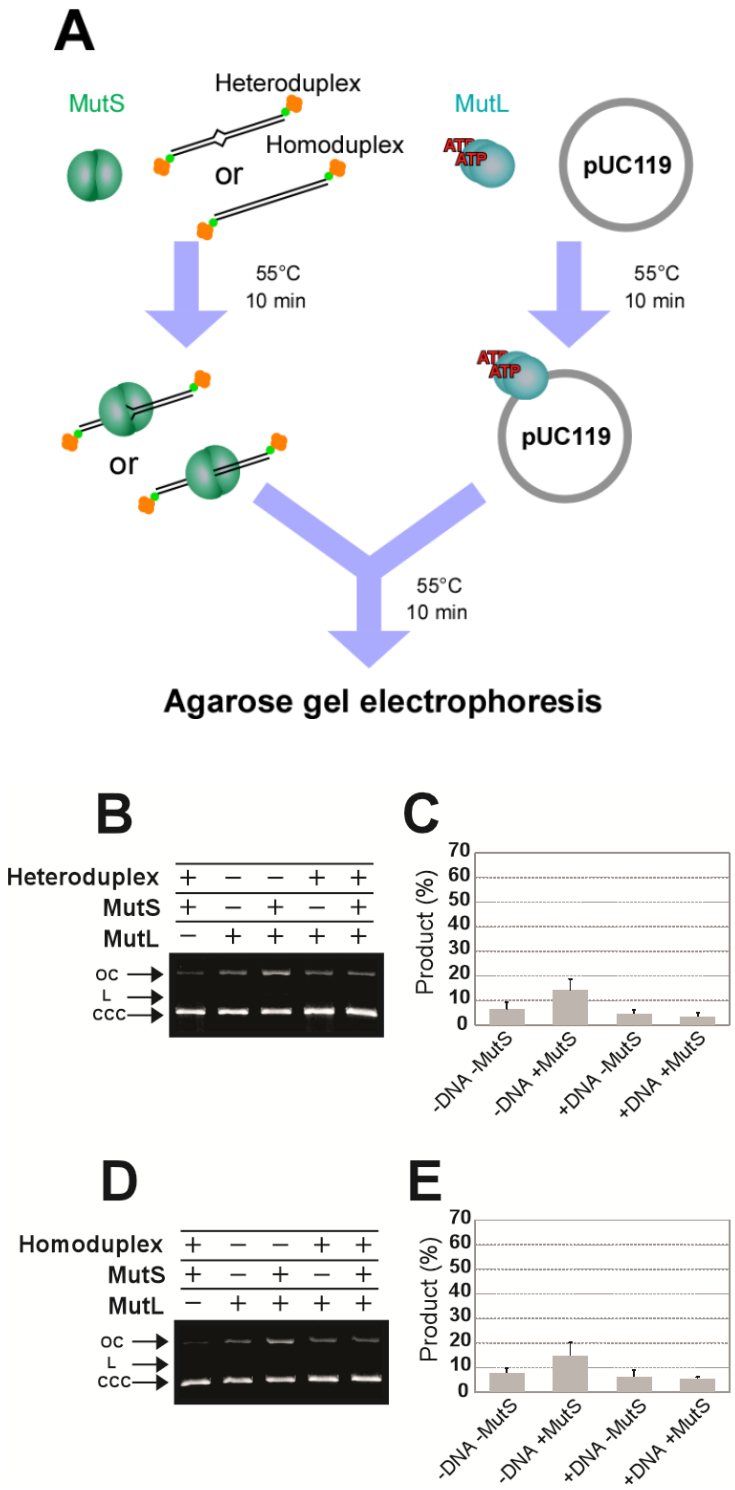

Figure II-21. *Trans*-activation analysis using homoduplex plasmid DNA. (A) Scheme for *trans-activation* analysis. Briefly, ttMutS and ttMutL were separately pre-incubated with 120-bp double-stranded DNA and CCC form of homoduplex plasmid DNA (pUC119) at 55°C for 10 min, respectively. Then, pre-incubated ttMutS and ttMutL solutions were mixed and incubated at 55°C for 10 min. (B) Pre-incubation of ttMutS was carried out with 120-bp GT mismatched DNA. (C) The percentages of reaction products in (B) are shown. (D) Pre-incubation of ttMutS was carried out with 120-bp homoduplex DNA. (E) The percentages of reaction products in (D) are shown.

DISCUSSION

I determined that intracellular concentration of ttMutL is approximately 300 nM (Fig. II-6C). Hence, I used 500 nM ttMutL for *in vitro* analyses in this study. Although the endonuclease activity of 500 nM ttMutL was inhibited in the presence of ATP, the activity was activated in the presence of a mismatch and ttMutS despite of the presence of ATP (Fig. II-7 and 10). Thus, it is suggested that the nick introduction by ttMutL is prevented from degrading error-free strand until ttMutL accepts the signal of a mismatch base recognition by ttMutS. There could be two possible explanations for ATP-dependent suppression of the ttMutL endonuclease activity. First, ATP binding might induce ttMutL to adopt inactive conformation, which suppresses its nicking endonuclease activity. Because ATP-binding motif and endonuclease motif reside in NTD and CTD of ttMutL, respectively, ATP-binding signal in NTD could be transmitted to CTD via interdomain interaction. Second, the essential metal ion, Mn^{2+}, for the endonuclease activity might be chelated by ATP, and then the amount of Mn^{2+} might become insufficient to exhibit the activity. However, deletion of NTD from ttMutL showed no inhibition of its endonuclease activity by ATP (Fig. II-17). Hence, the observed inhibition of the ttMutL endonuclease activity in the presence of ATP is caused by the binding of ATP to NTD of ttMutL. To verify that intracellular ttMutL exists ATP-binding form in living cell, I examined the K_M and k_{cat} values of ttMutL for ATP. As a result, the K_M value for ATP was sufficiently smaller than cellular concentration of ATP, approximately 10 mM in a bacterial cell (Bennett *et al*., 2009), and k_{cat} value for ATP is extremely low. These results suggest that the endonuclease activity of ttMutL is tightly regulated *in vivo* by ATP binding.

My experiments indicated that ttMutS was stimulated the ttMutL endonuclease in the presence of ATP. This stimulation was not observed in the presence ADP or AMPPNP (Fig. II-14A, B, and K). Also in the presence of both ADP and AMPPNP, ttMutS was unable to stimulate the ttMutL endonuclease activity (Fig. II-14J). Moreover, the ttMutL

endonuclease was not activated by ATPase deficient mutants of ttMutS in the presence of both ADP and ATP (Fig. II-14H and I). These results strongly suggest that the ATP hydrolysis by ttMutS is necessary for the stimulation of the endonuclease activity of ttMutL. I propose two hypotheses to explain how ttMutL endonuclease is stimulated by ttMutS depending on ATP hydrolysis. First, ATP-bound ttMutS might search for ttMutL along the DNA with sliding formation after recognition of a mismatch, and then ATP-bound ttMutS might form a ternary complex with ttMutL, which leads to activation of ttMutL depending on the ATP hydrolysis (Fig. II-22). I demonstrated that ttMutS enhanced the endonuclease activity of ttMutL in *cis* (Fig. II-10) but not in *trans* (Fig. II-21), strongly indicating that two proteins, ttMutS and ttMutL, both need to be on the same DNA molecule to interact. Furthermore, the endonucleolytic products detected by Southern blotting analysis were smear (Fig. II-13). This result suggests that there is a variety of lengths in cleaved products. Based on these results, ATP-binding ttMutS moved away form a mismatched base and interacted with ttMutL, then ATP hydrolysis energy was transmitted to ttMutL from ttMutS.

Second, ATP hydrolysis might be employed to form the active complex of ttMutS, ttMutL and a mismatched base (Fig. II-22). In eukaryotic MMR, ATP binding, not hydrolysis, is required to form the sliding clamp of MutSα and to make interaction between MutSα and MutLα (Hargreaves *et al*., 2012). In the case of *T. thermophilus*, however, the stimulation of ttMutL endonuclease activity by ttMutS was not observed in the presence of both ADP and AMPPNP (Fig. II-14J and K). This can be explained if ATP hydrolysis by ttMutS is necessary to form the sliding clamp and/or the complex with ttMutL. Because AMPPNP-bound ttMutS (and ttMutL complex) is expected to be stable at the mismatched base, another ttMutS (and ttMutL complex) molecule would be unable to recognize the mismatched base, resulting in the decrease of turnover rate of nick introduction. In addition, the necessity of ATP hydrolysis by ttMutS is supported by the observation that the ATPase-deficient mutants were unable to stimulate ttMutL activity. It should be noted,

however, that it remains uncertain whether those mutants can form sliding clamp or not. Further experiments must be performed to clarify the precise role of the ATP hydrolysis by ttMutS.

Surface plasmon resonance experiments revealed that ttMutS interacts with the ttMutL CTD (Fig. II-19). Therefore, the stimulation of the endonuclease activity would involve direct interaction between ttMutS and the endonuclease domain of ttMutL. However, my results also clarified that unlike full-length ttMutL, the CTD of ttMutL was not activated by ttMutS (Fig. II-17 and 18). The ATP hydrolysis- and interdomain interaction-dependent conformational change in the ttMutL CTD may be necessary to enable activation by ttMutS.

ATP hydrolysis by ttMutL was also involved in the stimulation of ttMutL endonuclease activity. Several previous reports have suggested that ATP hydrolysis by MutL is needed for the mismatch-specific endonuclease activity of MutL. In *A. aeolicus*, even in the absence of MutS and mismatch, ATP (but AMPPNP) promotes the endonuclease activity of relatively high concentrations of MutL (Mauris and Evans, 2009), suggesting the potential of ATP hydrolysis by MutL to enhance its endonuclease activity. In this study, I demonstrated that ATP hydrolysis by ttMutL is also required for nick introduction. In my experiments, the difference between WT and ATPase-deficient mutants of ttMutL was observed only in the presence of ttMutS and a mismatch, suggesting that ATP hydrolysis by ttMutL was activated by interaction with a ttMutS-mismatch complex. Furthermore, the ATPase-deficient mutant of ttMutS did not affect the endonuclease activity of ttMutL. These results suggest ATP hydrolysis by the ttMutS-mismatch complex enhances the ATPase activity of ttMutL. Subsequent ATP hydrolysis by the ttMutL NTD would cause a conformational change in the ttMutL CTD via interdomain interaction.

As described above, I succeeded in the reconstruction of the mismatch-specific nick introduction by ttMutS and ttMutL. In eukaryotic and *E. coli* MMR, it is known that replicative DNA polymerase subunits interact with MutS and/or MutL homologues (Li *et al.*,

2008; Pluciennik *et al*., 2009). In *E. coli* clamp loaders, DNA polymerase III γ, τ, δ, and δ′ subunits, interact with MutL, but the function of these interactions is unclear (Li *et al*., 2008; Pluciennik *et al*., 2009). On the other hand, in eukaryotes, PCNA stimulates the endonuclease activity of MutLα, and the interaction between PCNA and MutLα is reported to be essential for MMR to distinguish between template and newly-synthesized strands (Pluciennik *et al*., 2010). Hence, I investigated the effects of DNA polymerase III subunits on ttMutL endonuclease activity. Regardress of the presence of ATP, however, DNA polymerase III subunits, γ, τ, δ, δ', and β subunits, were unable to stimulated the ttMutL endonuclease activity (Fig. II-10 and 13). I confirmed that recombinant DNA polymerase III subunits were in active form by analyzing the ATP hydrolysis activity of clamp loader complex (γ, τ, δ, and δ' subunits) (Fig. II-12) and β clamp loading assay using DNA immobilized with sepharose beads (Fig. II-11). Therefore, in *T. thermopholus*, it is suggested that DNA polymerase III subunits has no effects on the ttMutL endonuclease activity. However, the intracellular interaction between β clamp and ttMutL was implied by the immunoprecipitation analysis (Fig. II-9). Since the β clamp interaction motif is hardly found in the amino acid sequence of ttMutL (Fukui *et al*., 2011), it can be suspected that the observed co-immunoprecipitation of β clamp with both ttMutL reflects their indirect interaction that is mediated by ttMutS. It is known that MutS interacts with both MutL and β clmap, therefore anti-ttMutL antibody may catch the ttMutS-β clamp complex. Similarly, ttMutS-ttMutL complex may be co-immunoprecipitated with anti-β clamp antibody. I postulate that the interactions between bacterial MutL and DNA polymerase III subunits mediate the loading of MutL onto DNA for strand discrimination, or loading of the DNA polymerase III complex for DNA resynthesis.

The mechanism of strand discrimination, which is the most important aspect in MMR reaction, has been still unclear in *T. thermophilus*. As mentioned above, in eukaryotic MMR, the interaction between MutLα and PCNA play a critical role in strand discrimination,

suggesting that ttMutL utilizes the fixed orientation of PCNA loading (Pluciennik *et al*., 2010). Similar to the method used by Pluciennik, I investigated the endonuclease assay using a nick-containing DNA, clamp loader, β clamp, ttMutS, and ttMutL in the presence of ATP (Fig. II-13). However, ttMutL cleaved both strand in the presence of clamp loader and β clamp. This result raises the possibility that additional factors are required for strand discrimination other than clamp loader and β clamp in *T. thermophilus* MMR. Furthermore, because β clamp-interacting motif is not found in ttMutL sequence, there could be the possibility that a previously unidentified mechanism is utilized in *T. thermophilus*. If the strand discrimination of *T. thermophilus* does not employ neither the sequence specificity for the cleavage by ttMutL or the interaction between ttMutL and β clamp, it could be suggested that *T. thermophilus* possesses a novel MMR system other than eukaryotic and *E. coli* type MMR systems.

In conclusion, I elucidated that the ATP hydrolyses by both ttMutS and ttMutL are necessary for the nick introduction by ttMutL in *T. thermophilus*. From the results in this study, I constructed two models of the initial step of MMR. The first model is that ATP hydrolysis by ttMutS is required for the activation of ttMutL CTD (Fig. II-22 Hypothesis I). Binding to mismatch and ATP induces the conformational changes in ttMutS to form a sliding clamp. Then ATP-bound ttMutS slides along the DNA to interact with ATP-bound ttMutL suppressed its nicking activity. The ATP hydrolysis by ttMutS confers the conformational change adequate to exhibit the endonuclease activity on ttMutL CTD via the interaction between ttMutS and ttMutL NTD. Then, the ATP hydrolysis by ttMutL NTD causes the dissociation of NTD form CTD, and then more efficient cleavage by CTD is yielded. Second is that the ATP hydrolysis by ttMutS is required for the forming the active complex among ttMutS, ttMutL, and a mismatched base (Fig. II-22 Hypothesis II). ATP-binding ttMutS form stable complex with a mismatched base, then ATP hydrolysis by ttMutS cause the conformational change adequate to interact with ATP-binding ttMutL. ADP-binding

ttMutS and ttMutL complex translocats along the DNA, and then ttMutL introduced a nick after ATP hydrolysis by ttMutL.

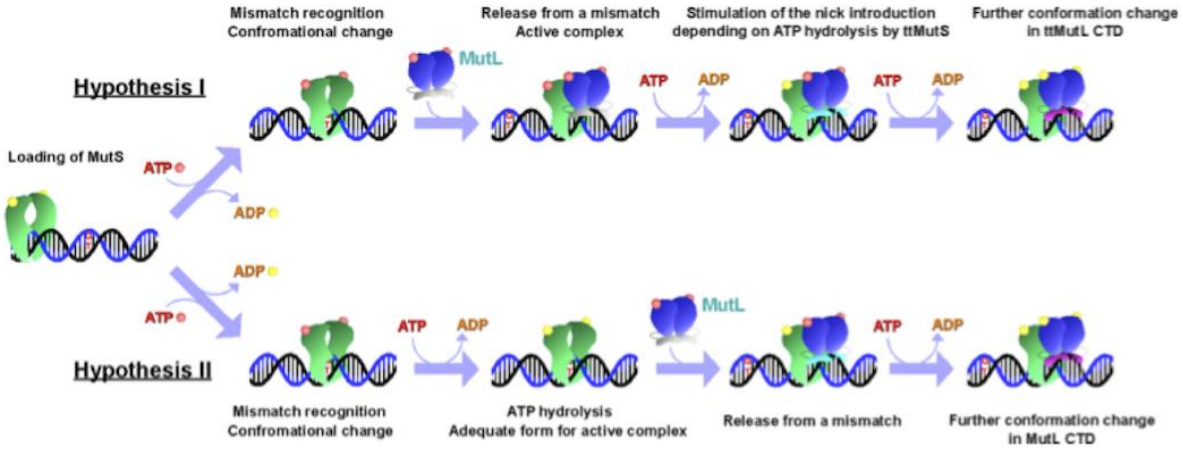

Figure II-22. The model of ttMutL activation. ADP-bound ttMutS binds on DNA and searches for a mismatch. Mismatch-bound ttMutS exchanges ADP with ATP. In hypothesis I, the nucleotide exchange results in formation of the clamp-like structure of ttMutS. The ATP-bound ttMutS releases from a mismatched base and interacts with the ATP-bound ttMutL. Then, ttMutS hydrolyzes ATP to activate ATP-bound ttMutL. In hypothesis II, ttMutS hydrolyzes ATP to form the active complex with ATP-bound ttMutL. ADP-bound ttMutS and ATP-bound ttMutL complex slide along the DNA. The ttMutL NTD hydrolyzes ATP, and the ATP-hydrolysis energy is utilized to stimulate the endonuclease activity of ttMutL CTD. A nick is introduced by activated ttMutL CTD.

REFERENCES

Agari Y., Sakamoto K., Tamakoshi M., Oshima T., Kuramitsu S., and Shinkai A. (2010) Transcription profile of *Thermus thermophilus* CRISPR systems after phage infection. *J. Mol. Biol.* **395:** 270-281

Akagawa M., and Suyama K. (2002) Oxidative deamination by hydrogen peroxide in the presence of metals. *Free Radic. Res.* **36:** 13-21

Allen D.J., Makhov A., Grilley M., Taylor J., Thresher R., Modrich P., and Griffith J.D. (1997) MutS mediates heteroduplex loop formation by a translocation mechanism. *EMBO J.* **16:** 4467-4476

Amin N.S., Nguyen M.N., Oh S., and Kolodner R.D. (2001) exo1-Dependent mutator mutations: model system for studying functional interactions in mismatch repair. *Mol. Cell. Biol.* **21:** 5142-5155

Antony E. and Hingorani M.M. (2003) Mismatch recognition-coupled stabilization of Msh2-Msh6 in an ATP-bound state at the initiation of DNA repair. *Biochemistry* **42:** 7682-7693

Antony E. and Hingorani M.M. (2004) Asymmetric ATP binding and hydrolysis activity of the *Thermus aquaticus* MutS dimer is key to modulation of its interactions with mismatched DNA. *Biochemistry* **43:** 13115-13128

Back J.H., Park J.H., Chung J.H., Kim D.S.H.L., and Han Y.S. (2006) A distinct TthMutY bifunctional glycosylase that hydrolyzes not only adenine but also thymine opposite 8-oxoguanine in the hyperthermophilic bacterium, *Thermus thermophilus*. *DNA repair* **5:** 894-903

Baitinger C., Burdett V., and Modrich P. (2003) Hydrolytically deficient MutS E694A is defective in the MutL-dependent activation of MutH and in the mismatch-dependent assembly of the MutS.MutL.heteroduplex complex. *J. Biol. Chem.* **278:** 49505-49511

Ban C., Junop M., and Yang W. (1999) Transformation of MutL by ATP binding and hydrolysis: a switch in DNA mismatch repair. *Cell* **97:** 85-97

Ban C. and Yang W. (1998) Structural basis for MutH activation in *E.coli* mismatch repair and relationship of MutH to restriction endonucleases. *EMBO J.* **17:** 1526-1534

Bennett B.D., Kimball E.H., Gao M., Osterhout R., Van Dien S.J., and Rabinowitz J.D. (2009) Absolute metabolite concentrations and implied enzyme active site occupancy in *Escherichia coli*. *Nat. Chem. Biol.* **5:** 593-599

Bernad A., Blanco L., Lazaro J., Martin G., and Salas M. (1989) A conserved 3′-->5′ exonuclease active site in prokaryotic and eukaryotic DNA polymerases. *Cell* **59:** 219-228

Biswas I. and Vijayvargia R. (2000) Heteroduplex DNA and ATP induced conformational changes of a MutS mismatch repair protein from *Thermus aquaticus*. *Biochem. J.* **347:**

881-886

Bonura T. and Smith K.C. (1975) Enzymatic production of deoxyribonucleic acid double-strand breaks after ultraviolet irradiation of *Escherichia coli* K-12. *J. Bacteriol.* **121:** 511-517

Bourre F., Benoit A., and Sarasin A. (1989) Respective roles of pyrimidine dimer and pyrimidine (6-4) pyrimidone photoproducts in UV mutagenesis of simian virus 40 DNA in mammalian cells. *J. Virol.* **63:** 4520-4524

Bowman G.D., O'Donnell M., and Kuriyan J., (2004) Structural analysis of a eukaryotic sliding DNA clamp-clamp loader complex. *Nature* **429:** 724-730

Bradley M.O. (1981) Double-strand breaks in DNA caused by repair of damage due to ultraviolet light. *J. Supramol. Struct. Cell Biochem.* **16:** 337-343

Breyer W.A. and Matthews B.W. (2000) Structure of *Escherichia coli* exonuclease I suggests how processivity is achieved. *Nat. Struct. Mol. Biol.* **7:** 1125-1128

Burdett V., Baitinger C., Viswanathan M., Lovett S.T., and Modrich P. (2001) *In vivo* requirement for RecJ, ExoVII, ExoI, and ExoX in methyl-directed mismatch repair. *Proc. Natl. Acad. Sci. U. S. A.* **98:** 6765-6770

Busam R. (2008) Structure of *Escherichia coli* exonuclease I in complex with thymidine 5′-monophosphate. *Acta Crystallogr. D Biol. Crystallogr.* **64:** 206-210

Courcelle J. and Hanawalt P.C. (2001) Participation of recombination proteins in rescue of arrested replication forks in UV-irradiated *Escherichia coli* need not involve recombination. *Proc. Natl. Acad. Sci. U. S. A.* **98:** 8196-8202

Cromie G.A., Connelly J.C., and Leach D.R.F. (2001) Recombination at double-strand breaks and DNA ends: conserved mechanisms from phage to humans. *Mol. Cell* **8:** 1163-1174

Crow Y.J., Hayward B.E., Parmar R., Robins P., Leitch A., Ali M., Black D.N., van Bokhoven H., Brunner H.G., Hamel B.C., Corry P.C., Cowan F.M., Frints S.G., Klepper J., Livingston J.H., Lynch S.A., Massey R.F., Meritet J.F., Michaud J.L., Ponsot G., Voit T., Lebon P., Bonthron D.T., Jackson A.P., Barnes D.E., and Lindahl T. (2006) Mutations in the gene encoding the 3′-5′ DNA exonuclease TREX1 cause Aicardi-Goutieres syndrome at the AGS1 locus. *Nat. Genet.* **38:** 917-920

de Silva U., Choudhury S., Bailey S.L., Harvey S., Perrino F.W., and Hollis T. (2007) The crystal structure of TREX1 explains the 3′ nucleotide specificity and reveals a polyproline II helix for protein partnering. *J. Biol. Chem.* **282:** 10537-10543

de Silva U., Perrino F.W., and Hollis T. (2009) DNA binding induces active site conformational change in the human TREX2 3′-exonuclease. *Nucleic Acids Res.* **37:** 2411-2417

Dillingham M.S., Spies M., and Kowalczykowski S.C. (2003) RecBCD enzyme is a bipolar DNA helicase. *Nature* **423:** 893-897

Dong Z., Onrust R., Skangalis M., and O′Donnell M. (1993) DNA polymerase III accessory

proteins. I. holA and holB encoding delta and delta′. *J*. *Biol*. *Chem*. **268:** 11758-11765

Duppatla V., Bodda C., Urbanke C., Friedhoff P, and Rao D.N. (2009) The C-terminal domain is sufficient for endonuclease activity of *Neisseria gonorrhoeae* MutL. *Biochem*. *J*. **423:** 265-277

Dutta R. and Inouye M. (2000) GHKL, an emergent ATPase/kinase superfamily. *Trends*. *Biochem*. *Sci*. **25:** 24-28

Feng G., Tsui H.C., and Winkler M.E. (1996) Depletion of the cellular amounts of the MutS and MutH methyl-directed mismatch repair proteins in stationary-phase *Escherichia coli* K-12 cells. *J*. *Bacteriol*. **178:** 2388-2396

Fishel R., Ewel A., and Lescoe M.K. (1994) Purified human MSH2 protein binds to DNA containing mismatched nucleotides. *Cancer Res*. **54:** 5539-5542

Fishel R., Lescoe M.K., Rao M.R., Copeland N.G., Jenkins N.A., Garber J., Kane M., and Kolodner R. (1993) The human mutator gene homolog MSH2 and its association with hereditary nonpolyposis colon cancer. *Cell* **75:** 1027-1038

Franklin W.A. and Haseltine W.A. (1986) The role of the (6-4) photoproduct in ultraviolet light-induced transition mutations in *E*. *coli*. *Mutat*. *Res*. **165:** 1-7

Friedberg E.C., Walker G.C., and Siede, W. (1995) *DNA Repair and Mutagenesis*, pp. 1-685, N. W. Washington, D.C.: American Society for Microbiology.

Fukuda T., Sumiyoshi T., Takahashi M., Kataoka T., Asahara T., Inui H., Watatani M., Yasutomi M., Kamada N., and Miyagawa K. (2001) Alterations of the double-strand break repair gene MRE11 in cancer. *Cancer Res*. **61:** 23-26

Fukui K., Masui R., and Kuramitsu S. (2004) *Thermus thermophilus* MutS2, a MutS paralogue, possesses an endonuclease activity promoted by MutL. *J*. *Biochem*. **135:** 375-384

Fukui K., Nishida M., Nakagawa N., Masui R., and Kuramitsu S. (2008) Bound nucleotide controls the endonuclease activity of mismatch repair enzyme MutL. *J*. *Biol*. *Chem*. **283:** 12136-12145

Fukui K., Shimada A., Iino H., Masui R., and Kuramitsu S. (2011) Biochemical properties of MutL, a DNA mismatch repair endonuclease. In Storici F (ed.), *DNA Repair - On the Pathways to Fixing DNA Damage and Errors* (Storici F, ed.), pp. 123-142. InTech, Rijeka, Croatia.

Fukui K., Takahata Y., Nakagawa N., Kuramitsu S., and Masui R. (2007) Analysis of a nuclease activity of catalytic domain of *Thermus thermophilus* MutS2 by high-accuracy mass spectrometry. *Nucleic Acids Res*. **35:** e100

Genschel J., Bazemore L.R., and Modrich P. (2002) Human exonuclease I is required for 5′ and 3′ mismatch repair. *J*. *Biol*. *Chem*. **277:** 13302-13311

Georgescu R.E., Kim S.S., Yurieva O., Kuriyan J., Kong X.P., and O'Donnell M, (2008) Structure of a sliding clamp on DNA. *Cell* **132:** 43-54

Gorbalenya A.E. and Koonin E.V. (1990) Superfamily of UvrA-related NTP-binding proteins. Implications for rational classification of recombination/repair systems. *J. Mol. Biol.* **213:** 583-591

Gorman J., Chowdhury A., Surtees J.A., Shimada J., Reichman D.R., Alani E., and Greene E.C. (2007) Dynamic basis for one-dimensional DNA scanning by the mismatch repair complex Msh2-Msh6. *Mol. Cell* **28:** 359-370

Gorman J., Wang F., Redding S., Plys A.J., Fazio T., Wind S., Alani E.E., and Greene E.C. (2012) Single-molecule imaging reveals target-search mechanisms during DNA mismatch repair. *Proc. Natl. Acad. Sci. U .S. A.* **109:** E3074-E3083

Gradia S., Subramanian D., Wilson T., Acharya S., Makhov A., Griffith J., and Fishel R. (1999) hMSH2-hMSH6 forms a hydrolysis-independent sliding clamp on mismatched DNA. *Mol. Cell* **3:** 255-261

Han E.S., Cooper D.L., Persky N.S., Sutera V.A., Whitaker R.D., Montello M.L., and Lovett S.T. (2006) RecJ exonuclease: substrates, products and interaction with SSB. *Nucleic Acids Res.*, **34**: 1084-1091

Hargreaves V.V., Putnam C.D., and Kolodner R.D. (2012) Engineered disulfide-forming amino acid substitutions interfere with a conformational change in the mismatch recognition complex Msh2-Msh6 required for mismatch repair. *J. Biol. Chem.*, **287:** 41232-41244

Hashimoto Y., Yano T., Kuramitsu S., and Kagamiyama H. (2001) Disruption of *Thermus thermophilus* genes by homologous recombination using a thermostable kanamycin-resistant marker. *FEBS Lett* **506:** 231-234

Higashi T.L., Ikeda M., Tanaka H., Nakagawa T., Bando M., Shirahige K., Kubota Y., Takisawa H., Masukata H., and Takahashi T.S. (2012) The prereplication complex recruits XEco2 to chromatin to promote cohesin acetylation in Xenopus egg extracts. *Curr. Biol.* **22:** 977-988

Hoseki J., Yano T., Koyama Y., Kuramitsu S., and Kagamiyama H. (1999) Directed evolution of thermostable kanamycin-resistance gene: a convenient selection marker for *Thermus thermophilus*. *J. Biochem.* **126:** 951-956

Hsieh P. and Yamane K. (2008) DNA mismatch repair. Molecular mechanism, cancer, and ageing. *Mech. Ageing Dev.* **129:** 391-407

Iino H., Kim K., Shimada A., Masui R., Kuramitsu S., and Fukui K. (2011) Characterization of C- and N-terminal domains of *Aquifex aeolicus* MutL endonuclease: N-terminal domain stimulates the endonuclease activity of C-terminal domain in a zinc-dependent manner. *Biosci. Rep.* **31:** 309-322

Ishii T., Sootome H., Shan L., and Yamashita K. (2007) Validation of universal conditions for duplex quantitative reverse transcription polymerase chain reaction assays. *Anal. Biochem.* **362:** 201-212

Ivancic-Bace I., Salaj-Smic E., and Brcic-Kostic K. (2005) Effects of *recJ, recQ*, and *recFOR* mutations on recombination in nuclease-deficient *recB recD* double mutants of *Escherichia coli*. *J*. *Bacteriol*. **187:** 1350-1356

Jiricny J. (2006) The multifaceted mismatch-repair system. *Nat*. *Rev*. *Mol*. *Cell Biol*. **7:** 335-346

Joshi A., Sen S., and Rao B.J. (2000) ATP-hydrolysis-dependent conformational switch modulates the stability of MutS-mismatch complexes. *Nucleic Acids Res* **28:** 853-861

Junop M.S., Obmolova G., Rausch K., Hsieh P., and Yang W. (2001) Composite active site of an ABC ATPase: MutS uses ATP to verify mismatch recognition and authorize DNA repair. *Mol*. *Cell* **7:** 1-12

Kadyrov F.A., Dzantiev L., Constantin N., and Modrich P. (2006) Endonucleolytic function of MutLa in human mismatch repair. *Cell* **126:** 297-308

Kadyrov F.A., Holmes S.F., Arana M.E., Lukianova O.A., O'Donnell M., Kunkel T.A., and Modrich P. (2007) *Saccharomyces cerevisiae* MutLa is a mismatch repair endonuclease. *J*. *Biol*. *Chem*. **282:** 37181-37190

Kolodner R.D. and Marsischky G.T. (1999) Eukaryotic DNA mismatch repair. *Curr*. *Opin*. *Genet*. *Dev*. **9:** 89-96

Kondo N., Nishikubo T., Wakamatsu T., Ishikawa H., Nakagawa N., Kuramitsu S., and Masui R. (2008) Insights into different dependence of dNTP triphosphohydrolase on metal ion species from intracellular ion concentrations in *Thermus thermophilus*. *Extremophiles* **12:** 217-223

Korada C.S.K., Johns D.T., Smith E.C., Jones D.N., McCabe A.K., and Bell E.C. (2013) Crystal structures of Escherichia coli exonuclease I in coplex with single-stranded DNA provide insights into the mechanism of processive digestion. *Nucleic Acids Res*. **41:** 5887-5897

Krishna T.S., Kong X.P., Gray S., Burgers P.M., and Kuriyan J. (1994) Crystal strutre of the eukaryotic DNA polymerase processivity factor PCNA. Cell **79:** 1233-1243

Kunkel T.A. and Erie D.A. (2005) DNA misamtch repair. *Annu*. *Rev*. *Biochem*. **74:** 681-710

Lamers M.H., Perrakis A., Enzlin J.H., Winterwerp H.H., de Wind N., and Sixma T.K. (2000) The crystal structure of DNA mismatch repair protein MutS binding to a G x T mismatch. *Nature* **407:** 711-717

Lamers M.H., Georgijevic D., Lebbink J.H., Winterwerp H.H., Agianian B., de Wind N., and Sixma T.K. (2004) ATP increases the affinity between MutS ATPase domains. Implications for ATP hydrolysis and conformational changes. *J*. *Biol*. *Chem*., **279:** 43879-43885

Larkin M.A., Blackshields G., Brown N.P., Chenna R., McGettigan P.A., Valentin F., Wallace I.M., Wilm A., Lopez R., Thompson J.D., Gibson T.J., and Higgins D.G. (2007) ClustalW and ClustalX version 2. *Bioinformatics* **23:** 2947-2948

Larsen B., Wills N.M., Nelson C., Atkins J.F., and Gesteland R.F. (2000) Nonlinearity in genetic decoding: homologous DNA replicase genes use alternatives of transcriptional slippage or translational frameshifting. *Proc. Natl. Acad. Sci. U. S. A.* **97:** 1683-1688

Leach F.S., Nicolaides N.C., Papadopoulos N., Liu B., Jen J., Parsons R., Peltomäki P., Sistonen P., Aaltonen L.A., and Nyström-Lahti M. (1993) Mutations of a mutS homolog in hereditary nonpolyposis colorectal cancer. *Cell* **75:** 1215-1225

Lebbink J.K., Georgijevic D., Natrajan G., Fish A., Winterwerp H.H., Sixma T.K., and de Wind N. (2006) Dual role of MutS glutamate 38 in DNA mismatch discrimination and in the authorization of repair. *EMBO J.* **25:** 409-419

Lee S.D. and Alani E. (2006) Analysis of interactions between mismatch repair initiation factors and the replication processivity factor PCNA. *J. Mol. Bio.* **355:** 175-184

Lee-Kirsch M.A., Gong M., Chowdhury D., Senenko L., Engel K., Lee Y.A., de Silva U., Bailey S.L., Witte T., Vyse T.J., Kere J., Pfeiffer C., Harvey S., Wong A., Koskenmies S., Hummel O., Rohde K., Schmidt R.E., Dominiczak A.F., Gahr M., Hollis T., Perrino F.W., Lieberman J., and Hubner N. (2007) Mutations in the gene encoding the 3′-5′ DNA exonuclease TREX1 are associated with systemic lupus erythematosus. *Nat. Genet.* **39:** 1065-1067

Lehman I.R. (1960) The Deoxyribonucleases of *Escherichia coli*. *J. Biol. Chem.* **235:** 1479-1487

Lehman I.R. and Nussbaum A.L. (1964) The Deoxyribonucleases of *Escherichia coli*. *J. Biol. Chem.* **239:** 2628-2636

Leu F.P. and O'Donnell M. (2001) Interplay of clamp loader subunits in opening the b sliding clamp of Escherichia coli DNA polymerase III holoenzyme. *J. Biol. Chem.* **276:** 47185-47194

Li F., Liu Q,. Chen Y-Y, Yu Z-N, Zhang Z-P, Zhou Y-F, Deng J-Y, Bi L-J, and Zhang X-E (2008) *Escherichia coli* mismatch repair protein MutL interacts with the clamp loader subunits of DNA polymerase III. *Mutat. Res.* **637:** 101-110

Li G.M. (2008) Mechanisms and functions of DNA mismatch repair. *Cell Res.* **18:** 85-98

Lombardo M-J, Aponyi I., Ray M.P., Sandigursky M., Franklin W.A., and Rosenberg S.M. (2003) xni-deficient *Escherichia coli* are proficient for recombination and multiple pathways of repair. *DNA repair* **2:** 1175-1183

Luria S.E. and Delbruck M. (1943) Mutations of Bacteria from Virus Sensitivity to Virus Resistance. *Genetics* **28:** 491-511

Längle-Rouault F., Maenhaut-Michel G., and Radman M. (1987a) GATC sequences, DNA nicks and the MutH function in Escherichia coli mismatch repair. *EMBO J.* **6:** 1121-1127

López de Saro F.J., Marinus M.G., Modrich P., and O′Donnell M. (2006) The beta sliding clamp binds to multiple sites within MutL and MutS. *J. Biol. Chem.* **281:** 14340-14349

Marti T.M., Fleck C.K.O. (2002) DNA mismatch repair and mutation avoidance pathways. *J. Cellular Physiol*. **191:** 28-41

Mauris J. and Evans T.C. (2009) Adenosine triphosphate stimulates *Aquifex aeolicus* MutL endonuclease activity. *PLoS One* **4:** e7175

McLuckey S.A., Van Berkel G.J., and Glish, G.L. (1992) Tandem Mass Spectrometry of Small, Multiply Charged Oligonucleotides. *J. Am. Soc. Mass. Spectrom*. **3:** 60-70

Mechanic L.E., Frankel B.A., and Matson S.W. (2000) *Escherichia coli* MutL loads DNA helicase II onto DNA. *J. Biol. Chem*. **275:** 38337-38346

Melancon P., Lemieux C., and Brakier-Gingras L. (1988) A mutation in the 530 loop of *Escherichia coli* 16S ribosomal RNA causes resistance to streptomycin. *Nucleic Acids Res*. **16:** 9631-9639

Mendillo M.L., Hargreaves V.V., Jamison J.W., Mo A.O., Li S., Putnam C.D., Woods V.L., and Kolodner R.D. (2009) A conserved MutS homolog connector domain interface interacts with MutL homologs. *Proc. Natl. Acad. Sci. U. S. A*. **106:** 22223-22228

Michaels M.L., Tchou J., Grollman A.P., and Miller J.H. (2002) A repair system for 8-Oxo-7,8-dihydrodeoxyguanine. *Biochemistry* **31:** 10964-10968

Moazed D. and Noller H.F. (1987) Interaction of antibiotics with functional sites in 16S ribosomal RNA. *Nature* **327:** 389-394

Modrich P. (2006) Mechanisms in eukaryotic mismatch repair. *J. Biol. Chem*. **281:** 30305-30309

Modrich P. and Lahue R. (1996) Mismatch repair in replication fidelity, genetic recombination, and cancer biology. *Annu. Rev. Biochem*. **65:** 101-133

Moe A., Ringvoll J., Nordstrand L.M., Eide L., Bjoras M., Seeberg E., Rognes T., and Klungland A. (2003a) Incision at hypoxanthine residues in DNA by a mammalian homologue of the *Escherichia coli* antimutator enzyme endonuclease V. *Nucleic Acids Res* **31:** 3893-3900

Monti R.M., Miguel V., Borgogno V.M., and Argaraña E.C. (2021) Functional analysis of the interaction between the mismatch repair protien MutS and the replication processivity factor b clamp in Pseudomonas aeruginosa. *DNA repair (Amst)* **11:** 463-469

Morita R., Nakagawa N., Kuramitsu S., and Masui R. (2008) An O^6-methylguanine-DNA methyltransferase-like protein from *Thermus thermophilus* interacts with a nucleotide excision repair protein. *J. Biochem*. **144:** 267-277

Morita R., Nakane S., Shimada A., Inoue M., Iino H., Wakamatsu T., Fukui K., Nakagawa N., Masui R., and Kuramitsu S. (2010) Molecular mechanisms of the whole DNA repair system: a comparison of bacterial and eukaryotic systems. *J. Nucleic Acids* **2010:** 179594

Moser M.J., Holley W.R., Chatterjee A., and Mian I.S. (1997) The proofreading domain of *Escherichia coli* DNA polymerase I and other DNA and/or RNA exonuclease domains.

Nucleic Acids Res. **25:** 5110-5118

Niedziela-Majka A., Maluf N.K., Antony E., and Lohman T.M. (2011) Self-assembly of *Escherichia coli* MutL and its complexes with DNA. *Biochemistry* **50:** 7868-7880

Obmolova G., Ban C., Hsieh P., Yang W. (2000) Crystal structures of mismatch repair protein MutS and its complex with a substrate DNA. *Nature* **407:** 703-710

Oliver A., Baquero F., and Blázquez J. (2002) The mismatch repai system (mutS, mutL, and uvrD genes) in Pseudomonas aeruginosa: molecular characterization of naturally occuring mutants. *Mol*. *Microbiol*. **43:** 1641-1650

Ooga T., Ohashi Y., Kuramitsu S., Koyama Y., Tomita M., Soga T., and Masui R. (2009) Degradation of ppGpp by nudix pyrophosphatase modulates the transition of growth phase in the bacterium *Thermus thermophilus*. *J*. *Biol*. *Chem*. **284:** 15549-15556

Peltomäki P. (2005) Lynch syndrome genes. *Fam*. *Cancer* **4:** 227-232

Perrino F.W., de Silva U., Harvey S., Pryor E.E., Jr., Cole D.W., and Hollis T. (2008) Cooperative DNA binding and communication across the dimer interface in the TREX2 3′ --> 5′-exonuclease. *J*. *Biol*. *Chem*. **283:** 21441-21452

Perrino F.W., Harvey S., McMillin S., and Hollis T. (2005) The human TREX2 3′ -> 5′-exonuclease structure suggests a mechanism for efficient nonprocessive DNA catalysis. *J*. *Biol*. *Chem*. **280:** 15212-15218

Piersen C.E., McCullough A.K., and Lloyd R.S. (2000) AP lyases and dRPases: commonality of mechanism. *Mutat*. *Res*. **459:** 43-53

Pillon M.C., Lorenowicz J.J., Uckelmann M., Klocko A.D., Mitchell R.R., Chung Y.S., Modrich P., Walker G.C., Simmons L.A., Friedhoff P., and Guarné A. (2010) Structure of the endonuclease domain of MutL: unlicensed to cut. *Mol*. *Cell* **39:** 145-151

Pillon M.C., Miller J.H., and Guarné A. (2011) The endonuclease domain of MutL interacts with the β sliding clamp. *DNA Repair (Amst)* **10:** 87-93

Pluciennik A., Burdett V., Lukianova O., O′Donnell M., and Modrich P. (2009) Involvement of the beta clamp in methyl-directed mismatch repair in vitro. *J*. *Biol*. *Chem*. **284:** 32782-32791

Pluciennik A., Dzantiev L., Iyer R.R., Constantin N., Kadyrov F.A., and Modrich P. (2010) PCNA function in the activation and strand direction of MutLα endonuclease in mismatch repair. *Proc*. *Natl*. *Acad*. *Sci*. *U*. *S*. *A*. **107:** 16066-16071

Podust L.M., Podust V.N., Sogo J.M., and Hübscher U. (1995) Mammalian DNA polymerase auxiliary protiens: analysis of replication factor C-catalyzed proliferating cell nuclear antigen loading onto circular double-stranded DNA. *Mol*. *Cell Biol*. **15:** 3072-3081

Prasher D.C., Conarro L., and Kushner S.R. (1983) Amplification and purification of exonuclease I from Escherichia coli K12. *J*. *Biol*. *Chem*. **258:** 6340-6343

Ramilo C., Gu L., Guo S., Zhang X., Patrick S.M., Turchi J.J., and Li G.M. (2002) Partial reconstitution of human DNA mismatch repair *in vitro*: characterization of the role of

human replication protein A. *Mol*. *Cell Biol*. **22:** 2037-2046

Robertson A.B., Pattishall S.R., Gibbons E.A., and Matson S.W. (2006) MutL-catalyzed ATP hydrolysis is required at a post-UvrD loading step in methyl-directed mismatch repair. *J*. *Biol*. *Chem*. **281:** 19949-19959

Rosenstein B.S., and Ducore J.M. (1983) Induction of DNA strand breaks in normal human fibroblasts exposed to monochromatic ultraviolet and visible wavelengths in the 240-546 nm range. *Photochem*. *Photobiol*. **38:** 51-55

Sacho E.J., Kadyrov F.A., Modrich P., Kunkel T.A., and Erie D.A. (2008) Direct visualization of asymmetric adenine-nucleotide-induced conformational changes in MutL alpha. *Mol*. *Cell* **29:** 112-121

Salzano A.M., D′Ambrosio C., and Scaloni A. (2008) Mass spectrometric characterization of proteins modified by nitric oxide-derived species. *Methods Enzymol*. **440:** 3-15

Sandigursky M. and Franklin W.A. (1992) DNA deoxyribophosphodiesterase of *Escherichia coli* is associated with exonuclease I. *Nucleic Acids Res*. **20:** 4699-4703

Sandigursky M. and Franklin W.A. (1994) *Escherichia coli* single-stranded DNA binding protein stimulates the DNA deoxyribophosphodiesterase activity of exonuclease I. *Nucleic Acids Res*. **22:** 247-250

Schofield M.J. and Hsieh P. (2003) DNA Mismatch Repair: Molecular Mechanisms and Biological Function. *Annu*. *Rev*. *Microbiol*. **57:** 579-608

Seeberg E., Eide L., and Bjoras M. (1995) The base excision repair pathway. *Trends Biochem*. *Sci*. **20:** 391-397

Sharma R. and Rao D.N. (2009) Orchestration of *Haemophilus influenzae* RecJ exonuclease by interaction with single-stranded DNA-binding protein. *J*. *Mol*. *Biol*. **385:** 1375-1396

Shimada A., Masui R., Nakagawa N., Takahata Y., Kim K., Kuramitsu S., and Fukui K. (2010) A novel single-stranded DNA-specific 3′-5′ exonuclease, *Thermus thermophilus* exonuclease I, is involved in several DNA repair pathways. *Nucleic Acids Res*. **38:** 5692-5705

Shinkai A., Kira S., Nakagawa N., Kashihara A., Kuramitsu S., and Yokoyama S. (2007) Transcription activation mediated by a cyclic AMP receptor protein from Thermus thermophilus HB8. *J*. *Bacteriol*. **189:** 3891-3901

Simmons L.A., Davies B.W., Grossman A.D., and Walker G.C. (2008) β clamp directs localization of mismatch repair in *Bacillus subtilis*. *Mol*. *Cell* **29:** 291-301

Sorek R., Kunin V., and Hugenholtz P. (2008) CRISPR--a widespread system that provides acquired resistance against phages in bacteria and archaea. *Nat*. *Rev*. *Microbiol*. **6:** 181-186

Szankasi P. and Smith G.R. (1992) A DNA exonuclease induced during meiosis of *Schizosaccharomyces pombe*. *J*. *Biol*. *Chem*. **267:** 3014-3023

Tachiki H., Kato R., Masui R., Hasegawa K., Itakura H., Fukuyama K., and Kuramitsu S.

(1998) Domain organization and functional analysis of *Thermus thermophilus* MutS protein. *Nucleic Acids Res*. **26:** 4153-4159Tishkoff D.X., Boerger A.L., Bertrand P., Filosi N., Gaida G.M., Kane M.F., and Kolodner R.D. (1997) Identification and characterization of *Saccharomyces cerevisiae* EXO1, a gene encoding an exonuclease that interacts with MSH2. *Proc*. *Natl*. *Acad*. *Sci*. *U*. *S*. *A*. **94:** 7487-7492

Thomas K.R. and Olivera B.M. (1978) Processivity of DNA exonucleases. *J*. *Biol*. *Chem*., **253:** 424-429

Tran P.T., Simon J.A., and Liskay R.M. (2001) Interactions of Exo1p with components of MutLalpha in *Saccharomyces cerevisiae*. *Proc*. *Natl*. *Acad*. *Sci*. *U*. *S*. *A*. **98:** 9760-9765

Truglio J.J., Croteau D.L., Van Houten B., and Kisker C. (2006) Prokaryotic nucleotide excision repair: the UvrABC system. *Chem*. *Rev*. **106:** 233-252

Turner J., hingorani M.M., Kelman Z., and O'Donnell M. (1999) The internal workings of a DNA polymerase clamp-loading machine. *EMBO J*. **18:** 771-783

Umar A., Buermeyer A.B., Simon J.A., Thomas D.C., Clark A.B., Liskay R.M., and Kunkel T.A. (1996) Requirement for PCNA in DNA mismatch repair at a step preceding DNA resynthesis. *Cell* **87:** 65-73

Viswanathan M., Burdett V., Baitinger C., Modrich P., and Lovett S.T. (2001) Redundant exonuclease involvement in *Escherichia coli* methyl-directed mismatch repair. *J*. *Biol*. *Chem*. **276:** 31053-31058

Viswanathan M. and Lovett S.T. (1998) Single-strand DNA-specific exonuclease in Escherichia coli. Role in repair and mutation avoidance. *Genetics* **149:** 7-16

Viswanathan M. and Lovett S.T. (1999) Exonuclease X of *Escherichia coli*. A novel 3′-5′ DNase and DnaQ superfamily member involved in DNA repair. *J*. *Biol*. *Chem*. **274:** 30094-30100

Wakamatsu T., Kitamura Y., Kotera Y., Nakagawa N., Kuramitsu S., and Masui R. (2010) Structure of RecJ exonuclease defines its specificity for single-stranded DNA. *J*. *Biol*. *Chem*. **285:** 9762-9

Wakamatsu T., Kim K., Uemura Y., Nakagawa N., Kuramitsu S., and Masui R. (2011) Role of RecJ-like protein with 5'-3' exonuclease activity in oligo(deoxy)nucleotide degradation. *J*. *Biol*. *Chem*. **286:** 2807-2816

Wang T., Sun HL., Cheng F., Zhang XE., Bi L., and Jiang T. (2013) Recognition ant processing of double-stranded DNA by ExoX, a distributive 3'-5' exonuclease. *Nucleic Acids Res*. **41:** 7556-7565

Waters L.S. and Storz G. (2009) Regulatory RNAs in bacteria. *Cell* **136:** 615-628

Weinfeld M., Liuzzi M., and Paterson M.C. (1989) Enzymatic analysis of isomeric trithymidylates containing ultraviolet light-induced cyclobutane pyrimidine dimers. II. Phosphorylation by phage T4 polynucleotide kinase. *J*. *Biol*. *Chem*. **264:** 6364-6370

Weiss B. (2001) Endonuclease V of *Escherichia coli* prevents mutations from nitrosative

deamination during nitrate/nitrite respiration. *Mutat*. *Res*. **461:** 301-309

Weiss B. (2006) Evidence for Mutagenesis by Nitric Oxide during Nitrate Metabolism in *Escherichia coli*. *J*. *Bacteriol*. **188:** 829-833

Yamagata A., Masui R., Kakuta Y., Kuramitsu S., and Fukuyama K. (2001) Overexpression, purification and characterization of RecJ protein from *Thermus thermophilus* HB8 and its core domain. *Nucleic Acids Res*. **29:** 4617-4624

Yamagata A., Kakuta Y., Masui R., and Fukuyama K. (2002) The crystal structure of exonuclease RecJ bound to Mn^{2+} ion suggests how its characteristic motifs are involved in exonuclease activity. *Proc*. *Natl*. *Acad*. *Sci*. *U*. *S*. *A*. **99:** 5908-5912

Yamamoto T., Iino H., Kim K., Kuramitsu S., and Fukui K. (2011) Evidence for ATP-dependent structural rearrangement of nuclease catalytic site in DNA mismatch repair endonuclease MutL. *J*. *Biol*. *Chem*. **286:** 42337-42348

Yao N., Leu F.P., Anjelkovic J., Turner J., and O'Donnell M. (2000) DNA structure requirements for the Eschrichia coli gammacomplex clamp loader and DNA polymerase III holoenzyme. *J*. *Biol*. *Chem*. **275:** 11440-11450

Zhai J. and Hingorani M.M. (2010) *Saccharomyces cerevisiae* Msh2-Msh6 DNA binding kinetics reveal a mechanism of targeting sites for DNA mismatch repair. *Proc*. *Natl*. *Acad*. *Sci*. *U*. *S*. *A*. **107:** 680-685

Zhang X., Zhu L., and Deutscher M.P. (1998) Oligoribonuclease is encoded by a highly conserved gene in the 3′-5′ exonuclease superfamily. *J*. *Bacteriol*. **180:** 2779-2781

ACKNOWLEGEMENT

I would like to express my great appreciation to Profssor Seiki Kuramitsu and Drs. Ryoji Masui, Noriko Nakagawa, and Kenji Fukui for their many valuable discussions. I also would like to express my great appreciation to Professors Hisao Masukata and Tetsuro Yonesaki and Dr. Tatsuro Takahashi for their critical advices in this work. I wish to thank Dr. Akeo Shinkai and Yashihiro Agari for their helpful discussion in CHAPTER I. I also thank Dr. Yoshinori Koyama for providing pHG305 plasmid, and Naoko Aoki for her excellent help in the construction of the plasmid for gene-disruption. I am grateful to Dr. Tatsuro Takahashi and Mr. Yoshitaka Kawasoe for their help in the constructing the plasmid DNA using nicking endonuclease assay in CHAPTER II. I wish to thank Hirofumi Ohmori for DNA sequencing in this study. Finally, I thank my colleagues in Kuramitsu laboratory for their kind help in this study.

LIST OF PUBLICATION

Publications related to Chapter I

1. Shimada A., Masui R., Nakagawa N., Takahata Y., Kim K., Kuramitsu S., and Fukui K. (2010) A novel single-stranded DNA-specific 3′-5′ exonuclease, *Thermus thermophilus* exonuclease I, is involved in several DNA repair pathways. *Nucleic Acids Res*. **38**: 5692-5705.

2. Morita R., Nakane S., Shimada A., Inoue M., Iino H., Wakamatsu T., Fukui K., Nakagawa N., Masui R., and Kuramitsu S. (2010) Molecular mechanisms of the whole DNA repair system: a comparison of bacterial and eukaryotic systems. *J*. *Nucleic Acids* **Article ID 179594**, 32 pages **(review)**

Publications related to Chapter II

1. Iino H., Kim K., Shimada A., Masui R., Kuramitsu S., and Fukui K. (2011) Characterization of C- and N-terminal domains of Aquifex aeolicus MutL endonuclease: N-terminal domain stimulates the endonuclease activity of C-terminal domain in a zinc-dependent manner. *Biosci*. *Rep*. **31**, 309-322

2. Fukui K., Shimada A., Iino H., Masui R., and Kuramitsu S. (2011) Biochemical properties of MutL, a DNA mismatch repair endonuclease. In Storici F (ed.), *DNA Repair - On the Pathways to Fixing DNA Damage and Errors* (Storici F, ed.), pp. 123-142. InTech, Rijeka, Croatia. **(review)**

3. Shimada A., Kawasoe Y., Hata Y., Takahashi T.S., Masui R., Kuramitsu S., and Fukui K. (2013) MutS stimulates the endonuclease activity of MutL in an ATP hydrolysis-dependent manner. *FEBS J*. **280**, 3467-3479

Other publications

1. Shimada A., Ishikawa H., Nakagawa N., Kuramitsu S., and Masui R. (2010) The first crystal structure of an archaeal metallo-β-lactamase superfamily protein; ST1585 from *Sulfolobus tokodaii*. *Proteins* **78**: 2399-2402.

2. Fukui K., Bessho Y., Shimada A., Yokoyama S., and Kuramitsu S. (2013) Thermostable mismatch-recognizing protein MutS suppresses nonspecific amplification during PCR. *Int*. *J*. *Mol*. *Sci*. **14**: 6436-6453